U.PORTO

FEUP FACULDADE DE ENGENHARIA
UNIVERSIDADE DO PORTO

Master Thesis in Mechanical Engineering

Experimental and numerical study of contaminated adhesive joints

Author:
Ricardo Brandão Rodrigues

Supervisor:
Ricardo J. C. Carbas

Co-Supervisors:
Lucas F. M. da Silva
Eduardo A. S. Marques
Catarina S. P. Borges

Integrated Master in Mechanical Engineering

June, 2021

Acknowledgements

First and foremost, I'd want to express my gratitude to Professor Lucas da Silva, for giving me the opportunity to work on this project and for sharing his knowledge with me.

Special thanks to Professor Ricardo Carbas, and Professor Eduardo Marques, for their mentoring, knowledge sharing, and continual availability.

To Catarina, my deepest thanks for the friendship, help, sharing knowledge but above all for instilling in me a work ethic like I never had before and for the positive attitude with every problem we faced.

To all members of the adhesives unit, AJPU, for their unwavering availability, helpful advice, and friendship during this project. It was a joy to collaborate with all of you.

To all my friends during this wonderful period in FEUP, I am grateful for all the friendship and affection you gave me.

To my family, Mother, Father, Diana and Rafa. I'm beyond proud of being part of our family. Thank you for the support, the motivation and guidance. This victory is also yours. And finally, I dedicate this work in honor of my grandfather, my greatest wish would be that you could attend to the conclusion of this milestone.

Abstract

Adhesives, and particularly silicones, are employed in a variety of applications that require not only the bonding of two components but also the sealing of the whole assembly. Usually, these are non-structural and semi-structural applications that need flexible bonding, severe environment tolerance and long-term bond endurance. Therefore, silicone adhesive joints are often exposed to moist and contaminated environments. The adhesive studied is used to join a polybutylene terephthalate with 30% of glass fiber (PBT-GF30) housing for electronic components used in the automotive sector, as well as seal the housing, protecting the electronic components from exterior contamination, and, given its heat insulator properties, to bond an aluminum heat sink to the housing.

The main aim of this work is to analyze the effect of contamination on the properties of aluminum/silicone and PBT-GF30/silicone adhesive joints. Regarding the aluminum/silicone adhesive joints, the contamination arises from a surfactant used to clean oils from the substrates. The effect of this surfactant on the silicone was analyzed by mixing different amounts of surfactant to the adhesive, and studying its mechanical and chemical properties. Afterwards, double cantilever beam (DCB) and single lap joints (SLJ) with aluminum substrates with different amounts of surfactant were prepared. It was seen that the adhesive suffers chemical changes when surfactant is added, decreasing its strength and stiffness. When in a joint, the surfactant is absorbed by the adhesive close to the substrate (at the interphase), weakening this region and moving the failure surface progressively towards the interface. There is a moment at which the amount of contaminant surpasses the adhesive absorption limit, and it acts as a physical separation between adhesive and substrate, promoting adhesive failure. The properties of the interphase were obtained through reverse engineering from numerical simulation.

Regarding the PBT-GF30/silicone joints, contamination arises from environmental moisture. It had also been studied that the PBT-GF30, if immersed in water at temperatures above 85 °C suffers chemical changes, which may release contaminants that establish at the interface. Thus, the effect of water immersion at 70, 90 and 130°C was investigated. The adhesive, substrate and adhesive joints (SLJ and DCB) were tested in three states (dried, aged and dried after aging) to understand the effect of temperature on the dried state, the combined effect of temperature and moisture in the aged state and if the changes introduced were reversible through the dried after aging state. At 70 °C, joint strength follows a behavior similar to that of the adhesive, increasing with humidity. However, with increasing immersion temperature the degradation of the substrate became clearer, and the failure presented areas of cohesive failure closer to the interface, adhesive failure or even failure at the substrate for the DCB joints. All experimental results were validated with a numerical simulation using *Abaqus*, showing good agreement.

Resumo

Os adesivos, e particularmente os silicones, são utilizados numa variedade de aplicações que requerem não só a colagem de dois componentes, mas também a selagem do conjunto final. Normalmente, estas são aplicações não-estruturais e semi-estruturais que necessitam de ligação flexível, tolerância a ambientes severos e resistência de ligação a longo prazo. Assim, as juntas adesivas com silicone são frequentemente expostas a ambientes húmidos e contaminados. O adesivo estudado é utilizado para unir uma caixa para componentes eletrónicos utilizada na indústria automóvel, fabricada em polibutileno tereftalato com 30% de fibra de vidro (PBT-GF30), bem como selar a caixa, protegendo os componentes eletrónicos da contaminação exterior, e, dadas as suas propriedades térmicas isolantes, unir um dissipador de calor de alumínio à caixa. O principal objetivo deste trabalho é analisar o efeito da contaminação nas propriedades de juntas adesivas de alumínio/silicone e PBT-GF30/silicone. Relativamente às juntas adesivas de alumínio/silicone, a contaminação resulta de um tensioativo utilizado para limpar óleos do alumínio. O efeito do tensioativo no silicone foi analisado, misturando diferentes quantidades de contaminante ao adesivo, e estudando as suas propriedades mecânicas e químicas. Posteriormente, foram preparadas juntas *double cantilever beam* (DCB) e juntas de sobreposição simples (SLJ) com substratos de alumínio com diferentes níveis de contaminação. Verificou-se que o adesivo sofre alterações químicas quando o tensioativo é adicionado, diminuindo a sua resistência e rigidez. Nas juntas este é absorvido pelo adesivo próximo do substrato, enfraquecendo esta região e deslocando progressivamente a superfície de rutura em direção à interface. Há um momento em que a quantidade de contaminante ultrapassa o limite de absorção do adesivo e atua como uma separação física entre o adesivo e o substrato, promovendo falha adesiva. As propriedades da interfase foram obtidas por engenharia inversa através de simulação numérica. Nas juntas de PBT-GF30/silicone, a contaminação surge da humidade ambiental. Tinha sido estudado que o PBT-GF30, se imerso em água a temperaturas superiores a 85 °C sofre alterações químicas, podendo libertar contaminantes que se alojam na interface. Assim, foi investigado o efeito da imersão em água a 70, 90 e 130°C. O adesivo, substrato e juntas (SLJ e DCB) foram testados em três estados (seco, envelhecido e seco após o envelhecimento) para compreender o efeito da temperatura sobre o estado seco, o efeito combinado da temperatura e humidade no estado envelhecido e se as alterações introduzidas eram reversíveis através do estado seco após o envelhecimento. A 70 °C, a resistência das juntas segue um comportamento semelhante à do adesivo, aumentando com a humidade. No entanto, com o aumento da temperatura de imersão, a degradação do substrato torna-se mais clara e a falha apresenta áreas de falha coesiva mais próximas da interface, falha adesiva, ou mesmo falha do substrato para os DCBs. Todos os resultados experimentais foram validados numericamente usando *Abaqus*.

Contents

List of Figures

List of Tables

1 Introduction

1.1 Background and motivation

The use of adhesive joints has been increasing in the aerospace, automotive and maritime industries [da Silva et al., 2018]. When compared to mechanical joints, such as bolts, welded joints and rivets, these joints can offer a reduction in the final component and the final cost of the products. Adhesive joints do not require the introduction of holes, as bolting or riveting, decreasing the stress concentrations in the joined parts, and do not require local damage of the material joined, as in welding processes. Additionally, complex geometries (with thin walls), composite materials and dissimilar substrates can be joined with this method [Adams et al., 1997].

In the automotive industry, adhesives can be used in structural and non-structural applications. Non-structural applications can consist, for instance, on the bonding of the housing for electronic components of the vehicle. The housing is typically manufactured from polybutylene terephthalate with 30% of glass fiber (PBT-GF30) and bonded using a silicone to take advantage of its sealing properties. In this application, the joint can be subjected to hot-humid environments and, due to the polymeric nature of adhesives, the joint performance can be compromised by the water ingress through the adhesive, through the substrate or through the adhesive/substrate interface. Additionally, water can establish chemical connections with water and experience degradation, releasing chemical substances that will accommodate in the adhesive/substrate interface [da Silva and Sato, 2013]. Therefore, it is important to understand the effect of water on the adhesive, substrate, and on the interface between them. The substrate was studied by Borges et al., that observed that PBT-GF30 is not stable at temperatures above 80-85 °C, experiencing chemical degradation. In this work, the substrate, adhesive and adhesive joint are going to be studied. Since it is wanted to understand the influence of the chemical changes of the substrate on the bondability of the joint, temperatures above 85 °C and below 80 °C are going to be analyzed (70, 90 and 130 °C). Additionally, three different humidity conditions are going to be studied (dried, aged, and dried after aging), to understand the effect of moisture on the materials and if it is reversible upon re-drying.

In the same components, silicone is also used to bond the housing to an aluminum heat sink. In the case of these aluminum joints, the contamination occurs commonly due to exterior agents, such as oils used to cut the aluminum. As part of the manufacturing process, after cutting, the aluminum is usually cleaned using detergents that contain surfactants. The effect of surfactants on adhesive joints, and especially using silicone adhesives, is not known. Therefore, it is also going to be addressed in this work.

1.2 Objectives

This thesis is done in the scope of a PhD project. The two main goals of the main project are the in-depth study of the effect of water and contamination on adhesive joints and the creation of testing methodologies to implement in industrial environments. The present thesis aims to contribute to the project by understanding the effect of contamination in adhesive joints. However, two different approaches are going to be followed. First, the water contamination in PBT-GF30/silicone joints and the one that may arise from the chemical degradation of the PBT-GF30 is analyzed. Then, the effect of the application of surfactants on aluminum prior to the bonding of the silicone adhesive is studied.

1.3 Research methodology

To accomplish the objectives of this work the following steps have been followed:

- A literature review was done, first to understand the effects of water intake in a PBT-GF30 substrate and on silicone adhesives, particularly concerning mechanical and chemical degradation. Contamination due to surfactant application prior to bonding was also addressed, as well as how several types of contaminant agents interfere with adhesive bonding, especially when silicone adhesives are used.
- Experimental analysis of the PBT-GF30, silicone and PBT-GF30/silicone joints when subjected at three different temperatures (70, 90 and 130°C) and at three different humidity conditions (dried, aged and dried after aging) was perfoned;
- Experimental tests of silicone and aluminum/silicone joints with different surfactant levels were conducted;
- Numerical simulations of the PBT-GF30/silicone joints at all of the conditions were performed;
- Numerical simulations of the aluminum/silicone joints were conducted to infer the properties of the interphase using reverse engineering.

1.4 Thesis outline

This dissertation is divided in seven parts: Chapter 1, is an introduction chapter that gives a brief and concise description of the problem of this dissertation, the objective and methodology used. Chapter 2, comprehends a literature review about adhesive bonding and the effect of contamination and humidity.

Chapter 3 summarizes the experimental procedure used throughout this work. Chapter 4 explains the numerical approach used in this work to validate the experimental procedure.

Chapter 5 presents a summary of the papers developed during this work. Chapter 6 presents the conclusions reached in this work, and in Chapter 7 future works are suggested.

2 Literature review

2.1 Adhesive bonding

An adhesive is, by definition, capable of joining two materials, whether they are similar or dissimilar, and resist their separation. The joined materials are usually called substrates before they are bonded and adherends, after bonding. The region between the adherend and the adhesive is the interphase, which contains the interface. The plane between the adhesive and the adherend is called interface.

Adhesive bonding is a technology increasingly implemented to replace traditional ones, such as the use of screws or welding, because it presents several advantages, such as a uniform stress distribution along the bonded area and an increase in stiffness and load transmission, while significantly reducing the weight of the final structure. It also features the possibility of connecting different materials, small joining areas, complex designs, and the ability to be implemented either manually or automatically [da Silva et al., 2018].

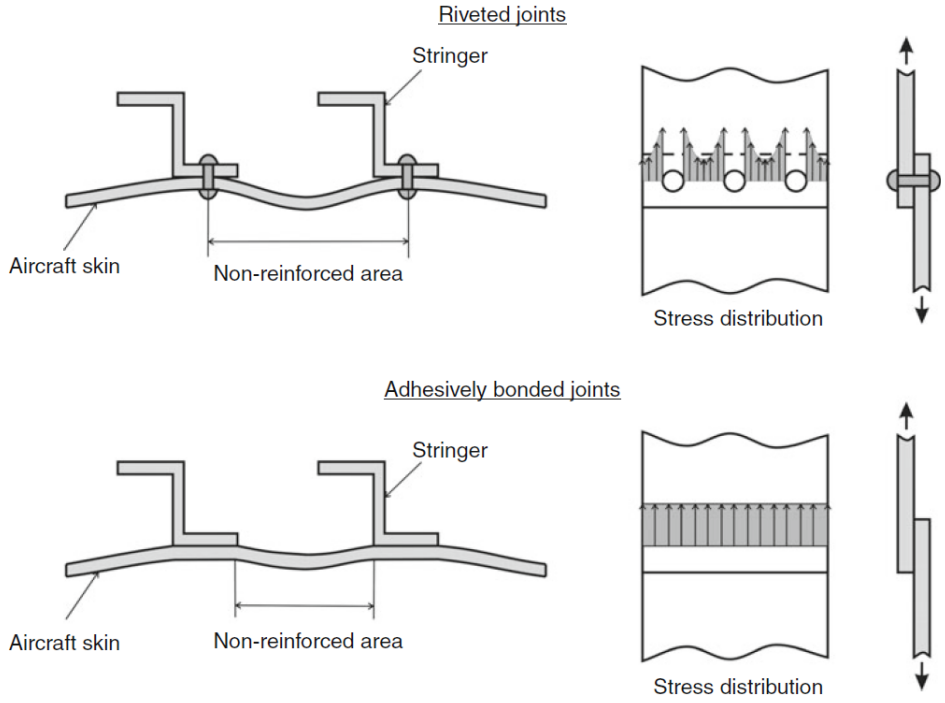

Figure 1: Comparison between riveted and adhesive bonded joints in terms of stiffness (left) and stress distribution (right) [da Silva et al., 2018].

However, there are some disadvantages to adhesive joints that must be considered. Since adhesives are polymeric materials by nature, they typically present a high sensitivity to harsh environments, such as high temperatures and humidity. Additionally, they generally present poor behavior under peel and cleavage stresses, as they concentrate the load in a small resistant area. The need for cleaning of the substrate, the need to keep

the substrate immobile while applying the adhesive and the curing process can also make adhesive application a time-consuming process, which may present a disadvantage in assembly lines. Disassembly of the bonded structures without damage is also a topic which is under research and quality control is difficult to perform.

2.1.1 Classification of adhesives

Adhesives can be distinguished on the basis of different criteria. They can be divided on the basis of their origin, i.e. natural or synthetic adhesives. Among the natural ones we find natural rubber, animal glue, casein-based and protein-based adhesives. However, the most widely used are synthetic adhesives, such as epoxies, polysters and silicones. At the basis of this work there is a silicone adhesive.

Adhesives can also be distinguished in terms of structure, i.e. thermosets, thermoplastics, elastomers or hybrid. Thermosets can not be melted or heated after curing and can be supplied as a one-part or two-part system (resin plus hardner), the one-part systems usually cure at an elevated temperature while the two-part systems cure at room temperature and have a longer life cycle despite temperature restrictions. Thermoplastics, on the other hand, are cured from a melted state or by loss of solvent and can be heated to temperatures up to the glass transition temperature, T_g [da Silva et al., 2018].

Elastomeric adhesives, such as the one used in this work, have a particular behavior, being very flexible and nearly incompressible. They may be supplied as solutions in organic solvents, latex cements, dispersions, pressure-sensitive tapes, and single- or multiple-part solvent-free liquids or pastes. In addition, the physical properties of elastomers are very rate and temperature dependent. Their curing varies, depending on the type and the form of adhesive. Quantifying the mechanical properties of elastomers is generally more difficult than typical engineering materials [Dillard et al., 2002, Ebnesajjad and Landrock, 2015]. Hybrid adhesives are a combination of two or more adhesive families, taking advantage of each of their particular advantages.

Another way to categorize adhesives is their function, and there are two main groups, structural adhesives and non-structural adhesives. The latter are used essentially as insulators and examples of these are polyester and synthetic rubbers, while the structural adhesives can bear high loads and as examples we have epoxies and polyurethanes [da Silva et al., 2018, Nunes, 2018]. Adhesives can additionally be categorized based on their physical form: liquid, paste, film, and powder. This is important for the industry because it will define how it should be applied, for example, a liquid adhesive can fill voids but can slide out of the joint when applied, which does not happen with the others. Finally, there is the reaction method that divides adhesives according to their curing method. Adhesives can cure by chemical reaction, by solvent loss, by water loss, or by cooling from

the molten state.

2.1.2 Failure modes and joint design

Adhesive joints can generally exhibit three types of failure: cohesive failure in the adhesive, adhesive failure and cohesive failure in the adherend. Cohesive failure in the adhesive occurs when a crack propagates in the adhesive, and after failure there is adhesive on both surfaces. Adhesive failure, occurs at the interface, that is, the failure is at the bond between the adhesive and one or both substrates. And, finally, the cohesive failure in the adherend happens when the limit of the substrate material is reach before that of the adhesive bond [da Silva et al., 2018].

Adhesive failure, an undesirable failure mode, occurs between the adhesive and one of the adherends and can be due to poor cleaning of the adherend surface, which leads to poor bonding with the adhesive, which can lead to an unstable and unexpected failure. Another catalyzer to this type of failure is contamination, because it interferes with the adhesive bonding in the interface.Adhesive failure, can also be due to thermal stresses, voids or other defects or inadequate overlap length. The third mode, cohesive failure in the adherend is the ideal case, since when it appears the bond region has not failed, it occurs when the adherent has reached its limit in terms of material strength and the adhesive bonding does not cause premature failure of the structure. It is still possible to obtain a mixed failure, a combination of cohesive and adhesive failure, when the failure happen near the substrate, and it is visible that in some parts of the failure it is adhesive and in others is it cohesive.

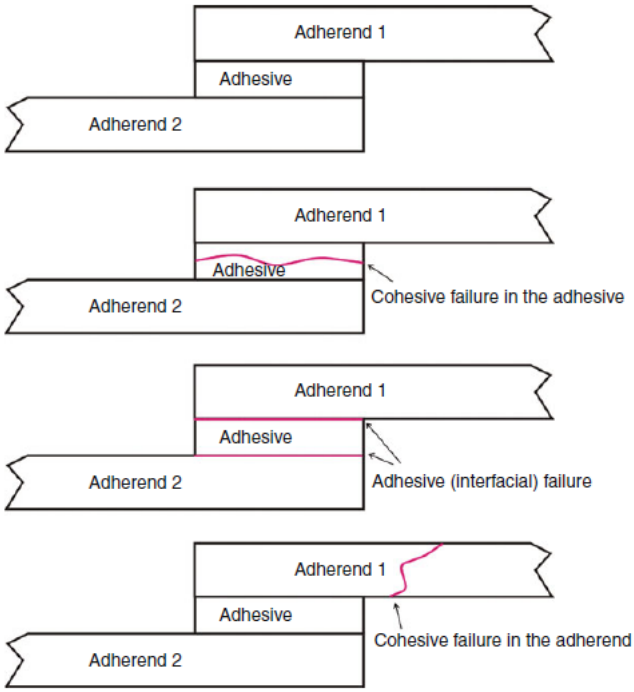

Figure 2: Schematic representation of cohesive and adhesive failures [da Silva et al., 2018].

The type of loading has a significant effect on the strength and durability of adhesive joints. There are four typical loading conditions that adhesive joints can be subject to: normal, shear, peel and cleavage.

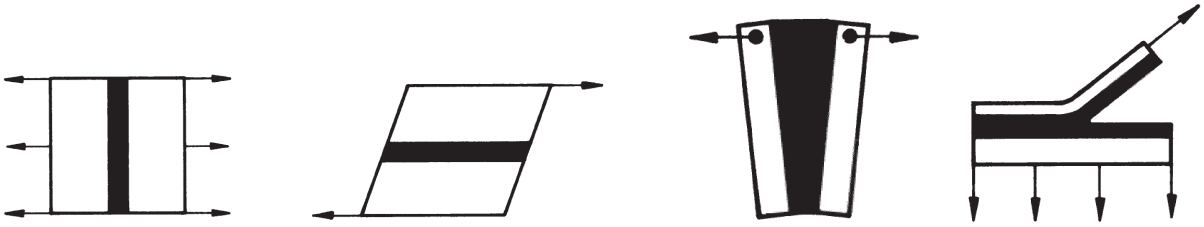

(a) Normal. (b) Shear. (c) Cleavage. (d) Peel.

Figure 3: Types of stress on adhesive joints. Adapted from [da Silva et al., 2018]

Adhesive joints must be designed to maximize the resisting area. Therefore, to suffer shear loading, where the whole adhesive layer is resisting the loading applied. Cleavage and peel load a specific thin region of the adhesive layer, which makes the load that the joint can withstand significantly smaller. With normal loading, purely tensile, theoretically the complete adhesive layer would be loaded, however, in real applications, a perfect parallel alignment would be impossible, and the loading would always tend to cleavage. Thus, the geometry of the joints must be carefully designed, taking into account the type of stress that they are subjected to. Among the most common joint configurations are single-lap joints (SLJ), double-lap joints (DLJ), scarf joints and stepped-lap joints, Figure

4. SLJs are one of the joint configurations that are going to be analyzed in this work.

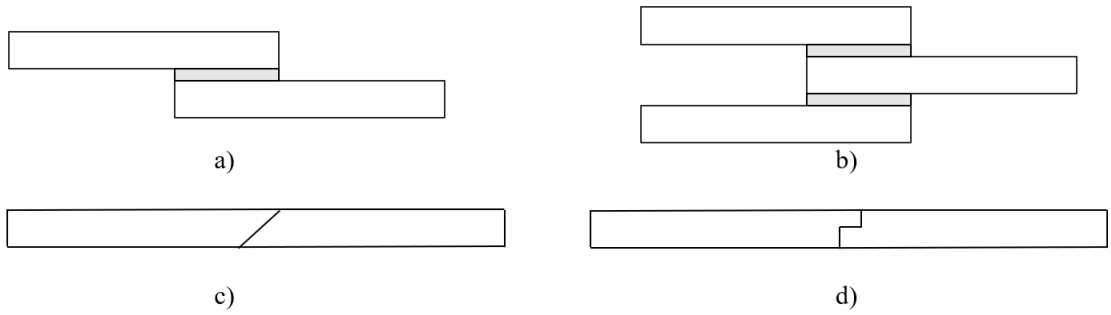

Figure 4: Different joint configurations: a) single lap joints; b) double-lap joints; c) scarf joints; d) stepped-lap joints.

2.2 Adhesives in the electronic industry

Modern electronic component assembly emerged in the 1960s, after the appearance of the integrated circuit in the 1950s. However, all the early electronic components were connected by metallic systems, such as soldering which is a joining process used to join different types of metals together by melting solder (e.g. tin-lead), and wire bonding (gold and aluminum), and were mounted on ceramic substrates until the 1980s. In fact, most applications for electronic systems at this time were for high reliability applications and were not driven by cost. With the introduction of electronics in consumer products, polymeric substrates and adhesives began to attract attention because of their low cost and high production rate [Alam and Bailey, 2011].

Adhesives are commonly used both as functional and structural materials in electronic packaging. They supply electrical connections, thermal paths to extract heat from a semiconductor, and can be relied upon to provide structural integrity of the package and system as well as package sealing properties, especially when silicone adhesives are used. In this work, the adhesive studied is a silicone adhesive used to join two parts of a housing for electronic components used in the automotive industry, as well as seal the housing, preventing water to contact the electronic components within.

Silicone adhesives, analyzed in this thesis, are finding extensive use in electrical and electronic applications where stable dielectric properties and resistance to harsh environments are important. Most of these applications are not truly structural in nature, in fact, they are often used in electronics as thermal fillers and mechanical stress buffers because of their flexibility, low ionic impurity, dielectric insulation properties, moisture resistance and wide operating temperature range [Dillard, 2010]. The simultaneous presence of

"organic" groups attached to an "inorganic" backbone gives silicones a combination of unique properties and allows their use in sealants and adhesives compositions in other different fields such as aerospace(for their low and high temperature behavior), medical (for their excellent biocompatibility) and the building industries(for their capability to seal materials of various nature, and their good resistance to weathering)

Another type of adhesive used in the industry regarding the housing bonding are moisture cure cyanoacrylate adhesives, since they can have a high temperature resistance and can be used also in wire-tacking applications. As for the heat sinks, a common adhesive used are heat cure single part epoxy with good thermal conductivity properties.

2.3 Strength prediction approaches

When designing adhesive joints, one must be aware of the type of stress that will be required by the joints, paying special attention to joint failure. The behavior of the adhesive can be characterized by three basic approaches: continuum mechanics, fracture mechanics, and damage mechanics

2.3.1 Continuum mechanics

Continuum mechanics is used to anticipate the strength of an adhesive joint. This approach is based on the analysis of different criteria, for instance the maximum stresses and maximum strains on both the adherent and the adhesive, as well as defining the maximum load that the joint can tolerate. For this purpose, the linear elastic finite element (FEM) is commonly used. However, this method does not assume any type of failure either in the adhesive or in the adherend, assuming a perfect bonding. In reality, this is not the case for several reasons, for instance, due to the singularities of the joint tip geometry, shown in Fig. 5. In this case, using finite element analysis, the stress value increases with mesh refinement and does not converge. As an alternative, the adhesive and/or substrate can be rounded to avoid singularities. [Banea and d. Silva, 2009,da Silva et al., 2007]

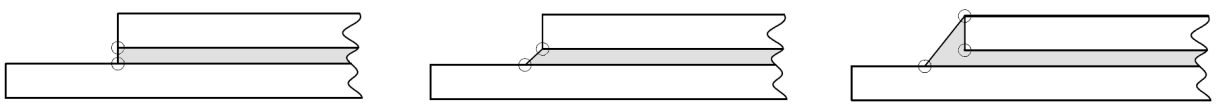

Figure 5: Singularities of the joint tip geometry. Adapted from [Chaves et al., 2014].

2.3.2 Fracture mechanics

Fracture mechanics assumes a non-continuous structure, allowing the existence of defects or damage caused during work. Imperfections such as delamination, debonding or

cracks are possible points of stress concentration, promoting fracture initiation and propagation, leading to an eventual failure of the structure. This approach can determine if the dimensions of any defect remain under the critical fracture size, which leads to structural failure [Chaves et al., 2014].

There are three distinct loading modes that can be distinguished according to the orientation of the load with respect to the crack plane: mode I, mode II and mode III as shown in the Figure 6.

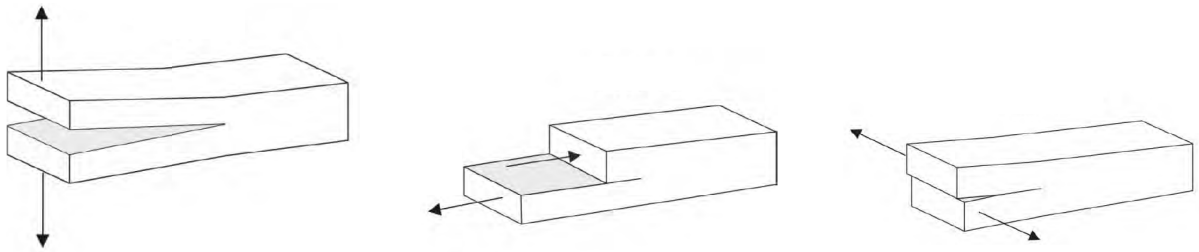

(a) Mode I. (b) Mode II. (c) Mode III.

Figure 6: Fracture modes for an adhesive joint [Chaves et al., 2014].

In mode I, the load is applied perpendicularly to the crack plane, leading to a tensile loading [Broek, 2012], whereas in mode II and III, the applied load is parallel to this plane. The difference between mode II and III is that the load is perpendicular and parallel to the front edge of the crack, respectively. However, as previously stated the failure in real service applications, does not occur in a pure mode of loading but in a combination of two or more modes. Fracture mechanics is based on two criteria: the stress intensity factor criterion and the energy criterion. The stress intensity factor, K, is a scalar parameter capable of quantifying the stress differences near the crack tip which originates from the infinite stress in that area. Considering a mode I loading, the stress intensity factor is described as [Chaves et al., 2014] :

$$K = Y\sigma_r\sqrt{\pi a} \tag{1}$$

where Y is a non-dimensional factor, dependent on the geometry and load distribution, σ_r is the remote tension applied and a is related to the crack length. The crack will propagate when the stress intensity factor, K, is equal to the material fracture toughness K_c. The first energy based criterion in fracture mechanics was proposed by Griffith. The Griffith criterion, which is an energy-based method, can only be used in pure mode I condition [Griffith, 1921]. Griffith et al. [Griffith, 1921], established that an internal defect will propagate when the available energy at the tip of the defect G - energy release rate), due to the loading, equals the energy needed for crack propagation G_c - critical energy release rate), that is a material property. Kinloch, et al. refers that it is advantageous

to use the energy criterion instead of the factor criterion, in what concerns adhesive joints [Kinloch, 2012]. The two criteria can be related, for plane stress, in by :

$$G = \frac{K^2}{E} \tag{2}$$

where E is the Young's modulus. And, for plane strain by [Broek, 2012]:

$$G = \frac{K^2}{E}(1 - \nu^2) \tag{3}$$

where v is the Poisson's ratio. Overall, this criterion tends to be preferred, as G is the material's ability to absorb energy, when fractured, without the progression of the crack [Anderson, 2005, Broek, 2012] This criterion is more widely used once it's more difficult to obtain true values of K, specially when the crack grows near the interface [Machado et al., 2019].

However, adhesive joints in service are not loaded under pure mode conditions. As such, it is necessary to determine the mixed mode ratio. Anderson et al. defined this ratio, for a combination of mode I and mode II, where G_I, the energy release rate in mode I, G_{II} the energy release rate in mode II, and α and β are constants [Anderson, 2005]:

$$\left(\frac{G_I}{G_{I_c}}\right)^{\alpha} + \left(\frac{G_I}{G_{II_c}}\right)^{\beta} = 1 \tag{4}$$

2.3.3 Damage mechanics

Damage mechanics takes into account crack initiation, combining continuum and fracture mechanics to overcome the specific limitations of each of these two methods. Typically, the cohesive zone model (CZM) is widely used for these studies, since it is based on zero thickness elements, establishing a connection between the two solid surfaces. Stress relaxation process based on fracture energy is used to simulate the material degradation. Because of stress relaxation, the mathematical stress singularities associated with continuous approaches do not occur [Anderson, 2005, Broek, 2012]. Through experimental and numerical studies, Campilho et al. [Campilho, 2013] showed that adhesive joints with ductile adhesives are strongly influenced by the CZM shape in the accuracy of strength prediction, with the trapezoidal shape fitting perfectly according to the experimental data. For brittle adhesives, on the other hand, the influence of the CZM shape was found to be null. Triangular and trapezoidal traction separation laws are schematically represented in the Figure 7.

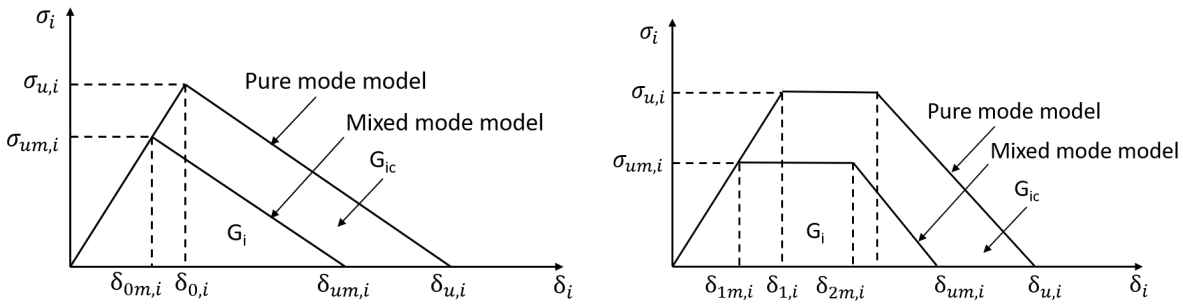

(a) Triangular traction-separation law. (b) Trapezoidal traction-separation law.

Figure 7: Schematic representation of traction separation laws, i=I,II.

2.4 Effect of contamination in adhesive bonding

One of the challenges adhesive joints present, when compared to other joining techniques, is that the bond quality is heavily dependent on the surface preparation of the substrates, since adhesives are susceptible to contaminants. If a substrate surface is contaminated prior to adhesion, the bond between the adhesive and the substrate will be weaker, resulting in a significantly smaller joint strength. Even if the surface is carefully prepared prior to the application of the adhesive, water or contaminants that may be in contact with the adhesive during its service life may deteriorate both the properties of the adhesive and the properties of the bond. For instance, when water is present in the adhesive-substrate system it may cause the substrate to corrode and, the oxidized layer of substrate, is going to decrease the bond strength [da Silva et al., 2018].

Moisture can be absorbed by the adhesive in two different ways, as free water, which occupies the free space of the adhesive and is directly responsible by the plasticization or as bonded water creating single or multiple hydrogen bonds with the adhesive polymer's chain, and can result in swelling of the adhesive, plasticization and a decrease on the strength and glass temperature [Viana et al., 2016]. The Fick's law of diffusion may generally be used to describe water uptake in polymeric materials as a function of time [Eftekhari and Fatemi, 2016]. This law is applied when the diffusion rate is significantly faster than the polymer's relaxation rate [Loh et al., 2005]. However, the compound may lose mass due to disintegration in the immersion environment which, in this case, is water [Borges et al., 2021b]. Considering the ongoing chemical phenomena during the absorption of water, mainly hydrogen bonds are formed with the non-binding electrons of the polymer chain and, as the water enters the polymer, it first binds to polar sites and then, when in higher concentration forms clusters [Cognard, 1994]. It is also known that adhesive plasticization is linked to the strong interaction between the dispersed water and some groups in the polymer chain of the material. The most common cause of damage in

bond connections caused by moisture infiltration is diffusion over the adhesive/substrate interface, which can result in the substrate and adhesive completely separating [Cavodeau et al., 2020].

When adhesives are exposed to moisture, they suffer a reduction in mechanical properties, such as stiffness, strength and toughness. Normally, with the decrease in strength comes an increase in ductility and, consequently, in strain to failure and creep strain [Costa et al., 2015]. The higher the temperature at which moisture exposure occurs, the greater the effect, since with temperature there is a consequent relaxation of the polymeric chain and the ratio between bound and free water increases with temperature [Zhou and Lucas, 1999].

In adhesive joints, composite materials are frequently utilized as substrates. Water diffusion occurs at the interface between the matrix and the fiber in these materials. As a result, water diffuses through composite materials and eventually reaches the interface and thus the adhesive. The physical behavior and diffusion processes of the adhesive/substrate interfaces and the fiber/matrix interfaces are similar [Borges et al., 2021b].

When bonding adhesive joints, an area, known as interphase, is formed. The interphase is a complex polymeric region with heterogeneous morphology and chemical structure, with multiple layers that are distinct from the adhesive and substrate [Crompton, 1989]. According to Possart et al., this interphase in adhesive joints with metallic substrates is formed due to component segregation at the metal interface, resulting in heterogeneities in the liquid adhesive stage [Possart et al., 2006]. Contaminants may affect the joint's mechanical, chemical, and thermal properties. When a substrate is contaminated, the contaminant can either be absorbed by the adhesive or persist at the adhesive/substrate interface. If the contaminant is absorbed by the adhesive, it can affect the mechanical properties, particularly of the interphase layer, since it is the one in proximity to the contaminated substrate. If the contaminant remains at the adhesive/substrate interface, it forms a thin segregation layer in a manometric scale, that can severely damage the adhesive bond due to the physical separation between adhesive and substrate, preventing mechanical interlocking and difficulties in chemical bonding. This can lead to interfacial defects like weak bonds or adhesion debonding. Surface contamination before to the application of the adhesive, incorrect curing of the adhesive, adhesive chemistry, or the environment surrounding the components during their service life are assumed to be the sources of these interfacial defects, or any combination of these reasons [Jeenjitkaew et al., 2010]. Contamination can occur at several stages of the process. For example, it can occur during substrate fabrication, resulting in a change in surface energy. Contamination can affect adhesion at various phases, as well as the surface's wettability, the curing process, and the mechanical qualities of the joint, such as strength [Akiyama et al., 2020].

When contaminant is applied to the surface, in order to avoid weak bonding or zero volume debonds and generate a strong bond between the adhesive and an oil-contaminated metal surface, regardless of superficial contamination, the adhesive must be able to do two things. First, the adhesive must be able to directly remove oil from the metal surface. The adhesive must also be able to absorb the majority of the oil [Pramanik et al., 2017].

3 Experimental procedures

3.1 Materials

3.1.1 Adhesive

The adhesive used in this study is a two-parts silicone elastomer adhesive, used to seal housings for electronic control units. The general properties of the adhesive, given by the manufacturer, can be seen in the Table 1.

Table 1: General properties of the adhesive used.

Type of adhesive	Supplied as	Cure cycle
Silicone elastomer	Two-part	120 °C / 25 min

The mechanical properties of the adhesive, given by the supplier, it can be seen in Table 2.

Table 2: Genera properties of the adhesive used, given by the supplier

Density/ g·cm^{-3}	1.28
Viscosity/ mPa·s	20000
Tensile strength/ MPa	2.2
Elongation at break/ %	120

3.1.2 Substrates

In this work two different substrates were used, PBT-GF30 (Paper **B**) and aluminum (Paper **C**).

PBT-GF30

PBT-GF30, polybutylene terephthalate with 30% glass fiber, is a commonly used material in the housing of electronics components, due to the good behavior in a large range of temperatures and because it is possible to manufacture complex parts using injection molding from this material. It is a material that has been subjected to several studies regarding the effect of water absorption and temperature, since these are two

variables that play a role in its main applications due to the heating of the outside of the housing or of the electronics and the environmental humidity should not be able to enter the housing, because it may damage the components enclosed.

The PBT-GF30 was studied in three different states (dried, aged and dried after aging) at three different temperatures (70, 90 and 130 °C). Borges et al. performed a study on PBT-GF30 at 35, 70 and 130 °C and stated that effect of temperature on the mechanical properties of the material was more significant than the effect of humidity and that there was chemical degradation of the material, in water immersion, between 80 and 85 °C. The main purpose of the present work is to understand if the chemical degradation of the material can release components that are going to accommodate at the adhesive/substrate interface during the degradation process and harm the adhesive bond. For that, joints at a temperature below chemical degradation, 70, and above, 90 and 130 °C, are going to be exposed to hot humid environments.

Aluminum

In Paper **C**, the joints were manufactured with 6082-T6 aluminum substrates. The aluminum substrates were used for the contamination study. This material was chosen since, in industrial processes, it is the material used in the heat sink to the PBT-GF30, which is bonded do the PBT-GF30.

In the Table 3 the general properties of this aluminum are shown.

Table 3: Mechanical properties of the substrate used.

Young's modulus/ MPa	70000
Poisson's ratio	0.33

3.2 Testing methods

All tests were performed by a universal testing machine, *INSTRON*® 3367 (Norwood, MA, USA), with a capacity of 30 kN, at room temperature and constant displacement rate of 2 mm/min.

3.2.1 Strength tests

Bulk specimen tensile test

The bulk specimens were manufactured by curing the adhesive between steel plates in a mold (Figure 8). A silicone rubber frame was used to prevent leakage of the adhesive, to ensure the thickness of the adhesive plate (1 mm) and to induce hydrostatic pressure in the adhesive, avoiding the presence of voids or other defects. The adhesive is then cured on a hot plates press at a 2 MPa pressure at temperature of 125 °C for 25 minutes.

In Paper **A**, neat adhesive was tested dried, aged and dried after aging for different temperatures. Adhesive with different amounts of water and contaminant mixed prior to curing was also analyzed.

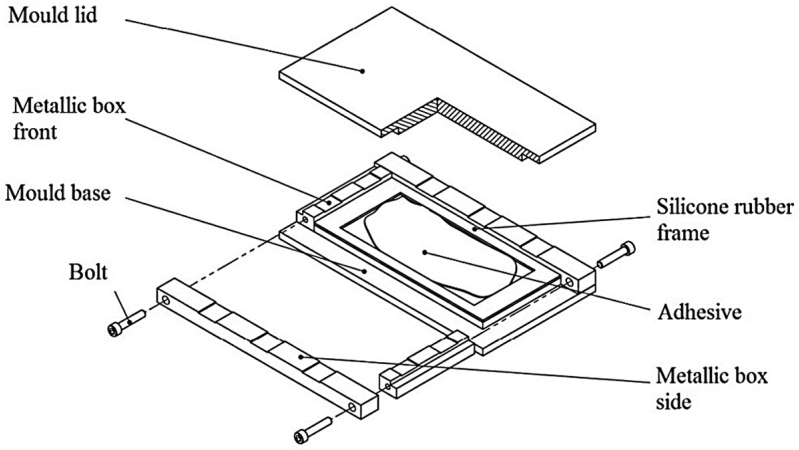

Figure 8: Mold used in the manufacture of adhesive bulk plates [Viana et al., 2017]

For the bulk tensile tests of PBT-GF30, the material plates were already prepared, with 1 mm of thickness, by *Robert Bosch GmbH, Corporate Research and Advance Engineering*. The bulk tensile tests of this material were used in Paper B. For both materials, reduce scale "dogbone" specimens were used. These specimens were, previously, used by Viana et al. and Borges et al. and proved to have accurate stress-strain curves, reducing the amount of material used and improving the storage of the specimens in water [Costa et al., 2015, Viana et al., 2017, Borges et al., 2021a].

In Paper **B**, the PBT-GF30 was tested for dry, aged and dried after aging for three different temperatures (70, 90 and 130°C).

Single lap joints (SLJ)

SLJs were manufactured both using PBT-GF30 (Paper **B**) and aluminum (Paper **C**) substrates. In both cases, the overlap length was 25 mm. Both geometries can be seen in Fig.9

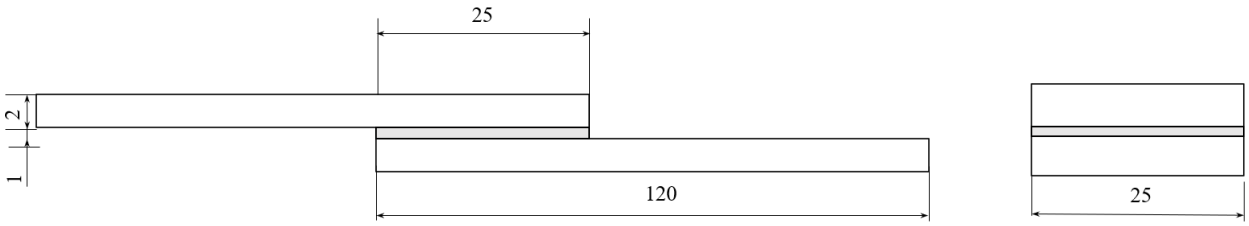

Figure 9: Geometry of the SLJ used, dimensions in mm.

The substrates received surface treatments before bonding. The aluminum substrate were treated with sand paper, degreased with acetone and anodized using phosphoric acid anodization (PAA) according to ASTM D3933 standard [D3933-98, 2017]. As for the PBT-GF30 substrate, the overlap was cleaned with acetone before bonding.

3.2.2 Fracture properties

Double cantilever beam (DCB)

To determine the fracture energy in mode I, double cantilever beam specimens were used, in Sub-Chapter 3.3 an optical method is presented that permitted the calculation of the G_{IC}. The DCBs specimens are composed by two substrates of the same length, width and thickness bonded with an adhesive, such as shown in Figure 10. Where L is the length of the DCB, a_0 is the initial crack length or pre-crack and h is the thickness of the substrates and t is the thickness of the adhesive.

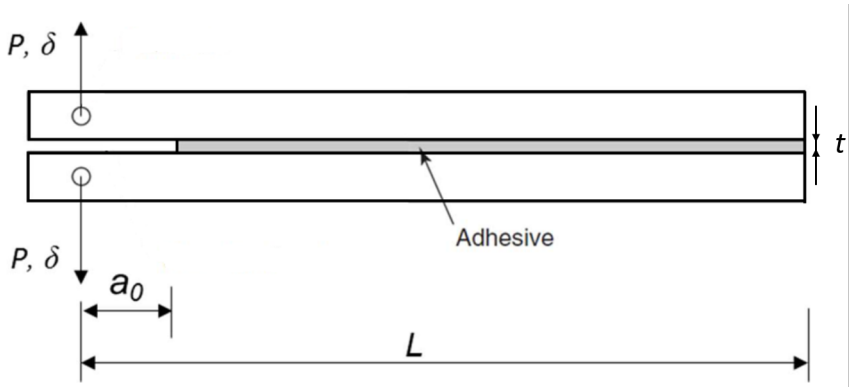

Figure 10: Schematic representation of DCB test.

In Paper **B**, two different DCB shapes were used, one with high strength steel substrates, used for the characterization of the silicone adhesive, and one with substrates of PBT-GF30 with the insertion of steel cubes in order to be capable to test them. These geometries are shown in Figures 11a and 11b, respectively.

In Paper **C**, only one shape was used with aluminum substrates for the different levels of contamination, shown in Figure 11c.

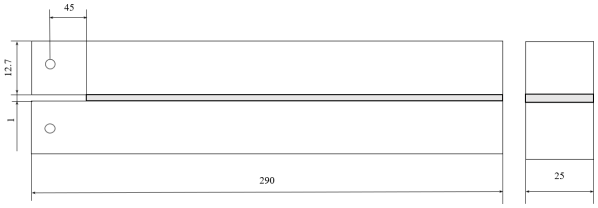

(a) High strength steel substrates DCB

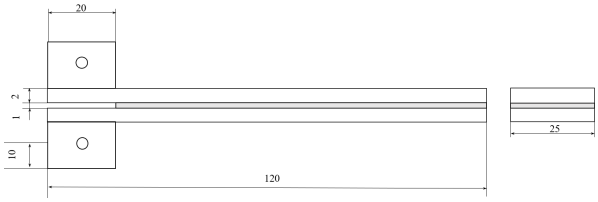

(b) PBT-GF30 substrates DCB

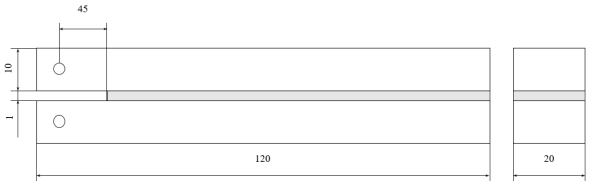

(c) Aluminum substrates DCB

Figure 11: Geometry of the DCB specimens used, dimensions in mm.

The substrates received a similar treatment as the SLJ substrates before bonding. The aluminum ones were sand blasted, degreased with acetone and phosphor acid anodized (PAA) according to ASTM D3933 standard [D3933-98, 2017]. The high strength steel substrates were sand blasted and degreased with acetone. As for the PBT-GF30, the overlap area was cleaned with acetone before bonding.

3.3 Data reduction scheme

As said, high strength steel DCB joints were prepared to characterize the silicone adhesive in terms of fracture toughness in mode I. However, having load and displacement information is important to use an appropriate data reduction scheme to obtain the strain energy release rate in mode I, G_{Ic}. In previous works when silicones adhesives were studied, it was showed that the most suitable approach was the J-integral direct method and therefore, it was the method applied in the work.

J-integral

The J-integral, introduced by Rice et al., is a continuous mechanical value that indicates the resistance of a material to crack propagation under a constant stress, and it is a mean of reporting the toughness of the material in geometries containing flaws [Rice, 1968]. It is measured at the onset of fracture and is defined as the critical value of fracture toughness. It has also an excellent applicability for modelling with current finite element modelling tools [K.H. Jürgen Buschow, 2001, Kurtz, 2016].

$$G_{IC} = 12\frac{(P_u a)^2}{E_a h^3} + P_u \theta_0 \tag{5}$$

or

$$G_{IC} = P_u \theta_p \tag{6}$$

Where P_u is the load applied per unit length at adjacent extremities, a is the crack length, h is the substrate thickness, E_a is the Young's modulus of the substrate and θ_p the relative rotation of the substrate at the line as showed in Figure 12. The J-integral is defined along an arbitrary path surrounding the beginning of the adhesive layer [Zhu et al., 2009] :

$$G_n = \int_0^{\delta_{nc}} t_n(\delta_n) d\delta_n \tag{7}$$

where δ_n and δ_{nc} are the normal opening and the normal end opening of the cohesive law at the tip of the initial crack and t_n is current normal traction. G_{IC} is the value of G_n at the crack tip. As for $t_n(\delta_n)$, it is obtained by differentiation of the equation 7 with respect to δ_n, giving the cohesive law [Zhu et al., 2009].

$$t_n(\delta_n) = \frac{\partial G_1}{\partial \delta_n} \tag{8}$$

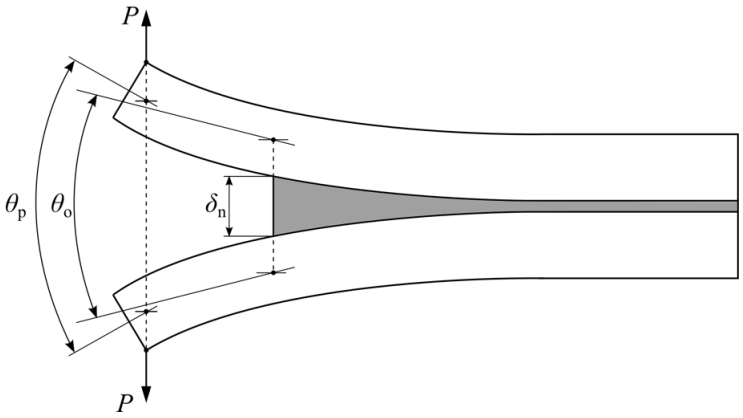

Figure 12: DCB specimen under loading, with description of the analysis parameters.

For the determination of δ_n and θ_0, a digital image correlation (DIC) software, *GOM*, was used. This software has the ability of following manually defined target points and gives the displacement accordingly to a coordinate system. This method was previously used by Campilho et al. [Campilho et al., 2014].

The used technique to create the tracking points consists in painting the specimen with white ink and, afterwards, black ink is carefully sprayed in order to obtain a speckled pattern, as shown in Figure 13. Two points (p_1, p_2) were used to obtain the current opening of the crack tip between the two substrates, t_A, and during the upload of the

video is defined as (t_A^{CT}). Two points in the top of the specimen (p_1, p_3) and the two points on the bottom of the specimen (p_2, p_4) were used to obtain θ_p. The points used for one specimen in DIC software are shown in Figure 13.

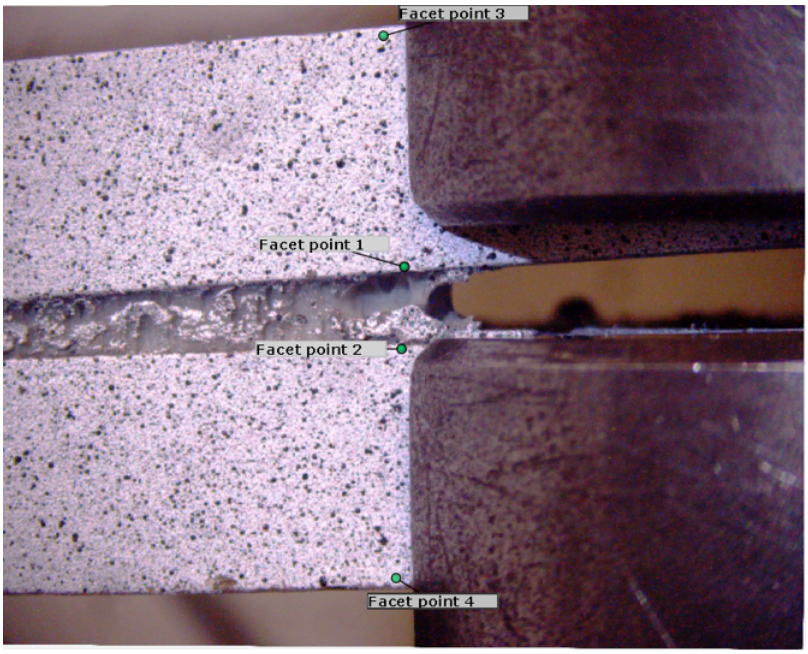

Figure 13: Points taken by the optical method for measuring G_{IC}, θ_p .

The value of t_A^{CT} in S.I units (mm) is the following equation:

$$t_A^{CT} = |p1 - p2| \tag{9}$$

and δ_n comes as :

$$\delta_n = t_A^{CT} - t_A \tag{10}$$

where t_A is the initial thickness of the adhesive, which is 1 mm. So, δ_n starts with an initial value of 0.

The relative rotation between two substrates was defined using two vectors u and t using all the four points (p_1, p_2 ,p_3, p_4). Both vectors are collinear with the top and bottom substrates [F.Loureiro, 2020].

$$\vec{u} = (p_{1x} - p_{3x}, p_{1y} - p_{3y}) \tag{11}$$

$$\vec{t} = (p_{4x} - p_{2x}, p_{4y} - p_{2y}) \tag{12}$$

In Figure 14, it is shown a vector representation of θ_P.

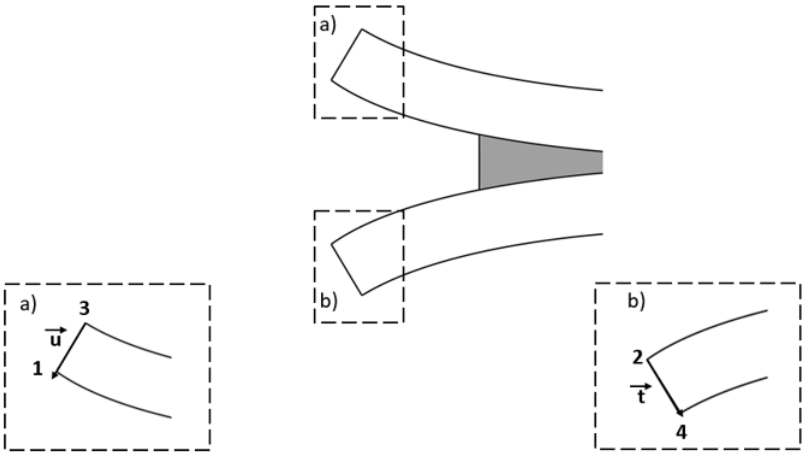

Figure 14: Vector representation of θ_P determination: (a) top substrate vector, u ; (b) lower substrate vector, t

In addiction, in order to relate both vectors, the vector product between the vectors u and t results in the vector t:

$$\vec{s} = \vec{u} \wedge \vec{t} \tag{13}$$

and

$$|\vec{s}| = \sqrt{s_X^2 + s_Y^2} = |\vec{u}| \cdot |\vec{t}| \cdot \sin\theta_p \tag{14}$$

So, we can rewrite the Equation 14 in order to θ_p as:

$$\theta_p = \arcsin \frac{|\vec{s}|}{|\vec{u}| \cdot |\vec{t}|} \tag{15}$$

4 Numerical details

Traditional stress/strain criteria have yielded satisfactory results in the study of adhesive joints using the finite element method (FEM). These standards are based on the examination of structural stresses and strains. It is feasible to determine the stress and displacement field around a specific location using the FEM. Real structures, on the other hand, have places where the stress concentration factor approaches infinity. The solution obtained by the FEM in these solitary spots are mesh-dependent and inaccurate. The point stress criteria, which computes stresses at a predetermined distance from the single point, can help to solve this type of problem and with the average stress criteria, which computes an average stress along a predetermined path [da Silva and Campilho, 2012].

Unlike stress/strain-based criteria, fracture mechanics-based criteria can predict when a crack will begin to propagate by taking into consideration the presence of single points in the structure. These approaches, however, are difficult to apply in adhesive joints because, while every material contains flaws, determining their size or position is difficult.

Further than traditional continuum mechanics modeling, a CZM can illustrate the fracture process and location. This is accomplished by incorporating a sequence of discontinuities in the model, which are represented by cohesive components that employ both strength and energy characteristics to mimic the formation and progression of a fracture crack [da Silva and Campilho, 2012]. Cohesive models apply fracture mechanics principles to simulate crack development in a material by integrating strength and energy characteristics.

Several cohesive laws may be employed to model material softening depending on the material's characteristics. Triangular, linear-parabolic, polynomial, exponential, and trapezoidal rules are among them. Although cohesive laws can be modified to better match the material's behavior, the triangular CZM is frequently utilized and produces satisfactory results in most real-world circumstances owing to its simplicity. Every simulation in this thesis was carried out using a triangular cohesive zone model.

In this regard, different models were created to simulate the experimental behavior of SLJ and DCB using FEM with *Abaqus* (Dassault Systèmes Simulia Corp.Providence, USA).

In **Paper B** in Section *Numerical model* a well detail explication of the models utilized to simulate the behavior of the PBT-GF30/silicone joints is given.

Models for contaminated joints

In **Paper C** a numerical model was created to obtain the properties of the interphase, via reverse engineering, since the properties of the PBT-GF30 were well known.

The substrate and adhesive were characterized as elastic components, whereas the contaminated layer was modeled through cohesive elements. When considering uncontaminated joints, the cohesive elements were included just in the adhesive layer joints since the failure was cohesive through the adhesive and the interphase was not modelled. However, contaminated joints fail through the interphase, therefore the cohesive elements were placed in this section. Various publications claim that the interphase is about 1 and 100 μm long [Gao and Mäder, 2002]. The size of the elements was set to 0.1 mm in *Abaqus*, however it's worth noting that the size of the elements has almost no impact on the cohesive zone models [Avendaño et al., 2016]. In Figure 15 is shown the different layers used in this model.

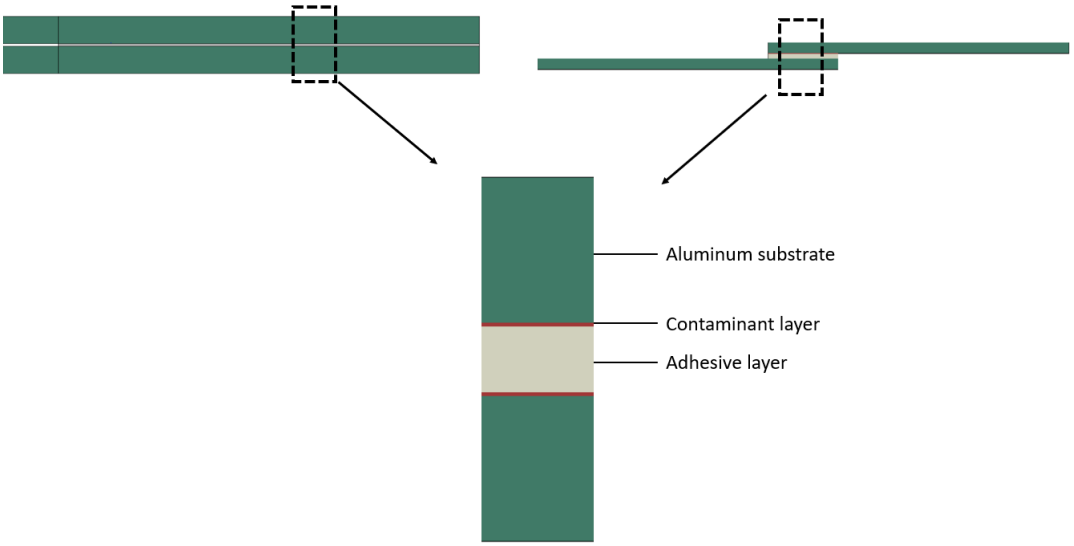

Figure 15: Numerical model of DCB and SLJ with contaminant layer

5 Summary of appended papers

Paper A	This paper studied the effect of water and surfactant contamination prior to curing and after the curing of a silicone adhesive. To study the effect prior to adhesive curing, 2, 5 and 10% of contaminant (water or surfactant) was added to the adhesive. To study the effect after curing, the neat adhesive was immersed in water at three different temperatures (70, 90 and 130°C) and three different states (dried, aged and dried after aging) were tested. All the conditions were analyzed through bulk tensile tests, to understand the effect on the mechanical properties; Fourier-transform infrared spectroscopy (FTIR), to understand the effect on the chemical profile and scanning electron microscopy (SEM), to understand the effect on the morphology of the adhesive.
Paper B	This paper aims to characterize the behavior of PBT-GF30/silicone joints with water uptake. For this, three different temperatures were studied (70, 90 and 130°C) and three different states (dried, aged and dried after aging). Bulk tensile tests were performed on "dogbone" specimens of PBT-GF30 in those conditions and SLJ and DCB with PBT-GF30/silicone adhesive exposed to the same temperatures and states were tested. Finally, through numerical analysis, a correlation was made between the behavior of the joints and the behavior of the bulk PBT-GF30. The failure surfaces of the joints were also analyzed.
Paper C	This paper investigates the impact of surfactant contamination on aluminum/silicone joints. Four levels of surfactant were applied on aluminum substrates before bonding, governed by the number of sprays, ranging from 0 to 10 sprays of contaminant. This experiment was done through DCB, to evaluate the effect on the mode I fracture properties and mode II strength properties were evaluated through SLJs. It was analyzed with SEM analysis if the silicone adhesive was capable of absorbing the surfactant. A detail characterization of the failure types evolution with the quantities of surfactant was done. A numerical study was carried out, and the inverse method was applied to find the mechanical properties of the contaminated interphase layer.

6 Conclusions

The mechanical properties of PBT-GF30 and a silicone adhesive were determined to different temperatures and different states of water intake. SLJ and DCBs under the same conditions were also studied in order to fully comprehend the impact of the PBT-F30 substrates and silicone adhesive had on adhesive joints. The results showed that while there was no severe substrate degradation, the water intake behavior of the silicone was the main influence, as the properties increase with water intake and, after the substrate degradation, the joints' behavior became strongly dependent on the substrate reducing their strength. A numerical model was created for both joints utilizing the bulk tensile experimental results of the PBT-GF30 and silicone for all conditions, and it was achieved a good agreement.

The silicone adhesive capacity to absorb contaminant was also studied, as well how the mechanical properties varied with the absorption. The silicone was mixed with surfactant contaminant in several quantities before curing and afterwards bulk tensile tests were performed. To further understand these phenomena, aluminum substrates for SLJ and DCBs were contaminated with the same surfactant before bonding and tested. The adhesive showed a capacity to absorb the contaminant of the surface until certain quantities and afterwards the failure type was completely adhesive due to remaining of contaminate on the surface, creating an interphase that does not allow a proper adhesion. The results showed a severe decrease of the bonding strength even for the smallest contaminant quantity and as the quantities increase the strength become less and less noticeable. A numerical model was created to simulate this behavior, via indirect method, to discover the mechanical properties of a small layer with cohesive elements. It was reached a good approximation of the $P - \delta$ curves of both SLJ and DCBs.

7 Future work

As future work, it would be interesting to study the behavior of both PBT-GF30/silicone at different temperatures in the range of 70 - 90°C in order to further characterize the detection of the materials. Perform a study similar to **Paper B** but with aluminum substrates, to isolate the effect of silicone adhesive on a joint at different temperatures and states without a degraded substrate.

Make a comparable investigation to the **Paper C** with different types of contaminants, such as oil silicones, to understand which type of contaminant has a bigger impact in the mechanical behavior in adhesive joints while using silicone adhesive. The numerical model could also be modified to each contaminant.

References

[Adams et al., 1997] Adams, R. D., Adams, R. D., Comyn, J., Wake, W. C., and Wake, W. (1997). *Structural adhesive joints in engineering*. Springer Science & Business Media.

[Akiyama et al., 2020] Akiyama, H., Fukata, T., Sato, T., Horiuchi, S., and Sato, C. (2020). Influence of surface contaminants on the adhesion strength of structural adhesives with aluminium. *The Journal of Adhesion*, 96(15):1311–1325.

[Alam and Bailey, 2011] Alam, M. and Bailey, C., editors (2011). *1 - Introduction to adhesives joining technology for electronics*. Woodhead Publishing.

[Anderson, 2005] Anderson, T. (2005). *Fracture Mechanics: Fundamentals and Applications,Third Edition*.

[Avendaño et al., 2016] Avendaño, R., Carbas, R., Marques, E., da Silva, L., and Fernandes, A. (2016). Effect of temperature and strain rate on single lap joints with dissimilar lightweight adherends bonded with an acrylic adhesive. *Composite Structures*, 152:34–44.

[Banea and d. Silva, 2009] Banea, M. and d. Silva, L. F. M. (2009). Adhesively bonded joints in composite materials: an overview. 223:1–18.

[Borges et al., 2021a] Borges, C., Akhavan-Safar, A., Marques, E., Carbas, R., Ueffing, C., Weißgraeber, P., and da Silva, L. D. (2021a). Effect of water ingress on the mechanical and chemical properties of polybutylene terephthalate reinforced with glass fibers. *Materials*, 14.

[Borges et al., 2021b] Borges, C., Marques, E., Carbas, R., Ueffing, C., Weißgraeber, P., and da Silva, L. (2021b). Review on the effect of moisture and contamination on the interfacial properties of adhesive joints. *Proceedings of the Institution of Mechanical Engineers, Part C: Journal of Mechanical Engineering Science*, 235(3):527–549.

[Broek, 2012] Broek, D. (2012). *Elementary engineering fracture mechanics,Third Edition*. martinus nijhoff publishers.

[Campilho, 2013] Campilho, R. (2013). Modelling adhesive joints with cohesive zone models: effect of the cohesive law shape of the adhesive layer. 44:48–56.

[Campilho et al., 2014] Campilho, R., Moura, D., Banea, M., and da Silva, L. (2014). Adherend thickness effect on the tensile fracture toughness of a structural adhesive using

an optical data acquisition method. *International Journal of Adhesion and Adhesives*, 53:15–22. Joint Design.

[Cavodeau et al., 2020] Cavodeau, F., Brogly, M., Bistac, S., Devanne, T., Pedrollo, T., and Glasser, F. (2020). Hygrothermal aging of an epoxy/dicyandiamide structural adhesive – influence of water diffusion on the durability of the adhesive/galvanized steel interface. *The Journal of Adhesion*, 96(11):1027–1051.

[Chaves et al., 2014] Chaves, F., da Silva, L., M Moura, D. D., and Esteves, V. (2014). Fracture mechanics tests in adhesively bonded joints: A literature review. *The Journal of Adhesion*, 90:955–992.

[Cognard, 1994] Cognard, J. (1994). Blistering of glass-epoxy amine adhesive joints in water vapour at high pressure. an indication of interfacial crumpling. *The Journal of Adhesion*, 47(1-3):83–93.

[Costa et al., 2015] Costa, M., Viana, G., Canto, C., da Silva, L., Banea, M., Chaves, F. and Campilho, R., and Fernandes, A. (2015). Effect of the size reduction on the bulk tensile and double cantilever beam specimens used in cohesive zone models. *Proceedings of the Institution of Mechanical Engineers, Part L: Journal of Materials: Design and Applications.*

[Crompton, 1989] Crompton, J. (1989). Interfacial properties and stability in bonded aluminium. *Journal of materials science*, 24(5):1575–1581.

[D3933-98, 2017] D3933-98, A. (2017). Standard guide for preparation of aluminum surfaces for structural adhesives bonding (phosphoric acid anodizing).

[da Silva and Sato, 2013] da Silva, L. and Sato, C. (2013). *Design of Adhesive Joints Under Humid Conditions.* Springer Science.

[da Silva and Campilho, 2012] da Silva, L. F. and Campilho, R. D. (2012). *Advances in numerical modelling of adhesive joints.* Springer.

[da Silva et al., 2018] da Silva, L. F., Ochsner, A., and Adams, R. D. (2018). *Handbook of adhesion technology.* Springer Science & Business Media.

[da Silva et al., 2007] da Silva, L. F. M., de Magalhaes, A. G., and de Moura, M. F. S. (2007). *Juntas adesivas estruturais.* Publindústria Portugal.

[Dillard et al., 2002] Dillard, D., Pocius, A., and Chaudhury, M., editors (2002). *Chapter 10 - Stresses and fracture of elastomeric bonds.* Elsevier Science B.V., Amsterdam.

[Dillard, 2010] Dillard, D. A., editor (2010). *4 - Advances in structural silicone adhesives*. Woodhead Publishing.

[Ebnesajjad and Landrock, 2015] Ebnesajjad, S. and Landrock, A. H., editors (2015). *Chapter 4 - Classification of Adhesives and Compounds*. William Andrew Publishing, third edition edition.

[Eftekhari and Fatemi, 2016] Eftekhari, M. and Fatemi, A. (2016). Tensile behavior of thermoplastic composites including temperature, moisture, and hygrothermal effects. *Polymer Testing*, 51:151–164.

[F.Loureiro, 2020] F.Loureiro, R. . R. (2020). J-integral analysis of the mixed-mode fracture behaviour of composite bonded joints. *The Journal of Adhesion*, 96(1-4):321–344.

[Gao and Mäder, 2002] Gao, S.-L. and Mäder, E. (2002). Characterisation of interphase nanoscale property variations in glass fibre reinforced polypropylene and epoxy resin composites. *Composites Part A: Applied Science and Manufacturing*, 33(4):559–576.

[Griffith, 1921] Griffith, A. A. (1921). The phenomena of rupture and flow in solids. 221.

[Jeenjitkaew et al., 2010] Jeenjitkaew, C., Luklinska, Z., and Guild, F. (2010). Morphology and surface chemistry of kissing bonds in adhesive joints produced by surface contamination. *International Journal of Adhesion and Adhesives*, 30(7):643–653.

[K.H. Jürgen Buschow, 2001] K.H. Jürgen Buschow, Robert W. Cahn, M. C. F. B. I. E. J. K. S. M. P. V. (2001). Fracture toughness testing of metallic materials. pages 3336–3340.

[Kinloch, 2012] Kinloch, A. J. (2012). *Adhesion and Adhesives: Science and Technology*.

[Kurtz, 2016] Kurtz, S. M. (2016). 29 - characterization of physical, chemical, and mechanical properties of uhmwpe. pages 531–552.

[Loh et al., 2005] Loh, W., Crocombe, A., Abdel Wahab, M., and Ashcroft, I. (2005). Modelling anomalous moisture uptake, swelling and thermal characteristics of a rubber toughened epoxy adhesive. *International Journal of Adhesion and Adhesives*, 25(1):1–12.

[Machado et al., 2019] Machado, J., Hayashi, A., Nunes, P., Marques, E., Carbas, R., Sato, C., and da Silva, L. (2019). Strain rate dependence of a crash resistant adhesive as a function of temperature for the automotive industry. 233.

[Nunes, 2018] Nunes, P. D. P. (2018). Impact strength of dissimilar joints for the automotive industry.

[Possart et al., 2006] Possart, W., Krüger, J. K., Wehlack, C., Müller, U., Petersen, C., Bactavatchalou, R., and Meiser, A. (2006). Formation and structure of epoxy network interphases at the contact to native metal surfaces. *Comptes Rendus Chimie*, 9(1):60–79.

[Pramanik et al., 2017] Pramanik, A., Basak, A., Dong, Y., Sarker, P., Uddin, M., Littlefair, G., Dixit, A., and Chattopadhyaya, S. (2017). Joining of carbon fibre reinforced polymer (cfrp) composites and aluminium alloys – a review. *Composites Part A: Applied Science and Manufacturing*, 101:1–29.

[Rice, 1968] Rice, J. R. (1968). A path independent integral and the approximate analysis of strain concentration by notches and cracks. *Journal of Applied Mechanics*, 35(2):379–386.

[Viana et al., 2016] Viana, G., Costa, M., Banea, M., and Silva, L. (2016). A review on the temperature and moisture degradation of adhesive joints. *Proceedings of the Institution of Mechanical Engineers, Part L: Journal of Materials Design and Applications*, 231.

[Viana et al., 2017] Viana, G., Costa, M., Banea, M. D., and da Silva, L. F. M. (2017). Behaviour of environmentally degraded epoxy adhesives as a function of temperature. *The Journal of Adhesion*, 93(1-2):95–112.

[Zhou and Lucas, 1999] Zhou, J. and Lucas, J. P. (1999). Hygrothermal effects of epoxy resin. part i: the nature of water in epoxy. *Polymer*, 40(20):5505–5512.

[Zhu et al., 2009] Zhu, Y., Liechti, K. M., and Ravi-Chandar, K. (2009). Direct extraction of rate-dependent traction–separation laws for polyurea/steel interfaces. *International Journal of Solids and Structures*, 46(1):31–51.

Appendices

A Paper A

Influence of water and surfactant contamination on the mechanical and chemical properties of a silicone adhesive, before and after curing

C.S.P. Borges[1], R. Brandão[2], A. Akhavan-Safar[1], E.A.S. Marques[1], R.J.C. Carbas[1], C. Ueffing[3], P.Weiβgraeber[3], F. Schmid[3], L.F.M. da Silva[2]

1 Instituto de Ciência e Inovação em Engenharia Mecânica e Engenharia Industrial (INEGI), Portugal

2 Departamento de Engenharia Mecânica, Faculdade de Engenharia (FEUP), Universidade do Porto, Portugal

3 Robert Bosch GmbH, Corporate Research and Advance Engineering, 71272 Renningen, Germany

Abstract: Adhesives are oftentimes polymeric materials, which are affected by their service conditions and by the quality and cleanliness of the surfaces they are being bonded to. One of the factors that influences the service quality of bonded joints is, therefore, the presence of contaminants during the different stages of its processing and service life. Silicone adhesives are a particularly interesting family of adhesives for this study since they are often used not only to joint but also seal components. Additionally, the effect of contaminants on the properties of bulk adhesives before curing, and particularly silicones is not very widely researched. This work aims to analyze the mechanical and chemical effects that contaminants can have prior to curing of the silicone adhesive, if they are present in the substrate or surrounding environment at adhesive application, as well as after curing when they appear during the service life of the adhesive joint. In this case, the contaminants are water and a surfactant present in detergents used to clear oils off aluminum surfaces. For this, 2% , 5% and 10% of contaminant was added to the adhesive prior to curing and neat adhesive after curing was immersed in contaminant at different temperatures. For all cases, the effect on the mechanical properties was evaluated through bulk tensile tests, the effect on the chemical profile was evaluated using Fourier-transform infrared spectroscopy (FTIR) and the morphology of the materials was studied with scanning electron microscopy (SEM). A dynamic mechanical analysis (DMA) was also conducted to understand if there is a transition temperature in the temperature range analyzed. The water immersion after curing increased the mechanical properties of the adhesive, however, the effect is reversible when redrying. The temperature to which the specimens are subjected when drying and aging damages the mechanical properties of the adhesive. The water added prior to curing introduces voids to the material but does not change its chemical profile or cross-linking. The surfactant absorbed by the adhesive when curing significantly changes its morphology, showing a difference in chemical profile, with the variation of the amplitude of vibration of the C-H bond. These changes translate into a lower strength and stiffness of the mixture.

A.1 Introduction

Adhesive joints are an alternative to classical joining methods in several industrial sectors, such as the automotive, aerospace and electronics. When compared to bolting or riveting, adhesives have the advantage of not needing the introduction of holes in the component, which is particularly important when joining notch sensitive composite materials, and contributes to a more uniform stress distribution [Da Silva et al., 2018]. When compared to welding, adhesives have the advantage of not needing the local heating of the components, which may lead to local degradation of the material and residual stresses in the final component. The application of adhesives relies on a careful surface preparation, since they are sensitive to moisture and other contaminants that can be accommodated on the substrate. Additionally, during their service life, due to their polymeric nature, adhesives are also able to absorb environmental moisture or other contamination.

The adhesive analyzed in this study was a silicone, used to bond a housing for electronic components used in the automotive industry. Silicones have both organic and inorganic groups, which gives them a combination of particular properties when compared to ordinary organic rubbers since, due to the Si-O bond, silicones have a higher heat resistance, chemical stability, electrical insulation and weatherability [Shit and Shah, 2013]. This array of properties makes silicone a great candidate for particular applications that require not only joining components but also the sealing of the assembly. Taking all the previously mentioned factors into consideration, it becomes clear that it is important to understand the effect of water and contamination both prior to the adhesive curing, if they are found in the substrate or in the manufacturing environment, and after curing, if the silicone adhesive is supposed to seal the component from that fluid. As contaminants, water and a surfactant that can be used or clean cutting oils from aluminum substrates prior to adhesive bonding were analyzed.

Silicones are usually considered when designing sealant joints, since they are generally more hydrophobic than other polymers used as adhesives. However, it must be considered that they are not completely resistant to water absorption [Khalilullah et al., 2017]. After the curing process of the adhesive, water can be absorbed by the adhesive as free water or bound water. Free water only fills the micro cavities in the polymeric chain of the adhesive, as bound water forms hydrogen bonds with the chain, which can cause chemical changes in the material [Barbosa et al., 2015, Viana et al., 2017b, Borges et al., 2021b]. The diffusion of water into a polymeric material is usually described through the variation of mass as a function of time. There is no universal law to describe this water uptake behavior, however, in most cases, the Fick's law is used with good approximation [Pethrick, 2015, Crank, 1979, Malpot et al., 2015, Mohd Ishak et al., 2000, Boubakri et al., 2010]. The Fick's law of diffusion is defined as a function of two variables: water uptake at saturation

(or infinite water uptake), M_∞, which is the point at which even immersed in water the mass of the sample will stop increasing since the material can not absorb more water, and the coefficient of diffusion, D, which translates the diffusion rate.

Dai et al. [Dai et al., 2006] investigated the ingress of deionized water, NaCl and HNO_3 on filled silicone rubber using temperatures between 20 and 60 °C. It was concluded that the water uptake of these silicones can be defined by the Fick's law of diffusion and that the coefficient of diffusion increases with increasing temperature, as stated above, while the infinite mass uptake is relatively insensitive to the change. Khalilullah et al. [Khalilullah et al., 2017] studied the moisture absorption of silicone/phosphor composites at different temperatures, between 30 and 80 °C and different relative humidities, between 30% and 80%, and also concluded that the material follows a Fickian model, adding that the diffusivity follows the Arrhenius law of difusion, increasing with temperature and relative humidity.

The Fick's law of diffusion is not the only one used to describe the behavior of the ingress of water in silicones. Lutz et al. [Lutz et al., 2012] studied the water diffusion in high temperature vulcanized silicone rubber (HTV-SR) and found that the behavior followed a Langmuir model. Similar findings were reported by Fang et al. [Fang et al., 2007].

Generally, adhesives exposed to humid environments experience a decrease in their mechanical properties, such as strength, stiffness and toughness. The decrease in strength is usually paired with an increase in ductility and, consequently, strain to failure and creep strain [Viana et al., 2017a, Sugiman et al., 2013, Hua et al., 2006, Ashofteh and Khoramishad, 2019]. This behavior is particularly pronounced at higher temperatures, due to the relaxation of the polymeric chain and to the ratio between bound and free water, which increases with temperature [Zhou and Lucas, 1999]. However, for silicones that is not the case. Fan et al. [Fan et al., 2019] studied the effect of moisture on the mechanical properties of phosphor/silicone composites, through the exposure of different samples to a controlled temperature of 55 °C and 85% of relative humidity (RH). The tensile strength and Young's modulus of materials with 0% and 10% of phosphor over an aging time of 42 days were studied. Over the aging time, the specimens were periodically withdrawn and tested. For all the samples analyzed, the pure silicone, with 0% of phosphor, was stronger and more flexible. However, both materials increased in strength and stiffness over the aging period. It was observed that the increase in strength of the pure silicone is higher than that of phosphor/silicone composites. This was also related to the hydrolisis of phosphor particles, which increases their surface roughness, promoting an uneven contact between the particles and silicone that culminates in gaps between them and decreases the rate of tensile strength increase. Regarding the Young's modulus, it was seen that

the increase for the composite is more pronounced than for pure silicone. This was attributed to the hydrolysis of the phosphor particles, which accelerated the stiffening of the material. Ali and Hackman [Ali and Hackam, 2008] studied the loss of hydrophobicity of high temperature vulcanized (HTV) silicone rubber using the contact angle between saline water and silicone, and concluded that, during immersion, this property decreases sharply, to 15% of its initial value, after 3000h of immersion at 98 °C.

Most studies conducted on this topic regard the effect of water contamination, however, it must be noted that, what is said about water diffusion into the material can be extrapolated to other contaminants, such as surfactants, remembering that this will occur with different laws of diffusion and different chemical effects on the structure of the material.

As two substrates are bonded using an adhesive, there is a formation of a zone called interphase. This region is different from the adhesive and substrate, both morphologically and chemically [Da Silva et al., 2018, Barthés-Labrousse, 2012]. The interphase is a transitional region with gradients of glass transition temperature, crosslinking and residual stresses, presenting a layered structure [Crompton, 1989], which makes it a complex zone, with heterogeneous morphology. The properties of the adhesive joint are dependent on the properties of the adhesive, the substrate and the interphase [Barthés-Labrousse, 2012].

If there is contamination at the surface of the substrates prior to bonding, it can either be absorbed by the substrate, by the adhesive (pior to curing or during the curing process), or remain at the adhesive/substrate interface. The second situation is the most concerning one, since the contaminant may act as a physical separation between the adhesive and substrate, constraining the inter-molecular interactions between them and creating weak bonds or, in the worst scenario, debonding [Borges et al., 2021b, Jeenjitkaew et al., 2010, Brotherhood et al., 2002, Holtmannspötter et al., 2010]. To avoid this, the adhesive must have the capacity of absorbing some of the contaminant present at the substrate surface. However, this absorption, specially before the curing process is complete, may have severe consequences to in the final adhesive properties, particularly at the interphase. The effect of contamination on adhesives is a highly complex topic, since it depends on the contaminant, adhesive and interactions between them. In this study, a silicone adhesive and water and surfactant contamination are analyzed. However, to the authors best knowledge, there is not a significant range of research performed on silicone adhesives, and the work developed on surfact contamination, although it is more extensive, it is also limited. Therefore, for this literature review, the scope was increased to more materials.

Debski et al. [Debski et al., 1986] studied the effect of mineral oil, added pre-mixing to epoxy adhesives, on the glass transition temperature, T_g of the materials. It was concluded that the cross-linking kinetics changes with the addition of contaminant, since for the

same cross-linking time and temperature, the higher the amount of oil mixed, the lower the T_g. Hong et al. [Hong et al., 1996] analyzed the effect of oil on the curing of an epoxy adhesive through differential scanning calorimetry (DSC) and determined that, with the increase of oil content, there is a decrease in the cure exotherm, which indicates changes in the chemical reaction of the curing. Akiyama et al. [Akiyama et al., 2020] studied the influence of surface contamination on joints with aluminum substrates and acrylic and epoxy adhesives. Different contaminants were used, among which four surfactants: stearic acid, oleic acid, sodium dodecyl sulfate (SDS), and dodecyl trimethyl ammonium chloride (DTAC). The adhesion strength was shown to decrease with surfactant contamination and two possible motives were pointed out, the first was that the surface energy of the surface was significantly affected by the presence of contaminant lowering the wettability of the substrate and the second is that the surfactants have low diffusivity into the adhesive, remaining at the interface. However, this hypotesis were not further analyzed its effects on the adhesive are not known.

As said, most projects developed regarding the effect of contamination on adhesive joints concern epoxy adhesives. Therefore, it is important to wide the scope of research and understand the effect on silicone adhesives.

In this work, the effect of water and surfactant contamination prior to curing was analyzed by adding 2, 5 or 10% of the contaminant to the uncured adhesive and the effect after curing is studied by immersing the neat silicone adhesive in the contaminant at 70, 90 and 130 °C for water and 70 °C for surfactant. These three temperatures were chosen because they represent the higher temperatures of interest from the manufacturing, packaging and service life of the final component and these phenomena are enhanced by increasing temperature. For the surfactant only the lower temperature was used since the fluid is not stable at the higher temperatures. The mechanical properties were evaluated through bulk tensile tests, chemical profiles were analyzed using Fourier-transform infrared spectroscopy (FTIR), for comparison purposes, FTIR of the contaminant profile was also carried out. The morphology of the materials was detailed with scanning electron microscopy (SEM) with energy dispersive spectroscopy (EDS). A dynamic mechanical analysis (DMA) was also carried out to understand if there is a transition temperature in the temperature range analyzed.

A.2 Experimental details

A.2.1 Materials

The adhesive used in this study is a two-part silicone adhesive. The adhesive/catalyst ratio used was 1:1 and the mixture was performed using a speed mixer and cured at 120

°C for 25 minutes.

The water contamination was performed using destilled water.

The surfactant contamination was performed using Cocosalkylaminethoxylate manufactured by SysKem Chemie GmbH (Wuppertal, Germany). This surfactant is used to clean aluminum surfaces from the oils needed during the manufacturing process. In the following sections, the group of surfactant and water are going to be referred to, generally, as contaminant.

A.2.2 Specimen manufacturing

The specimens for the different studies were cut from adhesive plates. For this, first, the adhesive and hardener must be mixed. The mass required of each part was measured using a microbalance with 0.1 mg of accuracy (KernToledo, Balingen, Germany) and then mixed using a Hauschild SpeedMixer® DAC 150.1 FVZ-K (Hauschild GmbH & Co.KG, Hamm, Germany) at 2000 rpm for 15 seconds. For the plates manufactured to study the effect of surfactant and water after the curing of the adhesive, after these steps the adhesive was introduced in the mold, as described bellow. However, when the effect prior to curing was the object of study the process is more complex. The mass of contaminant desired is introduced in the mixture (since the mass of the uncured adhesive plate is 50 g, for the 2% of contaminant 1 g is added, 2.5 g for 5% and 5 g for 10%) and is mixed for an additional 5 seconds at the same speed.

The adhesive plate was manufactured following the French NF T 76-142 standard [NF, 1988]. The process consists on introducing the adhesive on a mold lined with a silicone frame with the thickness desired for the plate. The frame ensures hydro-static pressure and this process decreases the amount of defects found in the final specimen. Afterwards, the mold is placed on a hot plates press following the curing cycle required to cure the adhesive.

Plates with thicknesses of 2 mm and 1 mm were produced. The 2 mm thick plates were utilized for the DMA of the neat adhesive and bulk tensile tests, FTIR and SEM analysis where contaminant was added prior to the adhesive curing. The 1 mm thick plates were used for the gravimetric analysis and bulk tensile tests performed after water immersion. The main purpose of the 1 mm thick specimens for these two procedures is the reduction of the immersion temperature required to fully saturate the specimen.

Dynamic mechanical analysis (DMA)

DMA was conducted with the neat adhesive after manufacturing, i.e., without the introduction of water or contamination either prior to curing or after curing. For this, 2 mm thick specimens with 6 by 20 mm were prepared from the plates previously manufactured.

Gravimetric study

In the plates used for the gravimetric study, the thickness must be significantly smaller than the other dimensions so that is represents the preferential water uptake direction. The specimens used were square plates with a side length of 30 mm, since in previous work by the same authors [Borges et al., 2021a] it has been determined that this size gives the same diffusion curve as the plates with side length of 60 mm that follow the ISO 294-3 standard [ISO,] with a smaller material waste and higher storage capability when immersed in water.

Bulk tensile tests

Bulk tensile test specimens were cut using a punch-matrix system from the previously manufactured adhesive plates. The specimens were reduced scale, since they have been known to accurately represent the tensile behavior of polymeric materials [Borges et al., 2021a]. These reduced scale specimens are easier to store in water and decrease the overall extension imposed to the testing machine, since this silicone is a very resilient material. The specimens were dried in silica at the controlled temperature, and then tested for the dried condition. Afterwards, they were immersed in water until saturation was achieved, and tested for the aged condition. Finally, they were re-dried and tested for the dried after aging condition.

Fourier-transform infrared spectroscopy (FTIR) and scanning electron microscopy (SEM)

FTIR analysis were conducted using the specimens tested in the bulk tensile tests for the correspondent condition, cutting into the specimen to remove the superficial layer of material and, therefore, surface contamination. For the SEM analysis, the fracture surfaces of the specimens after the bulk tensile test were analyzed.

A.2.3 Testing procedures

Dynamic mechanical analysis (DMA)

The DMA was conducted in a 242 E Artemis (NETZSCH-Gerätebau GmbH) machine scanning a range of temperatures from -110 °C to 130 °C at a rate of 3 °C/min. The material was analyzed for a frequency of 1 and 10 Hz. Three specimens were tested.

Gravimetric study

The gravimetric test has the main purpose of understanding how the contaminant diffuses into the specimen, after adhesive curing.

For the gravimetric analysis, the specimens were, first, dried in silica at 70 °C for two weeks. Afterwards, their mass was measured and this is considered the initial mass, m_0. Afterwards, the specimens were immersed in contaminant at the respective study temperature (70, 90 or 130 °C for water and 70 ° for the surfactant). At this point, it is crucial to ensure that the plates are fully covered in the immersion fluid and not in contact with the container or other plates, so that the surface is completely in contact with the surrounding contaminant and the absorption area is not compromised. To ensure the specimens remained under the contaminant, they were attached to 10x10x10 mm^3 stainless steel blocks. The temperature of immersion is controlled by placing the fluid container in a climatic chamber (Memmert GmbH, Büchenbach, Germany).

The mass of the specimens was measured periodically until a constant mass value was reached. When that happened, it was considered that the specimen was saturated, i.e., it reaches its maximum contaminant absorption level. When the mass of the specimens was going to be measured, the surface was cleaned with a paper towel just to remove excess fluid at the surface, not intending to remove fluid that may be free in the interior of the material. The mass measurements were conducted using a microbalance with 0.1 mg of accuracy (KernToledo, Balingen, Germany).

The contaminant uptake of the specimens for each time step was determined from:

$$M_t = \frac{m_t - m_0}{m_0} \cdot 100(\%) \tag{1}$$

where m_t is the mass at the time considered.

For the higher temperature, 130 °C it must be noted that, to avoid pressurization of the container, the lid was kept open and the water was added periodically. For each condition, at least four specimens were tested.

Bulk tensile tests

Bulk tensile tests were performed using a universal testing machine Instron® 3367, which has a load capacity of 30 kN, at a constant rate of 5 mm/min. Since the specimens are very reduced and thin, the addition of an extensometer would interfere with the results of the test. Additionally, the use of Digital Image Correlation (DIC) measurement required the painting of the specimen prior to the test which, since it is a time-consuming process, in the dried conditions could include ambient water in the specimen and, in the aged condition, could remove water from the specimen. Therefore, the displacement

obtained from the grips of the machine was used, after tunnning with controlled specimens through DIC to ensure a correct measurement of displacement. For each condition, at least three specimens were tested.

Fourier-transform infrared spectroscopy (FTIR)

FTIR analysis was conducted using a PerkinElmer Spectrum Two machine (Waltham, MA, USA). Wave lengths of 4000–500 cm^{-1} were scanned with intervals of 0.2 cm^{-1} and the tests were carried out in a machine with a KBr window and a $LiTaO_3$ detector (15,700–370 cm^{-1}). The spectra was recorded in attenuated total reflectance (ATR), which establishes spectra equivalent to transmittance. The specimens were removed from water and kept at room conditions for about 30 minutes prior to the performance of the FTIR analysis.

Scanning electron microscopy (SEM)

SEM analysis was conducted on two different microscopes: JEOL JSM 6301F/Oxford INCA Energy 350/Gatan Alto 2500 (Tokyo, Japan) and FEI Quanta 400FEG ESEM / EDAX Genesis X4M (Hillsboro, Oregon, United States). The analysis were carried out at CEMUP (University of Porto, Portugal). The samples were coated with an Au/Pd thin film, by sputtering, for 120 s with a current of 15 mA using the SPI Module Sputter Coater. The specimens were removed from water and kept at room conditions for about 12 hours prior to the performance of the SEM analysis, during this time, the specimens were cleaned using ultrasounds.

A.3 Experimental results

In this section, the different experimental results for each test are presented and some comments are made about the individual conclusions drawn from them. However, the complete analysis must be done is for each condition, throughout the scope of tests performed, which is going to be done in the *Discussion* section.

A.3.1 Dynamic mechanical analysis (DMA)

The DMA results are shown through a representative curve in Figure 1. The two curves represented refer to the same specimen (out of the three tested) for the two frequencies tested, 1 and 10 Hz. The transition temperature obtained, determined from the inflection points of the curves recorde, is at -56.3±0.9 °C, considering both the results for 1 and 10 Hz. This is a value of glass transition temperature (T_g), commonly found for silicones. It

can be concluded that on the range of temperatures under analysis (70 to 130 °C) there is no preponderant transition temperature.

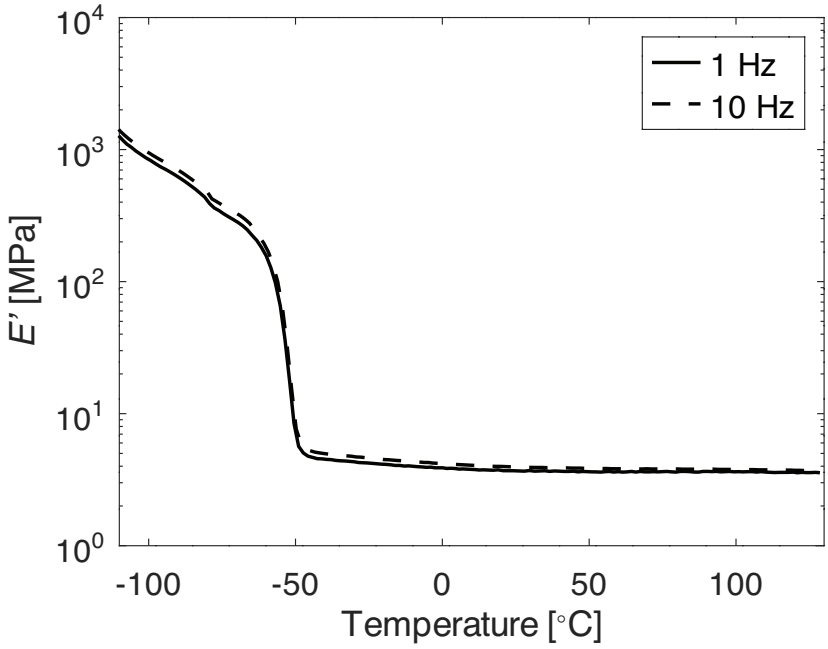

Figure 1: Representative curves obtained for the DMA for the same specimen, registered for 1 Hz and 10 Hz.

A.3.2 Gravimetric study

Effect of water after curing

The gravimetric study for the silicone immersed in water at 70, 90 and 130 °C can be seen in Figure 2.

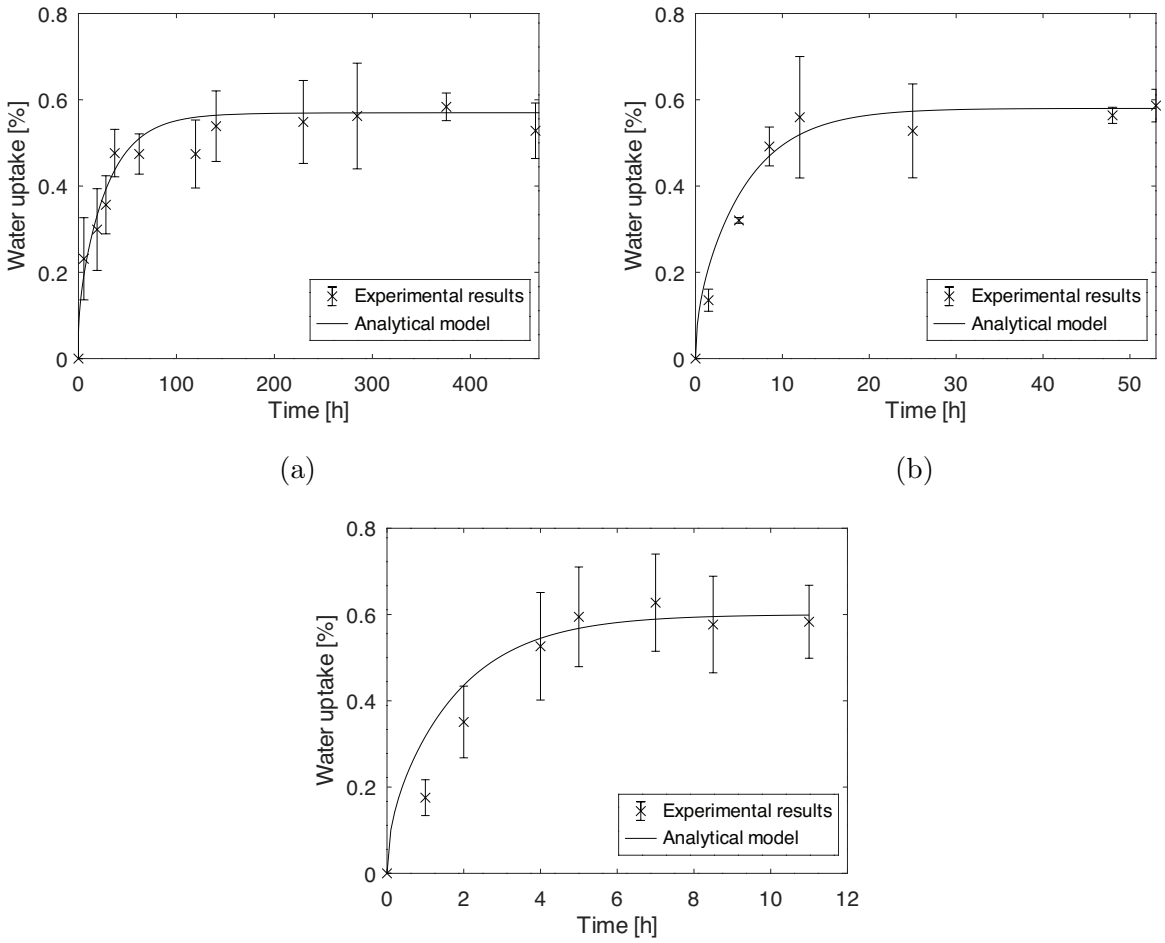

Figure 2: Water uptake as a function of time and respective analytical model following Fick's law of diffusion, for 70 °C (a), 90 °C (b) and 130 °C (c).

The analytical model represented is obtained from the second Fick's law of diffusion:

$$M_t = \left[1 - \frac{8}{\pi^2} \sum_{n=0}^{\infty} \frac{1}{(2n+1)^2} \, exp\left(\frac{-D(2n+1)^2\pi^2 t}{4h^2}\right)\right] M_\infty \tag{2}$$

where t is the time (starting from immersion) and h is the thickness of the specimen. The values determined for each temperature are given in Table 1.

Table 1: Parameters of the Fick's law of diffusion as a function of temperature.

Temperature [°C]	D [m^2/s]	M_∞ [%]
70	$9.1 \cdot 10^{-13}$	0.57
90	$4.8 \cdot 10^{-12}$	0.58
130	$9.8 \cdot 10^{-12}$	0.60

As temperature increases, there is also a slight increase of the maximum water content the silicone can absorb, due to the relaxation of the polymeric chain of the material.

Additionally, it is clear that, as the immersion temperature increases, the coefficient of diffusion also increases. Usually, this increase follows an Arrhenius relation, which is given by:

$$D = D_0 \, exp\left(\frac{-E_A}{RT}\right) \tag{3}$$

where D_0 is the permeability index, E_A is the activation energy for diffusion, R is the universal gas constant and T is temperature. Rearranging the equation:

$$\ln(D) = -\frac{E_A}{R} D_0 \frac{1}{T} \tag{4}$$

Which means that the law that describes D as a function of temperature is a line in a graph where the xx axis corresponds to the inverse of temperature and the yy axis corresponds to $\ln(D)$, Figure 3.

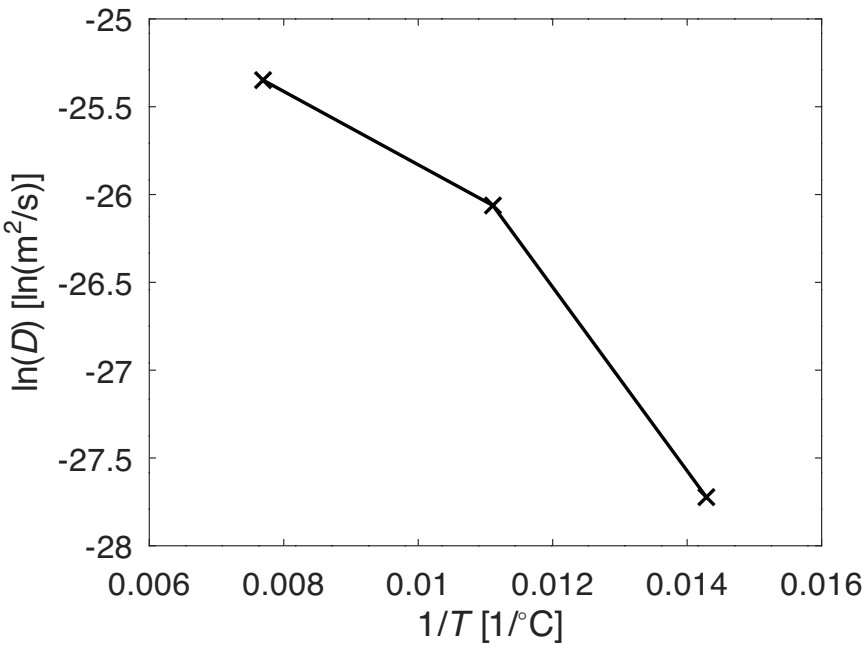

Figure 3: Relation between D and immersion temperature..

Effect of surfactant after curing

The gravimetric study for the silicone immersed in surfactant at 70 °C can be seen in Figure 4.

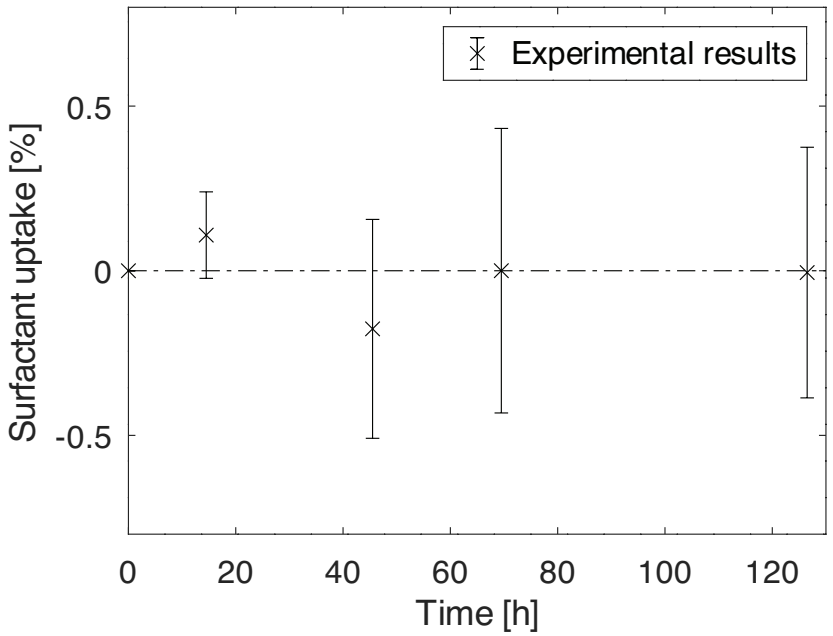

Figure 4: Surfactant uptake as a function of time, for 70 °C.

The average mass of the specimen is approximately the same along the time period analyzed. However, there is a high standard deviation, which is related to the contaminant that remained on the surface of the specimen after cleaning lightly with a paper towel. Since the results show that, on average, there is no surfactant ingress on the material, the mechanical and chemical analysis of the silicone after immersion in contaminant are not going to be carried out.

A.3.3 Bulk tensile tests

Bulk tensile test results are going to be divided according to what they aim to analyze. The effect of water prior to curing was evaluated by mixing water into the adhesive before curing, the same is valid for the surfactant. The effect of water after curing was evaluated from the specimens immersed in water at 70, 90 and 130 °C.

Effect of water after curing

The representative curves for the three humidity conditions tested (dried, aged and dried after aging) at the three different immersion temperatures (70, 90 and 130 °C) can be observed in Figure 5.

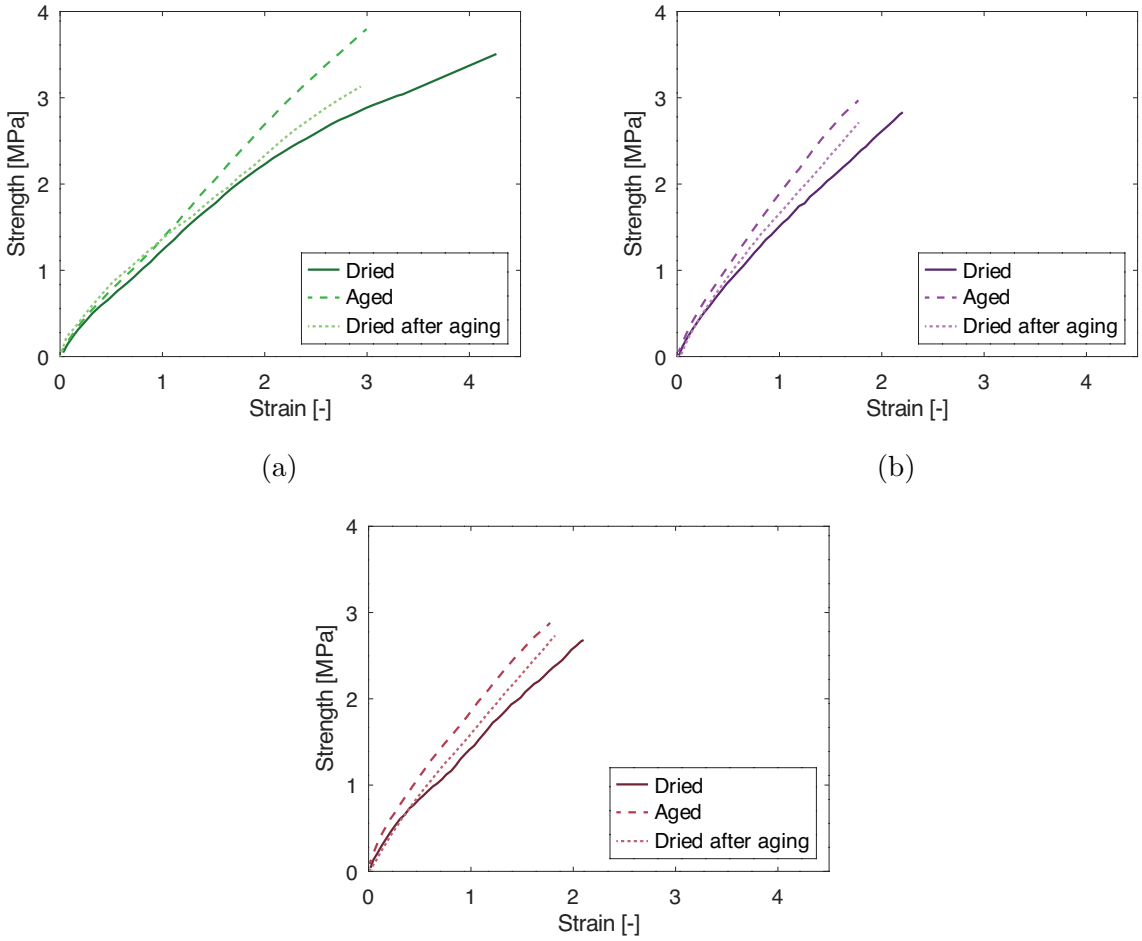

Figure 5: Representative stress-strain curves after the specimens are subjected to drying, aging and drying after aging at 70 °C (a), 90 °C (b) and 130 °C (c).

From the stress-strain curves represented it can be concluded that the stiffness and strength is higher for the aged condition of all the temperatures, which corroborates what Fan et al. [Fan et al., 2019] found for pure silicone and silicone with the addition of phosphorous. Comparing the strength of the tree conditions at each temperature tested, Figure 6, it is possible to infer that strength increases when the material is immersed in water (from the dried to the aged condition), being restored when the specimen is dried. This suggests that, although water in the polymeric chain helps stiffen it, this change is reversible. The differences between conditions are clearer at 70 °C, which suggests that the material is also subjected to temperature damage.

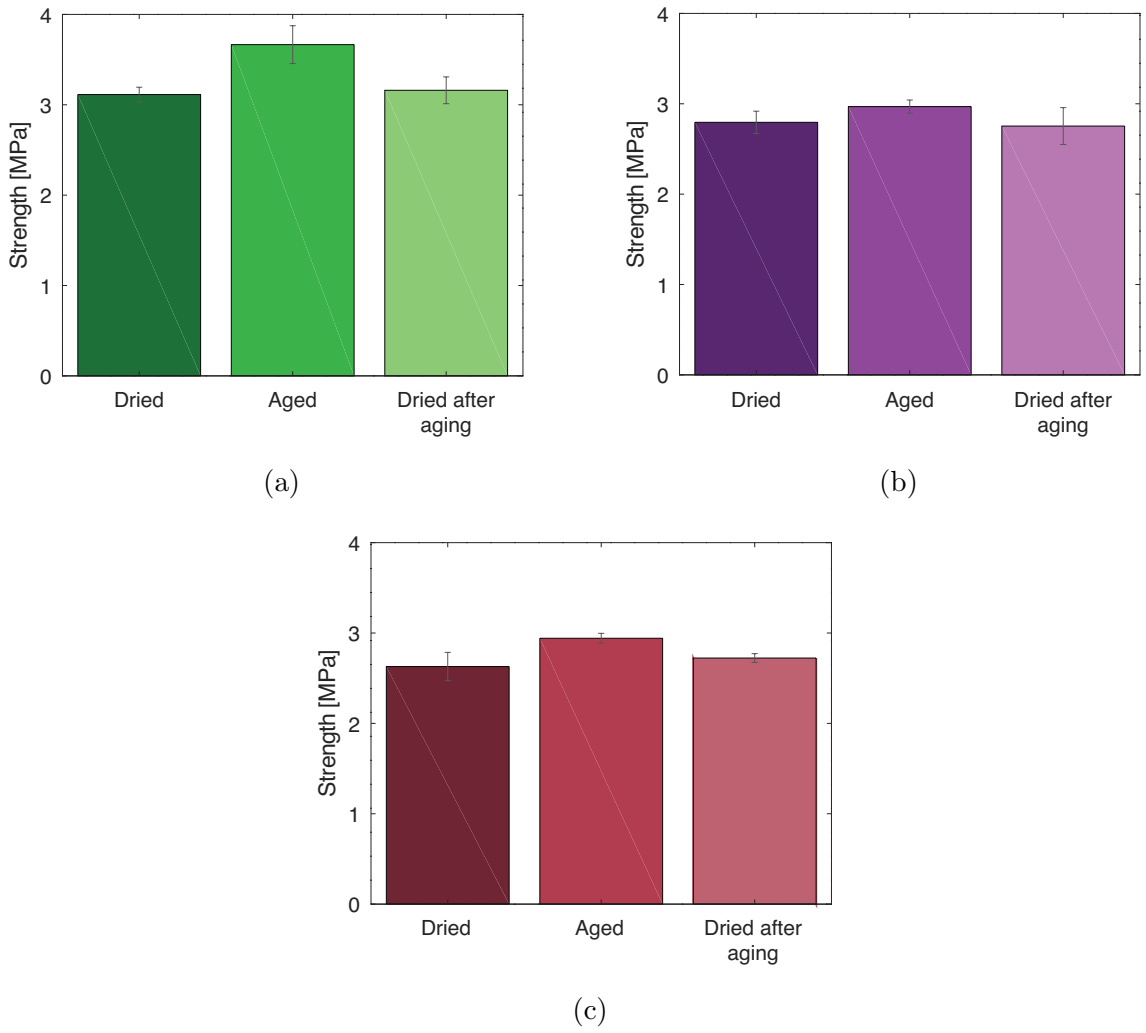

Figure 6: Strength of the specimens dried, aged and dried after aging for each temperature: 70 °C (a), 90 °C (b) and 130 °C (c).

Comparing the strength for the three different temperatures for each condition tested, Figure 7, it becomes clear that, for the dried condition strength decreases with increasing temperature and, for the other conditions it decreases from 70 °C to the other temperatures, being similar between them. It must be recalled that the tests were not performed at the temperatures indicated, but at room temperature after drying, aging and redrying at those temperatures. Therefore, it can be considered that the damage introduced to the material increases as the temperature to which it was subjected also increases.

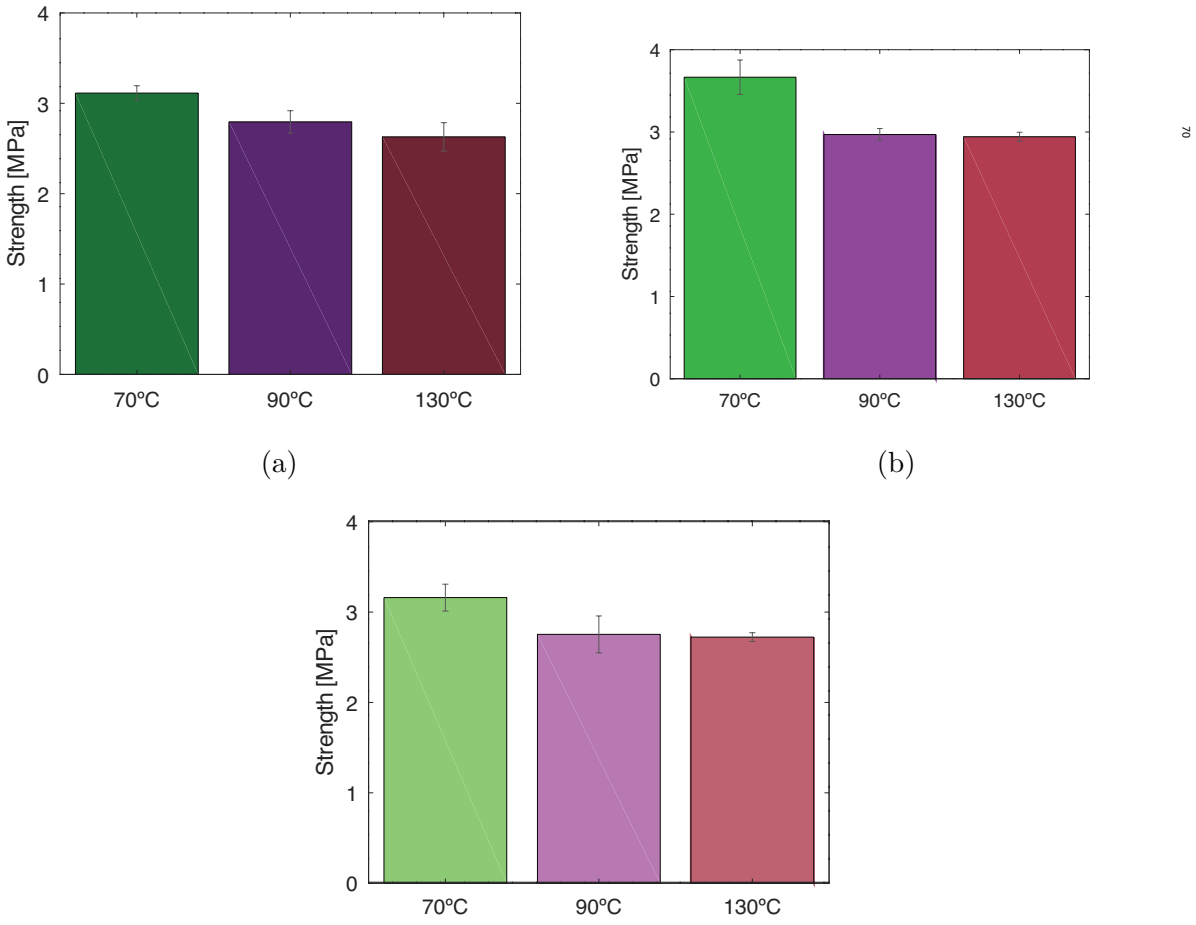

Figure 7: Strength of the specimens at 70 °C, 90 °C and 130 °C for each condition: dried (a), aged (b) and dried after aging (c).

Effect of water prior to curing

Representative stress-strain curves of the material as a function of the amount of water added prior to curing, as well as the strength for the different conditions analyzed can be seen in Figures 8a and 8b, respectively.

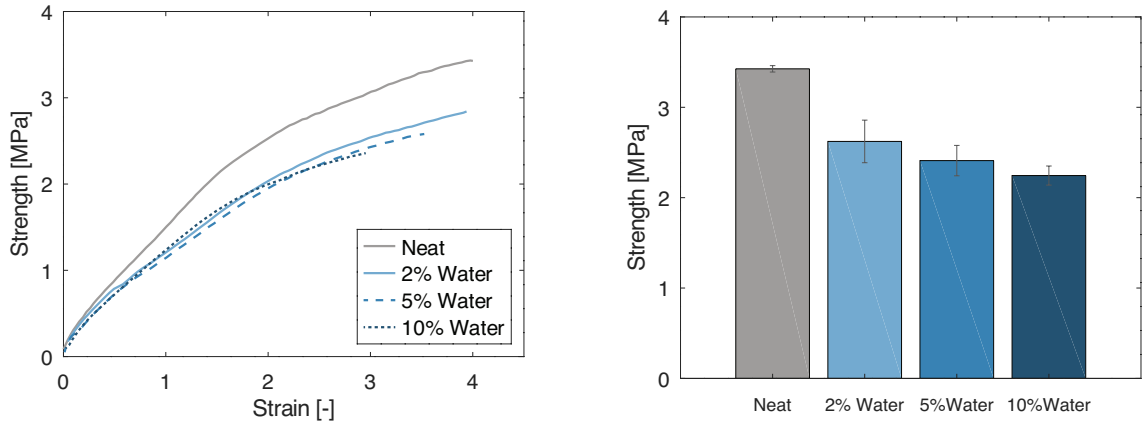

(a) (b)

Figure 8: Representative stress-strain curves for the adhesive with addition of water prior to curing (a) and strength for the different amounts of water added (b).

The strength, as shown, decreases as the water content added to the mixture prior to curing increases. However, the stiffness is lower than for the neat adhesive, but very similar between the specimens with water. Therefore, it may lead to the conclusion that, although there is degradation of the mechanical properties due to the inclusion of water, it does not change the properties of the material matrix itself, acting more as an introduction of defects. The strength and stiffness decrease as water is included but between the conditions with water, strength appears to decrease only due to an increase in the amount of defects added.

Effect of surfactant prior to curing

Representative stress-strain curves of the adhesive with surfactant added prior to curing and strength for the different amounts of surfactant are shown in Figures 9a and 9b, respectively.

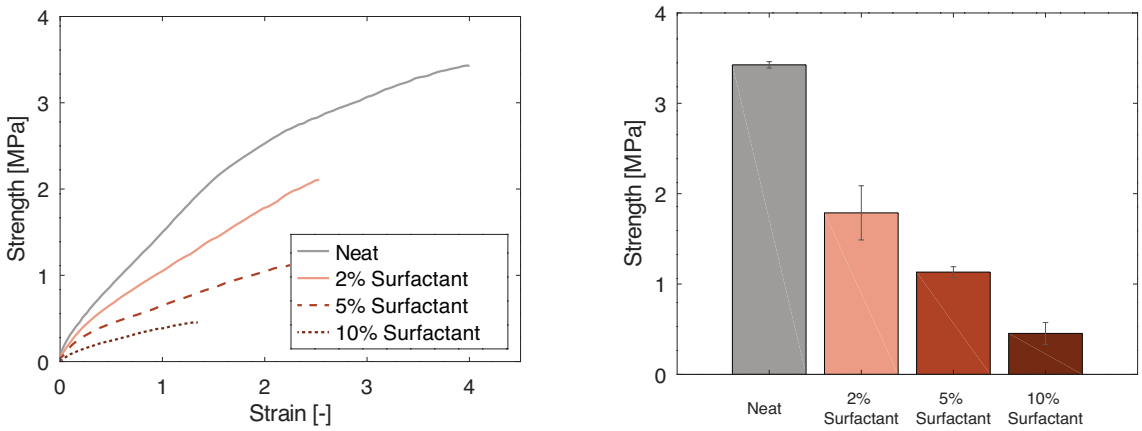

(a) (b)

Figure 9: Representative stress-strain curves for the adhesive with addition of surfactant prior to curing (a) and strength for the different amounts of surfactant added (b).

Unlike what was observed for the addition of water, with the addition of surfactant the decrease in strength of the specimens is accompanied by a decrease in stiffness, which leads one to believe that there is a morphological or chemical variation of the material, both of which are going to be analyzed through SEM and FTIR.

A.3.4 Fourier-transform infrared spectroscopy (FTIR)

Effect of water after curing

The effect of water after curing of the adhesive was analyzed form the FTIR profile of specimens dried after aging at the three different immersion temperatures analyzed, Figure 10.

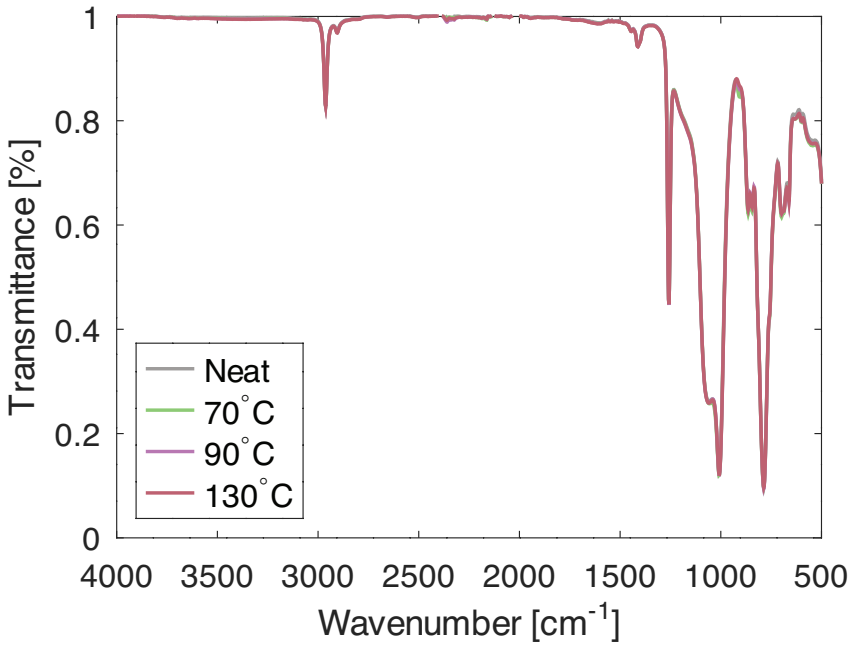

Figure 10: Representative curves obtained for the FTIR analysis of the specimens immersed in water, dried after aging as a function of immersion temperature.

From the curves presented, it is clear that, for all immersion temperatures, there is no irreversible chemical damage introduced to the material, since the profiles after aging perfectly overlap with the profile of the neat adhesive. Which means that, after water immersion at the three temperatures, the material retains its initial chemical structure.

Effect of water prior to curing

The chemical profiles, obtained from FTIR, of the material with water added in different quantities are presented in Figure 11 and compared to the neat adhesive.

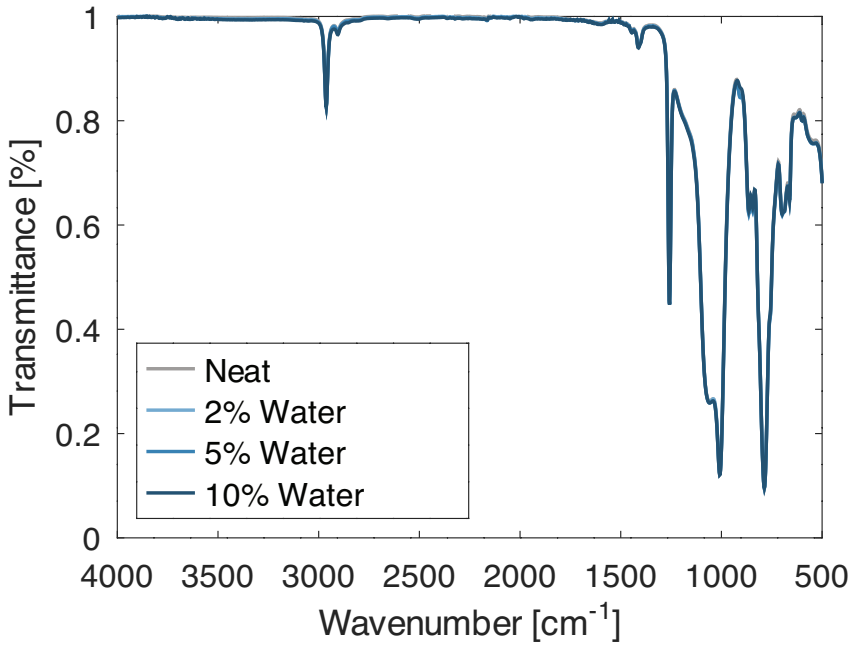

Figure 11: Representative curves obtained for the FTIR analysis as a function of water added prior to curing.

It can be concluded that the chemical profile of the material does not change when water is introduced prior to curing, which means that, as predicted, water does not form chemical bonds with the adhesive and it does not appear to influence the curing of the adhesive.

Effect of surfactant prior to curing

The FTIR profiles of the neat adhesive and adhesive with different quantities of surfactant added can be seen in Figure 12.

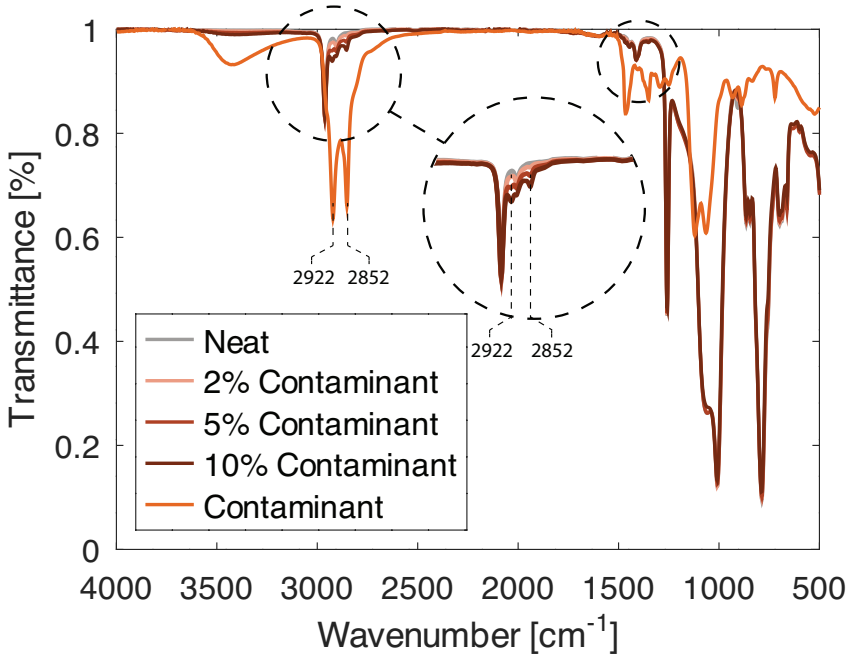

Figure 12: Representative curves obtained for the FTIR analysis as a function of surfactant added prior to curing.

The profile of the contaminant exhibits two peaks at around 2922 cm^{-1} and 2852 cm^{-1}. And, as the amount of contaminant added to the adhesive increases, small peaks appear in the profile of the adhesive at the same wavenumbers. This region is associated to the stretching of the C-H bond, which means the amplitude of vibration of these bonds increases with increasing surfactant contamination. This conclusion is supported by the intensification of the peak around 1450 cm^{-1}, related to the bending of the same bond, which means the bond angles are also changing. The peak associated with stretching exhibits a more clear change since differences in stretching are easier to detect than differences in angle. Therefore, it may be concluded that there are modifications in the structure of the adhesive due to the addition of contaminant. The fingerprint region, from about 900 to 1300 cm^{-1} remains unchanged.

A.3.5 Scanning electron microscopy (SEM)

The SEM images of the neat adhesive, without the addition of water or surfactant, are shown in Figure 13.

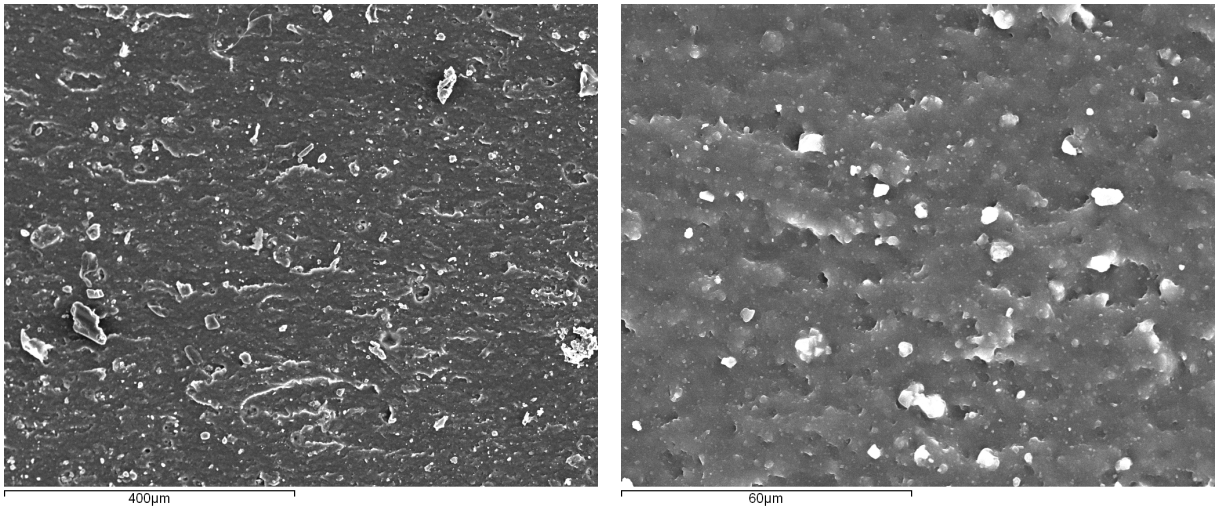

(a) (b)

Figure 13: SEM image of the neat adhesive with lower (a) and higher (b) magnification.

This surface is typical of silicone materials, with the note that the lighter regions have higher contents of phosphorus, which indicates the material under analysis is a silicone-phosphorus composite, such as the one analyzed by Fan et al. [Fan et al., 2019].

Effect of water after curing

The fracture surfaces of the specimens that were immersed in water after the curing of the neat adhesive are shown in Figure 14.

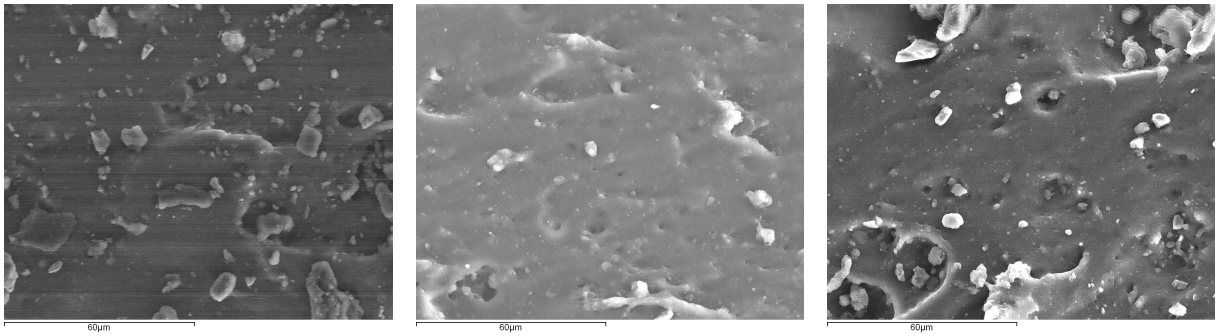

(a) (b) (c)

Figure 14: SEM image of the adhesive after water immersion at 70 °C (a), 90 °C (b) and 130 °C (c).

The fracture surfaces of the material appear to be increasingly smoother from neat adhesive to the adhesive immersed at 70 °C, 90 °C and finally 130 °C. However, the morphology of the material does not change abruptly from the neat condition, prior to water immersion, to the aged specimens, with the specimen that was saturated at 70 °C

being more similar to the neat adhesive than to the other immersion temperatures. This shows that, probably, the main differences denoted for the failure surface are not related to the water ingress but to the temperature at which it happens.

Effect of water prior to curing

The fracture surfaces of the specimens to which water was added prior to curing are shown in Figure 15. It must be noted that, when different machines were used to obtain the SEM images, the magnification were adapted to the focal length so that the images between machines are easily comparable.

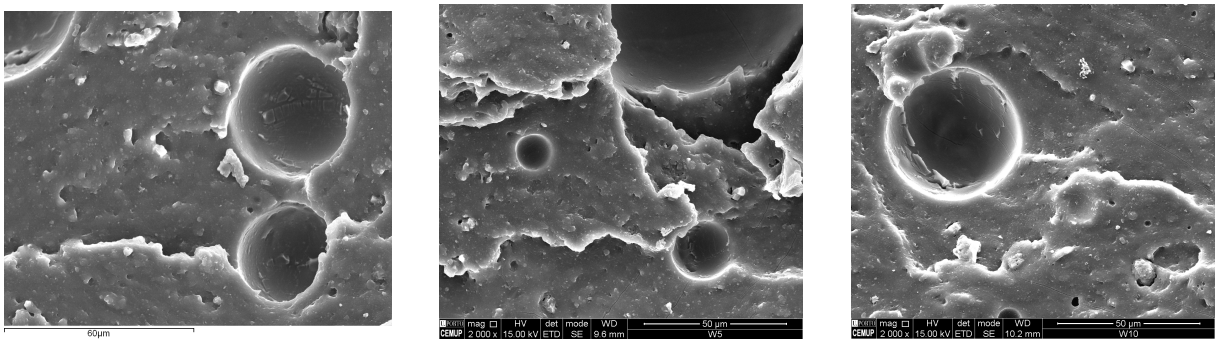

(a) (b) (c)

Figure 15: SEM image of the adhesive with the addition of 2% (a), 5% (b) and 10% (c) of water prior to curing.

With the addition of water to the adhesive prior to curing, the matrix of the adhesive is very similar to the neat adhesive and the same for the three amounts of water included. However, as water is added, it goes to specific locations in the adhesive and, as the temperature is raised to 120 °C to cure the adhesive, the water evaporates and forms voids. These voids have a pricking effect on the fracture of the specimen, evidenced by the fracture surfaces passing through them.

Effect of surfactant prior to curing

The fracture surfaces of the specimens to which surfactant was added prior to curing are shown in Figure 16.

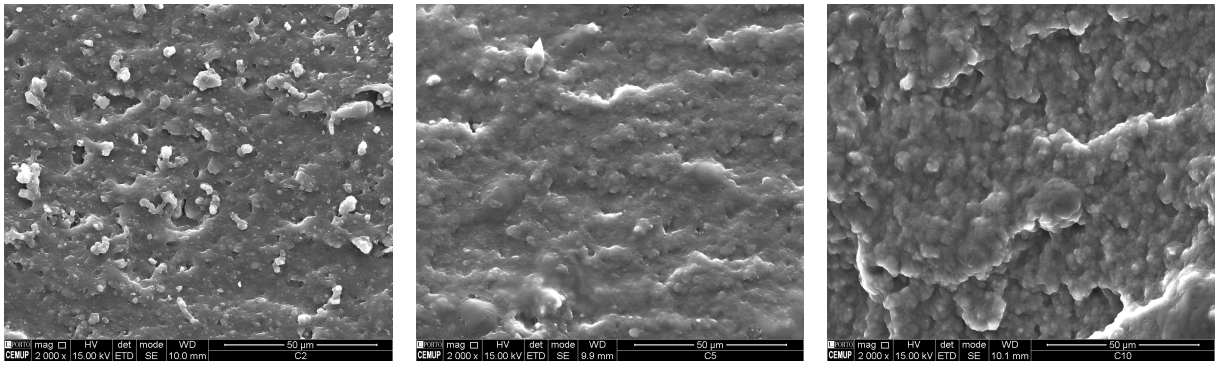

(a) (b) (c)

Figure 16: SEM image of the adhesive with the addition of 2% (a), 5% (b) and 10% (c) of surfactant prior to curing.

It is clear that the morphology of the adhesive changes from the neat condition to the contaminated ones, with a change intensification increasing surfactant content, which is also an indicator of chemical changes in the structure of the adhesive.

A.4 Discussion

A.4.1 Effect of water after curing

The gravimetric studies performed, Figure 2, exhibit that the coefficient of diffusion increases with increasing temperature, which was attributed to the relaxation of the polymeric chain at higher temperatures, and also explains the increase in maximum water uptake. However, from the FTIR analysis, Figure 10 it was seen that there is no change in the chemical profile of the adhesive, particularly in the region associated with OH bonds, indicating that water was absorbed as free water, and did not establish chemical bonds with the adhesive. From the bulk tensile tests, Figures 5 and 6, it was observed that strength increased, for all temperatures analyzed, as the specimens were aged. However, the increase was reversed as the specimens were redried.

From the data collected, it can be concluded that the changes introduced by water to the silicone adhesive are reversible, not changing the chemical profile or irreversibly damaging the material. Hoque et al. [Hoque et al., 2019] studied the water absorption and desorption of pure silicone and silicone with phosphorous and concluded that the water absorbed by the material was fully removed upon redrying.

From the SEM and EDS analysis, Figure 13, it was observed that the material in study also presents particles enriched in phosphorous, which, according to the data collected from Hoque et al. [Hoque et al., 2019], indicates that the material in study has enhanced sealing characteristics, when compared to pure silicone, having a lower maximum water

uptake. Fan et al. [Fan et al., 2019] also studied the effect of moisture on pure silicone and phosphorous/silicones composites and recorded an increase in strength and stiffness with aging, as in the present work. It was proposed that phosphorous particles interacted with water accelarating the stiffening of the material, however, water aging changed the interaction between phosphorous and silicone, exhibiting a smaller increase in strength for the mixed material, which can explain the small strength increase between the dried and aged conditions found in this work.

The SEM images of the fracture surface of the specimens tested after aging, Figure 14, appear to be smoother with increasing immersion temperature. Additionally, for all conditions tested (dried, aged and dried after aging), strength decreased with the increase of the temperature to which the material was subjected, Figure 7. Combined with the conclusion that the effect produced on the material by water is reversible, these results show that exposure to high temperatures for significant periods of time damages the mechanical properties of the silicone.

A.4.2 Effect of water prior to curing

The introduction of water to the adhesive prior to curing of the adhesive decreases its strength and stiffness, Figure 8a. However, the stiffness appears to be fairly insensitive to the amount of water added and the decrease in strength between the specimens with water addition is not very pronounced, although there is a clear decreasing trend with increasing water content mixed.

From the SEM analysis, Figure 15, it was shown that when water is added to the silicone adhesive prior to curing, it segregates in preferential locations, evaporating as the adhesive temperature is increased and forming voids. However, it does not appear to establish chemical interactions or damage the surrounding adhesive. The analysis of the FTIR profile of the silicone with different amounts of water added, also compared against the profile of the neat adhesive, Figure 11 showed that the water inclusion did not change the molecular structure of the material, which corroborates the conclusion that there is no expressive interaction between the silicone matrix and segregated water during the curing and cross-linking of the adhesive. This explains the results found for the bulk tensile tests, since it shows that the increase in the amount of water added to the adhesive only contributes to a higher unoccupied volume of adhesive, with the voids acting as a prick, causing the adhesive to fail progressively earlier with increasing water content, although the stiffness is similar.

Although the water prior to curing does not have a severe impact on the mechanical properties of the adhesive, the appearance of voids during curing and its presence during the service life of an adhesive bond, could lead to a higher water uptake through the pores

of the material or even positioning of the voids close to the interface, enhancing the water absorbed between adhesive and substrate and causing premature failure of the joint.

A.4.3 Effect of surfactant prior to curing

The introduction of surfactant prior to the curing of the adhesive showed a severe impact on the mechanical properties of the silicone, translated both in a decrease of stiffness and strength, Figure 9a. From the FTIR profile, Figure 12, it was seen that the contaminant inclusion contributes to an increase of the amplitude of vibration of the C-H bond, also detecting changes in the bond angle. This implies that, as the surfactant is added to the adhesive, its chemical instability increases, changing the cross-linking reactions and resulting in weaker adhesive. If the surfactant content was progressively increased to more than 10%, it is expected that it would reach a concentration at which the silicone would not cure. From the SEM analysis, these conclusions were supported, since a change in the molecular structure of the adhesive is expected to promote a difference in the morphology of the material, exposed in Figure 16.

These findings lead to the conclusion that, if surfactant contamination is found at the substrates prior to bonding, it could not only lead to a physical separation between the adhesive and substrate, resulting in a weaker bond, but also, even if removed from the interface by adhesive absorption, lead to an interphase much weaker that the neat adhesive at the middle of the overlap. Which would prevent adhesive failure, but would contribute to a failure close to the substrate at a load level much lower that predicted from the neat adhesive properties.

A.5 Conclusions

The main conclusions drawn from this work are that:

- When water is absorbed by silicone adhesives after aging, it contributes to an increase in strength and stiffness of the material. However, these changes are reversible, not changing the chemical profile of the material;

- The increase of temperature at which the specimens are dried and aged decreases its strength and changes the morphology of the fracture surface, indicating damaging of the adhesive;

- The presence of water prior to the curing of the silicone adhesive does not cause chemical changes to the adhesive, only contributing to the appearance of voids after curing;

- The surfactant added prior to curing is absorbed by the adhesive during cross-linking, changing the chemical profile of the final adhesive, showed by the difference in the C-H bond;

- The absorption of contaminant during the curing process significantly influences the mechanical properties of the adhesive, decreasing its strength and stiffness and alters its morphology.

Acknowledgments

The author(s) disclosed receipt of the following financial support for the research, authorship, and/or publication of this article: The authors wish to acknowledge and thank the funding and support provided by Robert Bosch GmbH, Corporate Research and Advance Engineering, Renningen.

References

[Akiyama et al., 2020] Akiyama, H., Fukata, T., Sato, T., Horiuchi, S., and Sato, C. (2020). Influence of surface contaminants on the adhesion strength of structural adhesives with aluminium. *The Journal of Adhesion*, 96(15):1311–1325.

[Ali and Hackam, 2008] Ali, M. and Hackam, R. (2008). Effects of saline water and temperature on surface properties of htv silicone rubber. *IEEE Transactions on Dielectrics and Electrical Insulation*, 15(5):1368–1378.

[Ashofteh and Khoramishad, 2019] Ashofteh, R. S. and Khoramishad, H. (2019). The influence of hygrothermal ageing on creep behavior of nanocomposite adhesive joints containing multi-walled carbon nanotubes and graphene oxide nanoplatelets. *International Journal of Adhesion and Adhesives*, 94:1–12.

[Barbosa et al., 2015] Barbosa, A., Da Silva, L., and Öchsner, A. (2015). Hygrothermal aging of an adhesive reinforced with microparticles of cork. *Journal of Adhesion Science and Technology*, 29(16):1714–1732.

[Barthés-Labrousse, 2012] Barthés-Labrousse, M.-G. (2012). Mechanisms of formation of the interphase in epoxy-amine/aluminium joints. *The Journal of Adhesion*, 88(8):699–719.

[Borges et al., 2021a] Borges, C., Akhavan-Safar, A., Marques, E., Carbas, R., Ueffing, C., Weißgraeber, P., and da Silva, L. (2021a). Effect of water ingress on the mechani-

cal and chemical properties of polybutylene terephthalate reinforced with glass fibers. *Materials*, 14(5):1261.

[Borges et al., 2021b] Borges, C., Marques, E., Carbas, R., Ueffing, C., Weißgraeber, P., and Silva, L. d. (2021b). Review on the effect of moisture and contamination on the interfacial properties of adhesive joints. *Proceedings of the Institution of Mechanical Engineers, Part C: Journal of Mechanical Engineering Science*, 235(3):527–549.

[Boubakri et al., 2010] Boubakri, A., Haddar, N., Elleuch, K., and Bienvenu, Y. (2010). Impact of aging conditions on mechanical properties of thermoplastic polyurethane. *Materials & Design*, 31(9):4194–4201.

[Brotherhood et al., 2002] Brotherhood, C., Drinkwater, B., and Guild, F. (2002). The effect of compressive loading on the ultrasonic detectability of kissing bonds in adhesive joints. *Journal of Nondestructive evaluation*, 21(3):95–104.

[Crank, 1979] Crank, J. (1979). *The mathematics of diffusion*. Oxford university press.

[Crompton, 1989] Crompton, J. (1989). Interfacial properties and stability in bonded aluminium. *Journal of materials science*, 24(5):1575–1581.

[Da Silva et al., 2018] Da Silva, L. F., Öchsner, A., and Adams, R. D. (2018). *Handbook of adhesion technology*. Springer Science & Business Media.

[Dai et al., 2006] Dai, J., Yao, X., Yeh, H., and Liang, X. (2006). Moisture absorption of filled silicone rubber under electrolyte. *Journal of applied polymer science*, 99(5):2253–2257.

[Debski et al., 1986] Debski, M., Shanahan, M., and Schultz, J. (1986). Mechanisms of contaminant elimination by oil-accommodating adhesives part 1: displacement and absorption. *International Journal of Adhesion and Adhesives*, 6(3):145–149.

[Fan et al., 2019] Fan, J., Wang, Z., Zhang, X., Deng, Z., Fan, X., and Zhang, G. (2019). High moisture accelerated mechanical behavior degradation of phosphor/silicone composites used in white light-emitting diodes. *Polymers*, 11(8):1277.

[Fang et al., 2007] Fang, S., Jia, Z., Gao, H., and Guan, Z. (2007). Influence of fillers on silicone rubber for outdoor insulation. In *2007 Annual Report-Conference on Electrical Insulation and Dielectric Phenomena*, pages 300–303. IEEE.

[Holtmannspötter et al., 2010] Holtmannspötter, J., Czarnecki, J., and Gudladt, H.-J. (2010). The use of power ultrasound energy to support interface formation for structural adhesive bonding. *International journal of adhesion and adhesives*, 30(3):130–138.

[Hong et al., 1996] Hong, S., Shu, H., Lin, J., and Young, J. (1996). The effects of a slushing oil on the curing and degradation behavior of an oil-accommodating epoxy adhesive. *Die Angewandte Makromolekulare Chemie: Applied Macromolecular Chemistry and Physics*, 238(1):129–141.

[Hoque et al., 2019] Hoque, M. A., Bradley, R. K., Fan, J., and Fan, X. (2019). Effects of humidity and phosphor on silicone/phosphor composite in white light-emitting diode package. *Journal of Materials Science: Materials in Electronics*, 30(23):20471–20478.

[Hua et al., 2006] Hua, Y., Crocombe, A., Wahab, M., and Ashcroft, I. (2006). Modelling environmental degradation in ea9321-bonded joints using a progressive damage failure model. *The Journal of Adhesion*, 82(2):135–160.

[ISO,] ISO, B. 294-3: 2003,(2003). *BS EN ISO 294-3: 2003-Plastics-Injection moulding of test specimens of thermoplastic materials-Part 3: Small plates*.

[Jeenjitkaew et al., 2010] Jeenjitkaew, C., Luklinska, Z., and Guild, F. (2010). Morphology and surface chemistry of kissing bonds in adhesive joints produced by surface contamination. *International journal of adhesion and adhesives*, 30(7):643–653.

[Khalilullah et al., 2017] Khalilullah, I., Reza, T., Chen, L., Mazumder, A. M. H., Fan, J., Qian, C., Zhang, G., and Fan, X. (2017). In-situ characterization of moisture absorption and hygroscopic swelling of silicone/phosphor composite film and epoxy mold compound in led packaging. In *2017 18th International Conference on Thermal, Mechanical and Multi-Physics Simulation and Experiments in Microelectronics and Microsystems (EuroSimE)*, pages 1–9. IEEE.

[Lutz et al., 2012] Lutz, B., Guan, Z., Wang, L., Zhang, F., and Lü, Z. (2012). Water absorption and water vapor permeation characteristics of htv silicone rubber material. In *2012 IEEE International Symposium on Electrical Insulation*, pages 478–482. IEEE.

[Malpot et al., 2015] Malpot, A., Touchard, F., and Bergamo, S. (2015). Effect of relative humidity on mechanical properties of a woven thermoplastic composite for automotive application. *Polymer Testing*, 48:160–168.

[Mohd Ishak et al., 2000] Mohd Ishak, Z., Tengku Mansor, T., Yow, B., Ishiaku, U., and Karger-Kocsis, J. (2000). Short glass fibre reinforcedpoly (butylene terephthalate) part 1–microstructural characterisation and kinetics of moisture absorption. *Plastics, rubber and composites*, 29(6):263–270.

[NF, 1988] NF, T. (1988). T 76-142. *Méthode de preparation de plaques d'adhésifs structuraux pour la réalisation d'éprouvettes d'essai de caractérisation*.

[Pethrick, 2015] Pethrick, R. A. (2015). Design and ageing of adhesives for structural adhesive bonding–a review. *Proceedings of the Institution of Mechanical Engineers, Part L: Journal of Materials: design and applications*, 229(5):349–379.

[Shit and Shah, 2013] Shit, S. C. and Shah, P. (2013). A review on silicone rubber. *National Academy Science Letters*, 36(4):355–365.

[Sugiman et al., 2013] Sugiman, S., Crocombe, A., and Aschroft, I. (2013). Experimental and numerical investigation of the static response of environmentally aged adhesively bonded joints. *International Journal of Adhesion and Adhesives*, 40:224–237.

[Viana et al., 2017a] Viana, G., Costa, M., Banea, M., and Da Silva, L. (2017a). Behaviour of environmentally degraded epoxy adhesives as a function of temperature. *The Journal of Adhesion*, 93(1-2):95–112.

[Viana et al., 2017b] Viana, G., Costa, M., Banea, M., and Da Silva, L. (2017b). A review on the temperature and moisture degradation of adhesive joints. *Proceedings of the Institution of Mechanical Engineers, Part L: Journal of Materials: Design and Applications*, 231(5):488–501.

[Zhou and Lucas, 1999] Zhou, J. and Lucas, J. P. (1999). Hygrothermal effects of epoxy resin. part i: the nature of water in epoxy. *Polymer*, 40(20):5505–5512.

B Paper B

The influence of humidity and immersion temperature on the properties and failure mode of PBT-GF30/silicone bonded joints

R.Brandão[1], C.S.P. Borges[2], E.A.S. Marques[2], R.J.C. Carbas[2], A. Akhavan-Safar[2], F. Schmid[3], C. Ueffing[3], P. Weiβgraeber[3], L.F.M. da Silva[1]

1 Departamento de Engenharia Mecânica, Faculdade de Engenharia (FEUP), Universidade do Porto, Portugal

2 Instituto de Ciência e Inovação em Engenharia Mecânica e Engenharia Industrial (INEGI), Portugal

3 Robert Bosch GmbH, Corporate Research and Advance Engineering, 71272 Renningen, Germany

Abstract: The housing of electrical components are commonly manufactured from polybutylene terephthalate with 30% of glass fiber (PBT-GF30). These housings can be subjected to severe conditions of temperature and humidity that can catalyze the degradation of their properties. In order to connect the different parts of the housing, a silicone adhesive is used, which also serves as a sealant preventing moisture from entering the final component. Therefore, the effects of temperature, water intake in joints with PBT-GF30 substrates and silicone adhesive were studied. For this purpose, single lap joints (SLJ) and double cantilever beam (DCB) joints were tested at three different temperatures, 70, 90 and 130°C. The joints were tested after dried and after aging at those temperatures. To understand if water immersion introduced irreversible damage to the joints, the re-dried condition was also analyzed. The tensile properties of the bulk substrate and adhesive for all conditions were also determined. It has been seen that, generally, the adhesive having a higher strength when aged, leads to a better joint performance at this condition. However, at 90°C and 130°C there is chemical degradation of the PBT-GF30 after aging, which lead to failure approaching the substrate in those conditions for the SLJ. This was attributed to the release of chemical compounds that stay at the adhesive/substrate interface. In the DCB, since the loading of the substrate is even more severe, there was substrate failure. Finally, a numerical model was created for all conditions tested, which showed that the joints can be simulated by the properties of the bulk adhesive and substrate, showing that the effect of the interface is not very significant.

B.1 Introduction

The bonding of two components can be done resorting to several different methods, such as riveting, bolting or welding. However, riveting and bolting require the introduction of holes in the parts being bonded, which is particularly concerning when joining notch sensitive composite materials, and welding requires the local heating of the components, which may introduce a region of degradated properties. Therefore, adhesive bonding is an interesting solution, also creating a more uniform stress distribution and sealing the final bond, specially if silicone adhesives are employed [da Silva et al., 2018]. Silicone adhesives are used for non-structural and semi-structural applications that require flexible bonding, resistance to extreme environments and high durability of the adhesive bond. They showcase extreme flexibility at low temperatures, since their glass transition temperature (T_g) in often below zero. Standard formulations remain flexible up to -60°C, special one-part formulations (with condensation cure) can go down to -90°C and special two-part formulations down to -115°C [White et al., 2009].

Therefore, adhesive joints with silicone adhesives are often subjected to humid environments. Water can diffuse into the adhesive joints through the adhesive, substrate or adhesive/substrate interface. As well as through pores and cracks of the final assembly.

Adhesives are usually polymeric materials, which can absorb water as free water, that fills the free spaces in the polymeric chain, or bound water, which establishes chemical bonds with that chain, causing chemical degradation of the adhesive [Borges et al., 2021a]. Water uptake in polymeric materials can usually be described, through water uptake as a function of time, by the Fick's law of diffusion [Eftekhari and Fatemi, 2016]. This law is suitable for cases where the diffusion rate is much quicker than the relaxation rate of the polymer [Loh et al., 2005]. However, there are situations for which this law is not suitable. The main factors that benefit a non-Fickian diffusion are the viscoelastic nature of the polymers and cracks that may arise in the material, increasing its free volume and changing the uptake behavior [Errajhi et al., 2005]. Most diffusion laws used focus on the fact that the material absorbs water and its mass increases. However, it is possible that the compound loses mass due to its dissolution on the immersion environment, in this case, water [Borges et al., 2021a]. In the present study, both the matrix of the substrate and the adhesive are polymeric materials, being the substrate polybutylene terephthalate with 30% of short glass fibers (PBT-GF30), and the adhesive silicone.

Borges et al. conducted an extensive study regarding the water uptake behavior of the same PBT-GF30 used in the present study, also investigating how the mechanical and chemical properties of the material are affected by water [Borges et al., 2021b]. Three temperatures were studied (35, 70 and 130°C) and it was showed that the uptake follows the Fick's law of diffusion, increasing the maximum water absorption, M_∞ with increasing

temperature as a result of a relaxation of the polymeric matrix as well as capillarity effects along the fiber/matrix interface. Regarding, the diffusion coefficient, D, it increased with temperature, following the Arrhenius relation. The authors explain this phenomenon with the increased energy and motion of the molecules, which increases the diffusion rate. The effect of temperature and water on the mechanical properties of the material was also analyzed following two different procedures: the specimens prior to moisture aging were tested at controlled temperature and the aged specimens were tested at room temperature after moisture aging at different temperatures. As most polymeric materials, PBT-GF30 significantly decreases its mechanical properties when tested at high temperature. Additionally, it also follows the common trend of decreasing its strength and stiffness with increasing moisture content [Viana et al., 2017, Borges et al., 2021a, Borges et al., 2021b, da Silva et al., 2018].

For silicones, on the other hand, this is not the case. Oldfield and Symes et al. tested several silicone adhesives in different environments (hot-dry and hot-wet environment), leaving the silicones at different locations on aluminum boxes that allowed free circulation of ambient air around the elastomers but excluded light and rain. The hot-dry place had an annual temperature of 32.3°C and an annual mean of 43 rainy days, while the hot-wet place had an annual temperature of 28.1°C and an annual mean of 174 rainy days. The experiment had a considerable period of time (from 2 years up to 20 year) and the authors stated that well-compounded silicone elastomers were mechanically very resistant to hot drying, hot water or tempered environments with some silicones (iron oxide pigmented, heat-vulcanized, dimethyl silicone rubber) exhibiting only reductions of less of 10% in tensile strength, less than 25% reduction in elongation at break and hardness increases of no more than 4%, after 20 years of exposure at either site [Oldfield and Symes, 1996].

Fan et al. analyzed the mechanical degradation mechanism of a phosphor/silicone composite over 1008 h of aging at 55°C, using samples with mass fractions 0% and 10% of phosphor. With aging, the Young's modulus increased for both samples since the moisture permeated into the silicone, the hydrolysis reaction of phosphor powders accelerated the stiffness of the composite. The tensile strength increment of pure silicone samples was higher than that of phosphor/silicone composites and the author stated the moisture-induced hydrolysis of the phosphor powders enhanced their surface roughness, thereby resulting in uneven contact between the phosphor particles and the silicone. This could produce gaps between them and slow down the rate of increase of tensile strength of the composite. [Fan et al., 2019].

A work developed by Kashi et al. [Kashi et al., 2018] focus how the mechanical properties of a silicone rubber change when it is aged in water at 195°C and found that there was a high deterioration of strength, Young's modulus and hardness. However, both tear

strength and hardness exhibited an initial increase in early stages of aging, followed by a decreasing trend as the aging continued and after two weeks there was a decrease of these values.

Although the water immersion of silicons increases its strength, when in a joint it was shown to have an important impact on the decrease of the sealing performance. Wu et al. studied the maximum contact pressure and contact area between silicone rubber and metal surface, conducting compression and hardness tests for several temperatures. The results showed that hardness and compression set increase with aging of silicone rubber. The authors stated that the aging process has a major impact on the sealing performance, with the results indicating that the maximum contact pressure and contact area between silicone rubber and metal surface were significantly reduced after aging, the maximum contact pressure decreasing with increasing aging temperature and 150 °C was the turning point of the aging effect time. In short, the contact area decreased when the aging time and aging temperature increased [Wu et al., 2017].

Bowditch et al. stated that when there is water absorption in the joint there can be also chemical degradation of the adhesive, the substrate or the chemical bonds across the interface. The absorbed water often plasticizes the organic adhesives, decreasing its strength. As for the effect of the temperature in the degradation of the material, it is commonly accepted that with increasing temperature there is an increase in the rate of degradation, and, therefore, a decrease in strength and stiffness [Bowditch, 1996].

This work aimed to add to the research on joint degradation due to aging, especially since there are not many studies available using silicone adhesives with polymeric substrates and since there is chemical degradation of the substrate at temperatures above 85°C, it is also intended to understand if this chemical change provides further contamination of the interface due to substances that may be released from the substrate when aging.

To understand if the aging creates irreversible effects on the joint, the joints were tested at three different states dried, aged and dried after aging at three different temperatures (70 and 90 and 130°C) to evaluate if they could restore the properties they presented prior to aging, and it was also examined whether this changed with temperature. To evaluate the effect on the strength properties of the joint single lap joints were used and, to evaluate the effect on fracture energy, double cantilever beam tests were carried out.

B.2 Experimental details

B.2.1 Materials

Adhesive

The adhesive used in this study is a two-component silicone elastomer adhesive, that cures at 120°C for 25 min. Borges et al. investigated the behavior of this silicone after aging at different temperatures [Borges et al., 2021c]. The cohesive strength regarding the states of dried, aged and dried after aging in the three temperatures analyzed in this work can be seen in Table 1. As for the stiffness, the authors stated that with water intake, the Young's modulus increased.

Table 1: Mechanical properties of the silicone

State	T(°C)	Strength (MPa)
Dried	70	3.1
Aged	70	3.7
Dried after aging	70	3.2
Dried	90	2.8
Aged	90	3.0
Dried after aging	90	2.8
Dried	130	2.6
Aged	130	2.9
Dried after aging	130	2.7

Substrates

The substrates used in this study are a polybutylene terephthalate with 30% glass fiber (PBT-GF30) and high strength steel. For all states, the general mechanical properties were determinate and are presented in the Chapter 3.

B.2.2 Specimen manufacturing

Gravimetric analysis

A gravimetric study was conducted on PBT-GF30 substrates at a temperature of 90°C. Borges et al. conducted a similar study for the temperatures of 70 and 130°C, which are also the temperatures analyzed in this paper [Borges et al., 2021b]. Similarly, Borges et al. performed the identical study for 70, 90 and 130°C but for the silicone adhesive of this work [Borges et al., 2021c]. All the values for the coefficient of diffusion, D, and the infinite water uptake, M_∞, are available in Table 2.

Table 2: Water uptake properties previous calculated of the materials.

Material	T(°C)	D (m^2/s)	M_∞ (%)
PBT-GF30	70	3.90×10^{-12}	0.50
PBT-GF30	130	1.37×10^{-11}	0.50
Silicone adhesive	70	9.1×10^{-13}	0.57
Silicone adhesive	90	4.8×10^{-12}	0.58
Silicone adhesive	130	9.8×10^{-12}	0.60

Regarding the plates used in this study, 30x30 mm^2 and 1 mm thick plates were used. Normally, 60x60 mm^2 and 1 mm plates are used, according to ISO 294-3 standard [ISO294-3, 2002]. However, Borges et al. performed an experiment comparing the two geometries and concluded that both had similar experimental values [Borges et al., 2021b]. Thus, in order to decrease the amount of PBT-GF30 used, plates of 30x30 mm^2 mm and 1 mm of thickness were used.

Bulk tensile tests

To study the effect of water and temperature on the mechanical properties of the PBT-GF30 bulk tensile test were performed for each state and for all temperatures to obtain the Young's Modulus (E), the strength (σ) and plastic behavior. However, the standard bulk "dog bone" specimens have high dimensions, and must be immersed in water, which would require large water containers and long immersion times. Therefore, reduced-scale specimens were used to expedite this process. These specimens were utilized in previous works and were proven to have accurate mechanical properties and, using these specimens,

it is also possible to it reduce the amount of PBT-GF30 used [Viana et al., 2017, Borges et al., 2021b]. The dimensions of the reduced scale "dogbones" are shown in Figure 1.

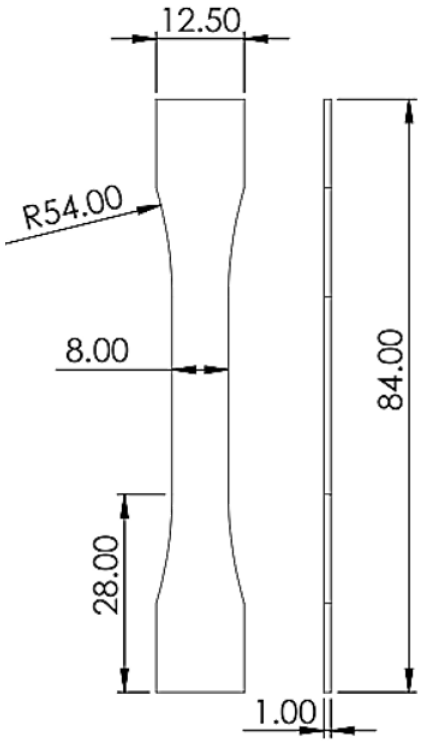

Figure 1: Schematic representation of the bulk tensile test specimen's geometry, dimensions in mm.

Single lap joints (SLJ)

Single lap joints with 1 mm thick adhesive and 25 mm of overlap length were manufactured.The adhesive thickness was chosen to mimic that of the housing for electronic components. In order to achieve that, packing shims were used to provide the necessary spacing between the two substrates. The schematic representation of the geometry is shown in Figure 2.

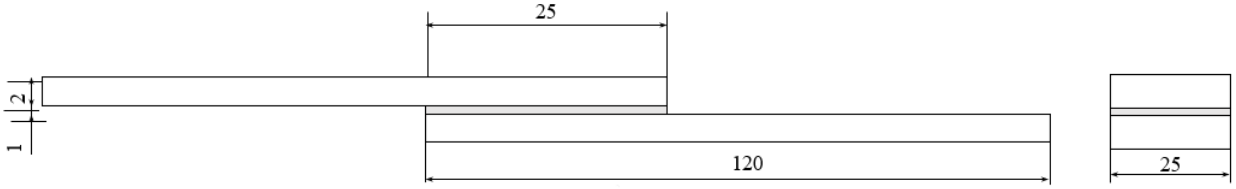

Figure 2: Schematic representation of the SLJ geometry, dimensions in mm.

Double cantilever beam (DCB)

The same substrates with 2 mm thickness and 25 mm width were used for the DCBs. The bond line thickness was set at 1 mm with the use of spacers (calibrated metal tape), which were positioned between the substrates prior to the application of the adhesive. To ensure a pre-crack in the adhesive, a razor blade was inserted mid-thickness. Before testing, stainless steel end-blocks were attached with cyanoacrylate adhesive on each specimen end respecting the ISO 15024 standard, which specifies that the crack-opening mode due to a load applied perpendicularly to the plane of delamination using the DCB specimen can be achieved with the use of hinges or load block [ISO, 2001]. The schematic representation of the geometry of the DCB joints is presented in Figure 3.

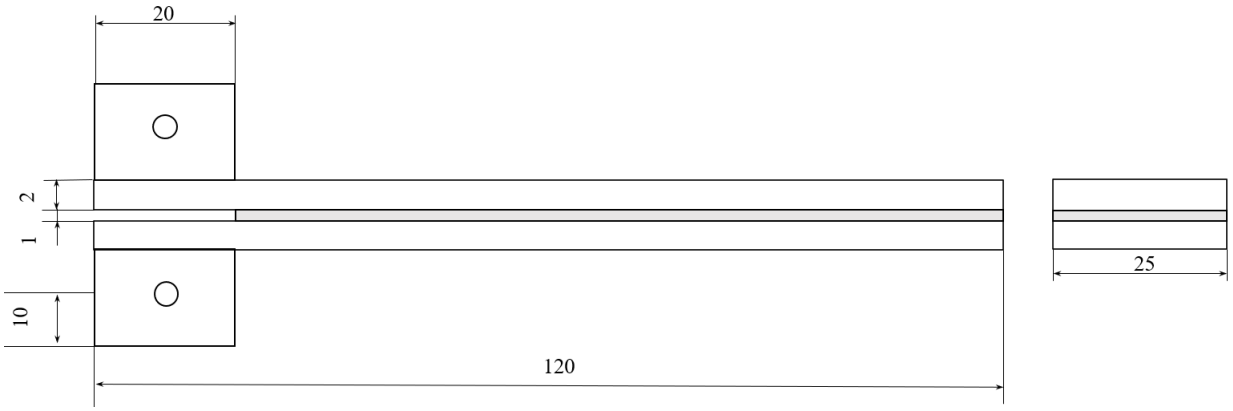

Figure 3: Schematic representation of the DCB geometry, dimensions in mm.

The joints with composite substrates have plastic deformation during testing. Therefore, to accurately simulate the process, the mode I fracture toughness of the adhesive must be determined from standard specimens. To determine that the fracture toughness in mode I, high strength steel substrates were used because there was plastic deformation with the PBT-GF30 substrates. The same adhesive thickness of 1 mm was applied, being ensured with the use of spacers. The value of the crack length, a_0 was 45 mm allowing a stable crack propagation. A pre-crack was introduced with a sharp blade positioned mid-thickness. The geometry of the DCB is shown in the Figure 4.

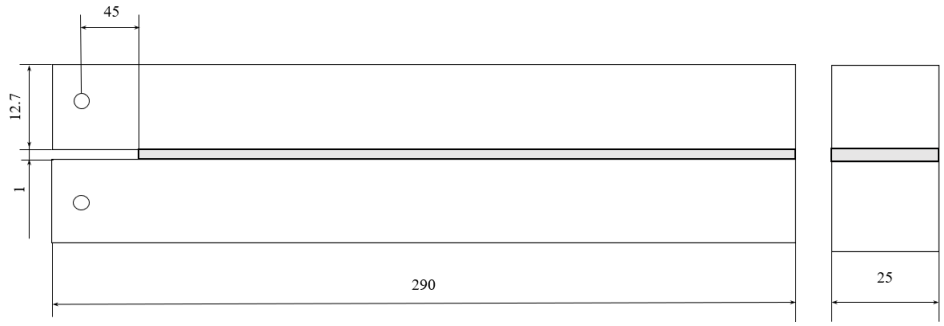

Figure 4: Schematic representation of the DCB geometry, dimensions in mm.

Prior to the application of the adhesive, the joint surfaces of the PBT-GF30 were degreased with acetone while the high strength steel were grit blasted and then degreased with acetone.

B.2.3 Experimental procedure

All tests were conducted with an *INSTRON*® 3367 universal test machine (Norwood, MA, USA), with a capacity of 30 kN. The testes were performed at room temperature and constant displacement rate of 2 mm/min. At least three specimens were tested for each condition

Gravimetric analysis

Before the immersion in water, the PBT-GF30 specimens were completely dried in silica at RT for two weeks to guarantee that no water was found in the material. Afterwards, the surfaces were treated with sand paper to remove any impurities and ensure minimum roughness. Before immersion, the masses of the specimens were determined. It was ensured that when the specimens were immersed, they were completely submerged in water and the surface was only in contact with water. The water temperature, at 90°C, was controlled by placing the water container in a climatic chamber (Memmert GmbH, Büchenbach, Germany). The mass was measured periodically until saturation was reached. Before all mass measurements, the specimens were dried with a paper towel to remove excess water from their surface. All mass measurements were performed on a microbalance with 0.1 mg accuracy (KernToledo, Balingen, Germany). The water uptake for each step is determined by:

$$M_t = \frac{m_t - m_0}{m_0} \times 100\ (\%) \tag{1}$$

where m_t is the mass of the specimen at the current step, and m_0 the initial mass. When the water uptake of the specimens reached a stable value, they were considered saturated.

Bulk tensile tests

In this work, bulk tensile tests of the PBT-GF30 were performed in three different states (dried, aged and dried after aging) and at three temperatures (70, 90 and 130 °C) All specimens were placed in a climatic chamber for enough time to reach saturation. To create a uniformly rough surface, the "dogbone" specimens were treated with sandpaper and mass was measured. Prior to testing, they were dried with paper towel. For each test performed, load-displacement (P-δ) curves were obtained up to failure. For each condition, at least three specimens were tested.

Single lap joints (SLJ)

Prior to testing, the SLJ were positioned and secured vertically using two grips (pressure was created using four screws and applying 20 Nm of torque with a torque wrench). Metal tabs were positioned below one side of each substrate of the SLJs to secure the specimens were horizontal when assembled. In addition, two center pins were utilized during testing to ensure proper positioning of the substrate, as well as to provide greater grip, minimizing or preventing the specimens from slipping. Load–displacement (P-δ) curves were recorded for all SLJs tested, allowing the determination of the tensile strength. For all states, the specimens were kept in the climatic chamber right until the testing procedure.

Double cantilever beams (DCB)

Load–displacement (P-δ) curves were determined for all DCBs with PBT-GF30 substrates tested.

As stated previously, due to the plastification of the PBT-GF30 substrates when in a DCB joint, it was not possible to determine the fracture toughness of the adhesive in mode I using these substrates. Therefore, it was assessed using standard joints with high strength steel substrates. The G_{IC} was determined using the J-integral method. The J-integral, introduced by Rice et al., is a continuous mechanical value that indicates the resistance of a material to crack propagation under a constant stress, and it is a mean of reporting the toughness of the material in geometries containing flaws [Rice, 1968]. It is measured at the onset of fracture and is defined as the critical value of fracture toughness. It has also an excellent applicability for modelling with current finite element modelling tools [K.H. Jürgen Buschow, 2001, Kurtz, 2016].

Defining the energy release rate from the concept of force from beam theory for a DCB [Rice, 1968]:

$$G_{IC} = 12\frac{(P_u a)^2}{E_a h^3} + P_u \theta_0 \tag{2}$$

or

$$G_{IC} = P_u \theta_p \tag{3}$$

Where P_u is the load applied per unit length at adjacent extremities, a is the crack length, h is the substrate thickness, E_a is the Young's modulus of the substrate and θ_p is the relative rotation of the substrate at the loadline as showed in Figure 5.

The J-integral is defined along an arbitrary path surrounding the beginning of the adhesive layer [Zhu et al., 2009]:

$$G_n = \int_0^{\delta_{nc}} t_n(\delta_n) d\delta_n \tag{4}$$

where δ_n and δ_{nc} are the normal opening and the normal end opening of the cohesive law at the tip of the initial crack and t_n is current normal traction. G_{IC} is the value of G_n at the tip of the crack. As for $t_n(\delta_n)$ is obtained by differentiation of the equation (4) with respect to δ_n, giving the cohesive law [Zhu et al., 2009].

$$t_n(\delta_n) = \frac{\partial G_1}{\partial \delta_n} \tag{5}$$

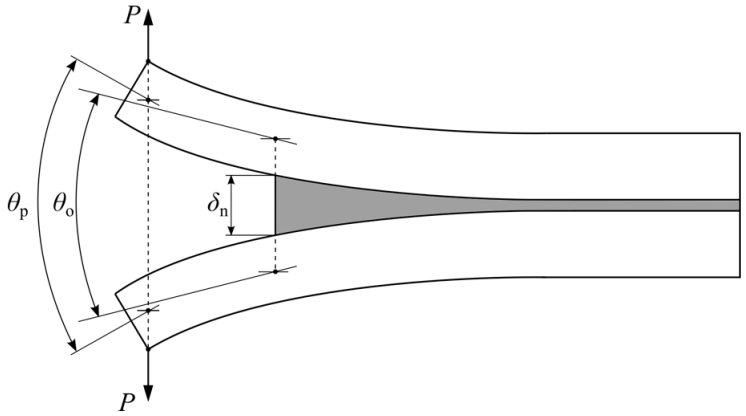

Figure 5: DCB specimen under loading, with description of the analysis parameters.

For the determination of δ_n and θ_p, a digital image correlation (DIC) software, *GOM*, was used. This software has the ability of following manually defined target points and gives the displacement relative to an imposed coordinate system. This method was previously used by Campilho et al. [Campilho et al., 2014].

The technique used to create the target points consists on painting the specimen with white ink and, afterwards, black ink is carefully sprayed in order to obtain a speckled

pattern as is shown in Figures 6 and 8. Two points (p_1,p_2) were used to obtain the current opening between the two substrates at the crack tip, t_A, and during the upload of the video is defined as (t_A^{CT}). Two points on top of the specimen (p_1,p_3) and two points on the bottom of the specimen (p_2,p_4) were used to obtain θ_p. The points used for one of the specimens in DIC software are shown in Figure 6.

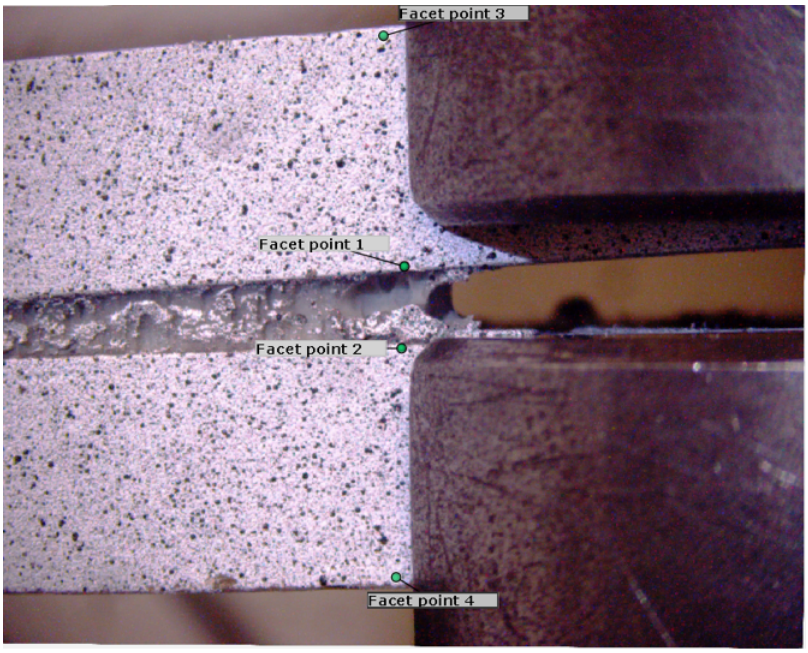

Figure 6: Points taken by the optical method for measuring θ_p .

The value of t_A^{CT} in S.I units (mm) is given by:

$$t_A^{CT} = |p1 - p2| \tag{6}$$

and δ_n comes as:

$$\delta_n = t_A^{CT} - t_A \tag{7}$$

where t_A is the initial thickness of the adhesive, which is 1 mm. Therefore, δ_n starts with an initial value of 0.

The relative rotation between two substrates was defined using two vectors u and t using all the four points (p_1,p_2,p_3,p_4). Both vectors are collinear with the top and bottom substrates [F.Loureiro, 2020].

$$\vec{u} = (p_{1x} - p_{3x}, p_{1y} - p_{3y}) \tag{8}$$

$$\vec{t} = (p_{4x} - p_{2x}, p_{4y} - p_{2y}) \tag{9}$$

Figure 7, shows a vectorial representation of θ_P.

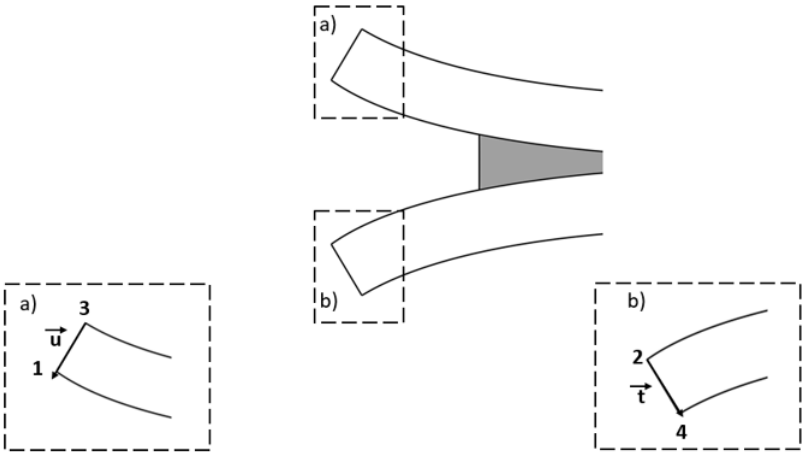

Figure 7: Vector representation of θ_P determination: (a) top substrate vector,u ; (b) lower substrate vector,t

In addiction, in order to relate both vectors, the vector product between the vectors u and t results in the vector$t$:

$$\vec{s} = \vec{u} \wedge \vec{t} \tag{10}$$

and

$$|\vec{s}| = \sqrt{s_X^2 + s_Y^2} = |\vec{u}| \cdot |\vec{t}| \cdot \sin\theta_p \tag{11}$$

So, we can rewrite the Equation 11 in order to θ_p as:

$$\theta_p = \arcsin \frac{|\vec{s}|}{|\vec{u}| \cdot |\vec{t}|} \tag{12}$$

In Figure 8 is shown a progressive crack growth process in the silicone adhesive.

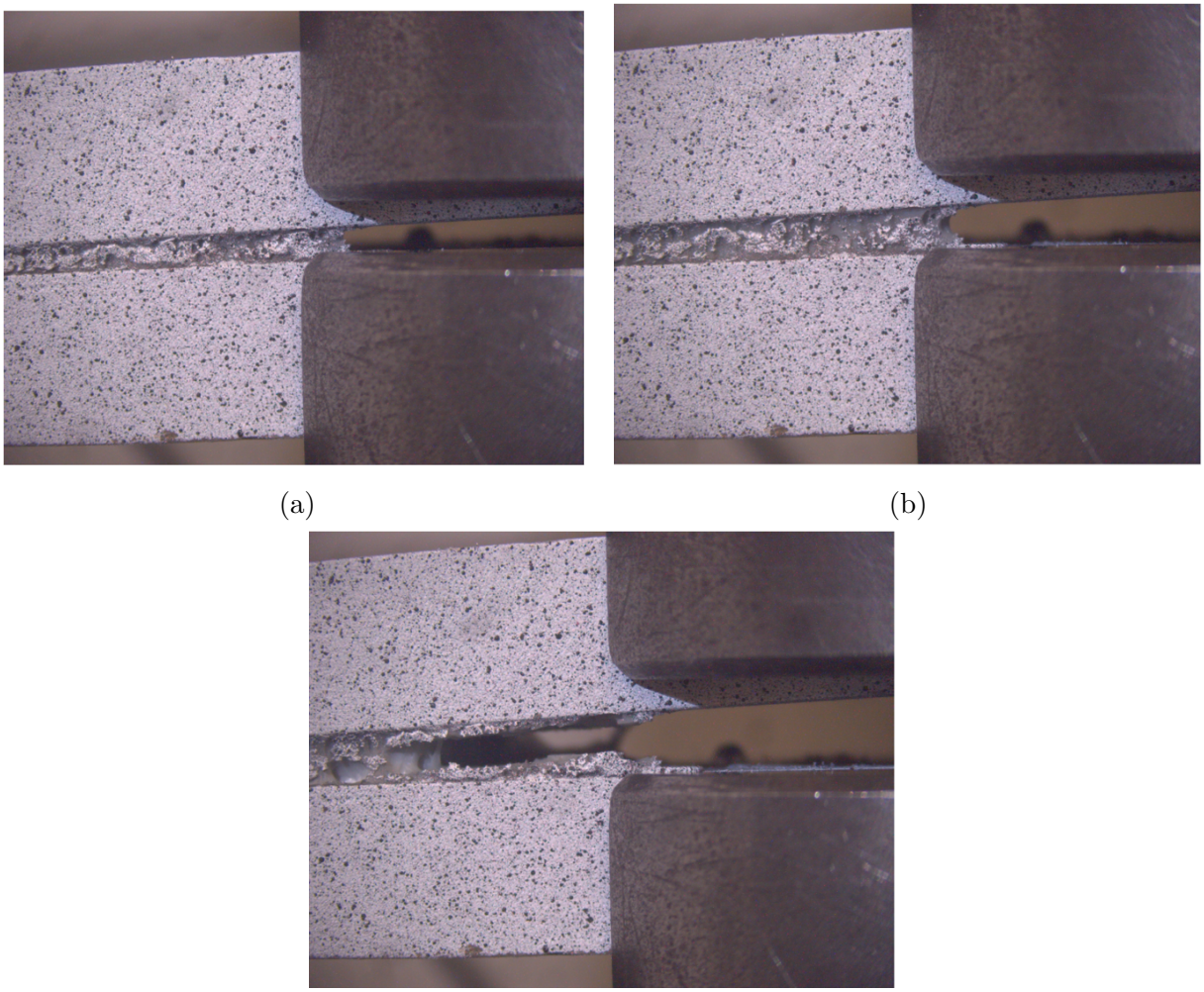

(a) (b)

(c)

Figure 8: Crack growth process

Calberger et al. studied the effects of temperature and strain rate on the cohesive parameters for an engineering epoxy adhesive and concluded that the fracture energy is shown to be relatively insensitive to the variation in temperature [Carlberger et al., 2009]. Gustafson et al. stated that for low values of cohesive strength the model shows to be insensitive to variations of the G_{IC} and, in fact, it is particularly sensitive to the cohesive strength [Gustafson and Waas, 2009]. So in the numerical models the value of 3.3 N/mm, calculated with high strength steel substrates, was used for all temperatures and states.

B.3 Numerical model

B.3.1 Water uptake of the joints

The water uptake of the joints at the moments the joints were removed from water were analyzed, with the main purpose of guaranteeing that, in the aged condition, the same water uptake in the adhesive and substrate was found for all the temperatures.

The water uptake was simulated using *Abaqus*, through a heat transfer analogy. The water uptake is, analogously, temperature and the coefficient of diffusion is the thermal diffusivity. It was considered that, when the material was placed under water, the nodes in direct contact with fluid immediately saturate. Therefore, in these nodes, a boundary condition of temperature equal to the maximum water uptake was defined and, the remaining temperature has temperature equal to zero.

For both joints, only one quarter of the joint was considered, taking advantage of symmetry, as shown in Figure 9 for SLJs.

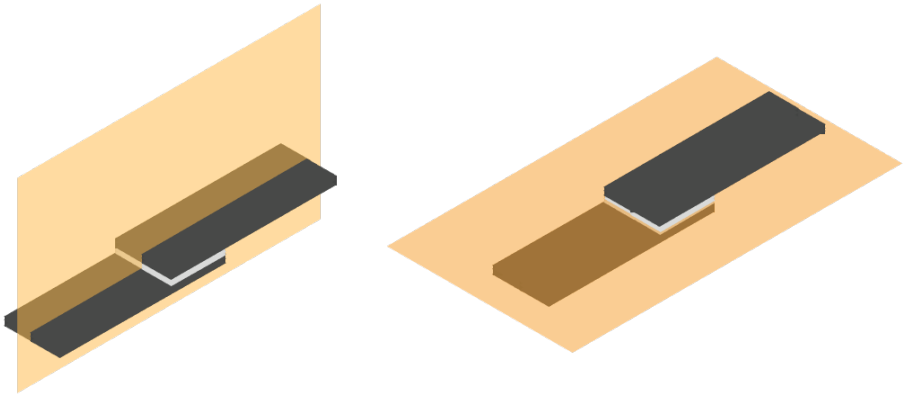

Figure 9: Schematic representation of the SLJ bondary condition.

The mesh used has cubic elements with a constant side length of 0.5 mm. The elements used are 8-node linear heat transfer bricks (DC3D8). The heat transfer through the adhesive/substrate interface was also considered.

B.3.2 Double cantilever beam and single lap joints

The FEM analysis was also performed using the software*Abaqus* with the main propose of simulating numerically the joint considering the effect of humidity on the mechanical properties of the bulk adhesive and substrate and understanding if they are similar to those obtained for the experimentally tested joint. The model employed cohesive elements with a triangular (bilinear) traction-separation law, based on the mechanical and cohesive properties of the silicone adhesive and considering the lack of any defect in the interface or within the adhesive layer. The adhesive layer, such as the experimental layer, was model with 1 mm thick cohesive elements.

The strength properties of the substrate and adhesive were set to those obtained from the bulk tensile tests performed for the correspondent tensing condition (dried, aged, dried after aging) and immersion temperature (70, 90 and 130°C). Since there is plastic deformation of the substrates, the plastic properties of the PBT-GF30 were also taken into consideration. The fracture toughness in pure mode I (G_{IC}) used was of 3.3 N/mm

obtain with the high strength steel DCB.

A static general step was chosen to solve the model. Regarding boundary conditions, in the SLJ FEM model, one of the ends was clamped, restrained in the two directions, while a longitudinal displacement was applied in the other end of the model, restrained in the transverse direction as well, Figure 10.

Figure 10: Schematic representation of the SLJ bondary condition.

As for the DCB model, the node in the middle of the lower steel cube was restrained in the plane, and the node in the middle of the upper cube was held horizontally and pulled vertically, Figure 11.

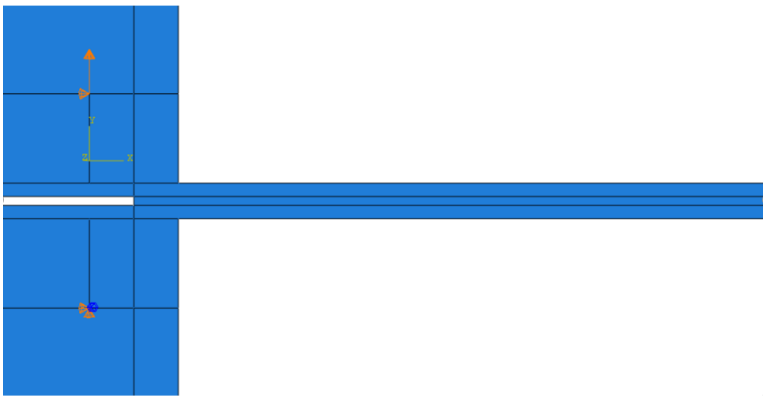

Figure 11: Schematic representation of the DCB bondary condition.

For the SLJ model, the size of the mesh was increased in areas away from the ends of the overlap, as the stress gradients are less severe, this technique allows a good compromise between accuracy and computational time. Regarding the elements type, for both models, a 4-node-two-dimensional cohesive elements (COH2D4) were used to define the bondline area, and a 4-node bilinear plane strain quadrilateral, reduced integration, hourglass control element (CPEAR) for the substrates and stainless steel cube. The mesh size of elements in the areas with severe stress was of 0.08 mm, while the cohesive elements were squares with 1 mm of side length. Both meshes are shown in Figure 12.

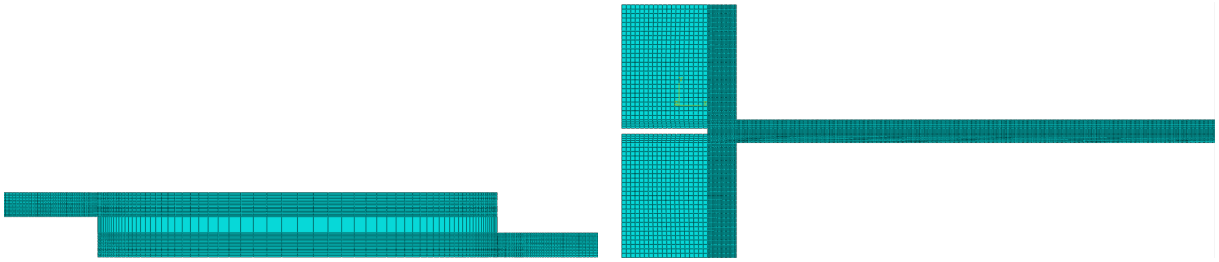

(a) SLJ mesh (b) DCB mesh

Figure 12: Mesh of the numerical models

B.4 Experimental results

Gravimetric analysis

As previously said, the gravimetric study of the PBT-GF30 at 70°C and 130°C and of the silicone for all the temperatures under analysis were already done by Borges et al. [Borges et al., 2021b,Borges et al., 2021c]. However, it was still necessary to understand the water uptake behevior or the PBT-GF30 at 90°C.

After the water uptake was defined for several time increments, to analyze the experimental results, the Fick's law of diffusion was used.

$$M_t = \left[1 - \frac{8}{\pi^2} \prod_{n=0}^{n} exp\left(\frac{-D(2n+1)^2\pi^2 t}{4h^2}\right)\right] M_\infty \tag{13}$$

where t is the time starting from immersion and h the thickness of the specimen. Table 3 presents the values for the coefficient of diffusion, D, and the infinite water uptake, M_∞, obtained.

Table 3: Water uptake properties of the PBT-GF30 at 90°C

Material	T(°C)	D (m^2/s)	M_∞ (%)
PBT-GF30	90	9.50×10^{-12}	0.49

The experimental results and analytical curves with the D and M_∞ is shown in Figure 13.

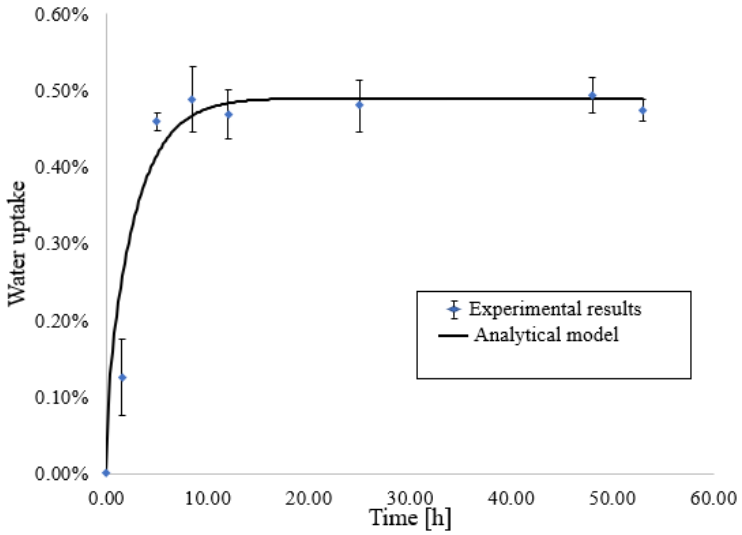

Figure 13: Experimental results and numerical details for the gravimetric tests of the PBT-GF30 at 90°C

B.4.1 Adhesive characterization

From the results obtain in the DCBs with high strength steel substrates, a representative curve of the variation of the J-Integral with the normal end-opening displacement (δ_n) is shown in Figure 14. This curve represents G_{IC} in the interval [0, δ_{nc}], where δ_{nc} is defined by the point when G_{IC} is at its maximum value. After reaching this point, testing always continue although only the region until this point is represented, since this fully defined the cohesive law [Högberg et al., 2007]. The value of the G_{IC} was 3.3 ± 0.38 N/mm.

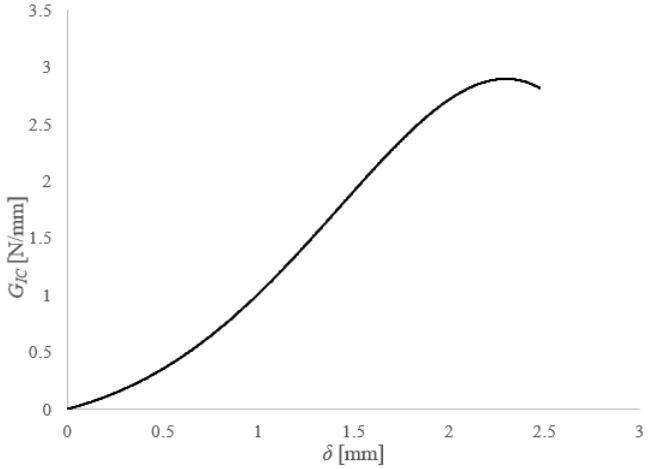

Figure 14: Representative curve of the G_{IC}

The cohesive law of the adhesive in mode I was obtained by differentiation of the G_{IC} with respect to (δ_n). From the most representative cohesive law in Figure 15, we infer

that the adhesive has a very little ductile behavior, being practically nonexistent. This shows that the adhesive has a brittle behavior, not being very tenacious.

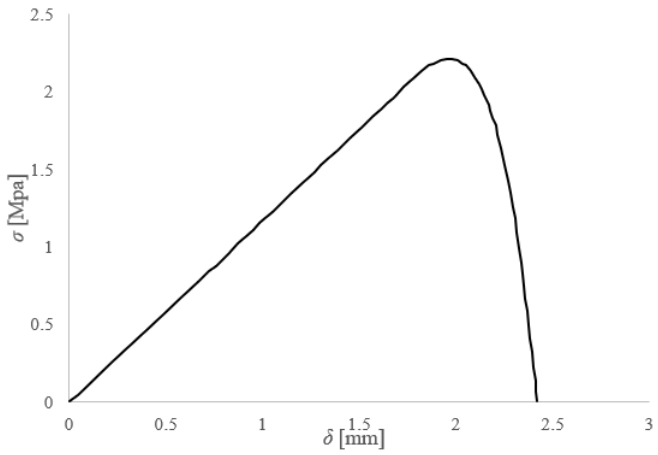

Figure 15: Cohesive law of the adhesive

B.4.2 Bulk tensile test

The results of the Young's modulus and strength of the different temperatures of the PBT-GF30 bulk tensile tests are showed in the following section.

70°C

Figure 16 shows the strength and Young's modulus of the PBT-GF30 dried, aged, and dried after aging at 70°C.

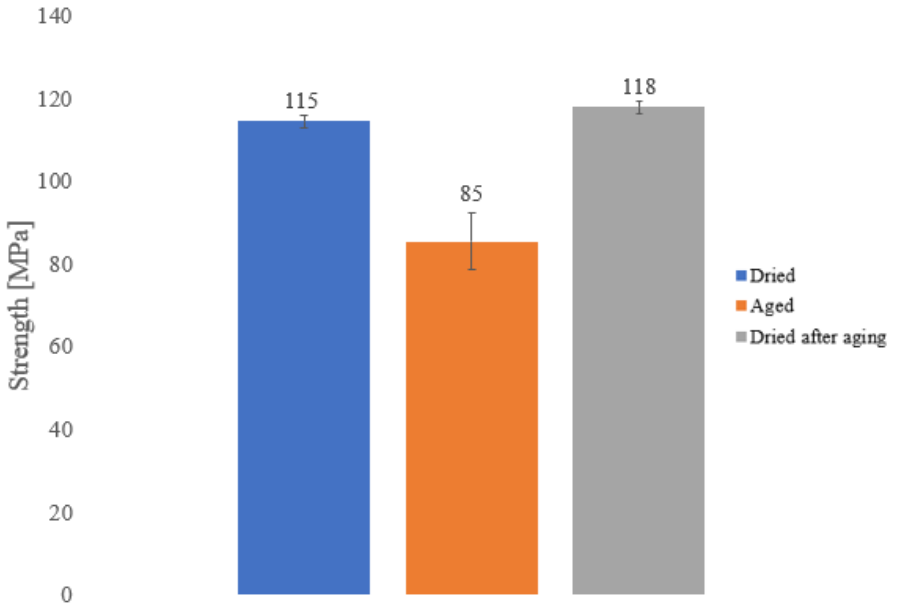

(a) Strength

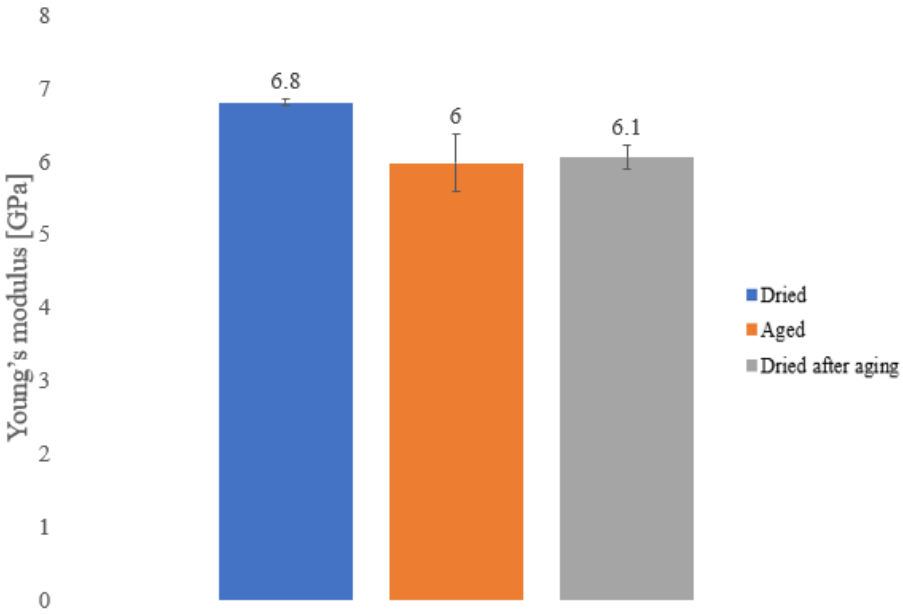

(b) Young's modulus

Figure 16: Mechanical properties of the PBT-GF30 for the different conditions at 70°C

For 70°C it is noticeable that there was a decrease of 26% in strength for the aged state in comparison with the dried state, however the PBT-GF30 was capable to recover after re-drying, which indicates that, after immersion at 70°C, the degradation caused by water intake to the PBT-G30 is not irreversible. Regarding the Young's modulus, the decrease in the aged state is not as pronounced in relation to the dried state. With these results, we can infer that degradation of the properties occurred due to water absorption, however the material was able to recover the tensile properties. This result is in agreement with a study by Ishak et al. who inferred that PBT with 30% glass fibers in a 100% RH

environment at 80°C are able to recover tensile properties [Mohd Ishak et al., 2000].

90°C

Figure 17 shows the strength and Young's modulus of the PBT-GF30 dried, aged, and dried after aging at 90°C.

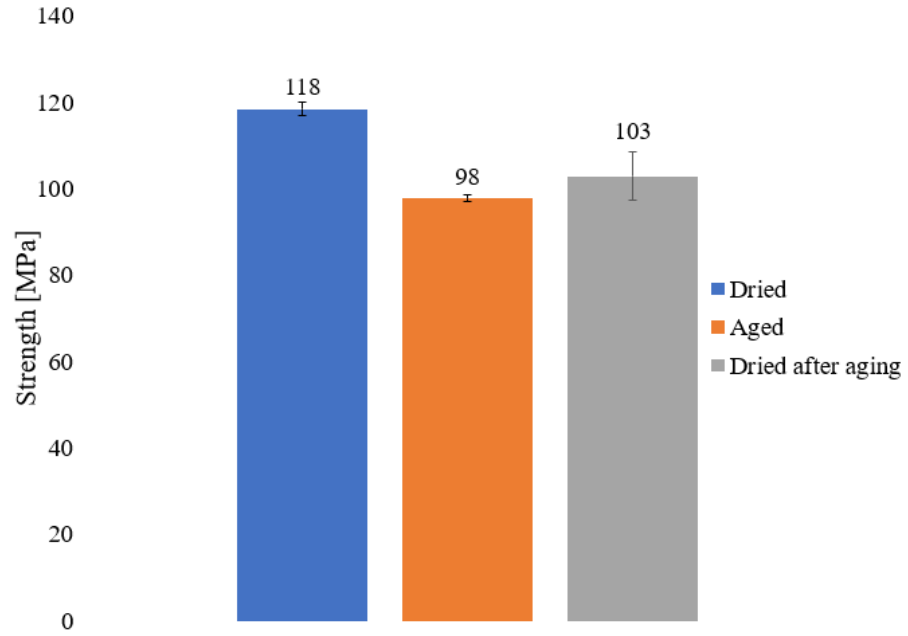

(a) Strength

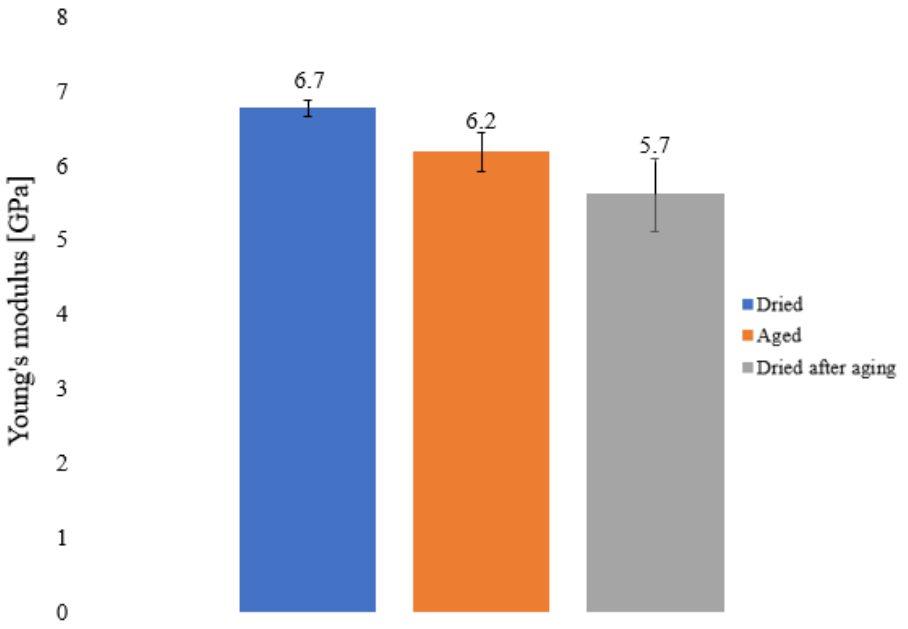

(b) Young's modulus

Figure 17: Mechanical properties of the PBT-GF30 for the different conditions at 90°C

When analyzing the results at 90°C, three situations were evident. First, in compar-

ison with the 70°C dried state, there was not a significant difference which leads to the conclusion that the effect of the temperature from 70° to 90° was not significant either to the Young's modulus or the strength. Secondly, the difference in the drop in properties between the dry and aged states does not change significantly between temperatures, Borges et al. who analyzed the mechanical properties of PBT-GF30 and PBT across different temperatures stated that there was no clear trend in any temperature for the evolution of the strength and Young's modulus as function of water uptake [Borges et al., 2021b].

Finally, and most important, at 90°C the PBT-GF30 was not capable to recover its mechanical properties when dried after aging what leaves to the conclusion that between 70°C-90°C there is mechanical degradation due to water intake, caused by a relaxation on the polymeric chain. This result is in line with an experiment by Borges et al. that stated that the PBT-GF30 starts to suffer chemical interaction with water around 80°-85° [Borges et al., 2021a].

130°C

Figure 18 shows the strength and Young's modulus of the PBT-GF30 dried, aged, and dried after aging at 130°C.

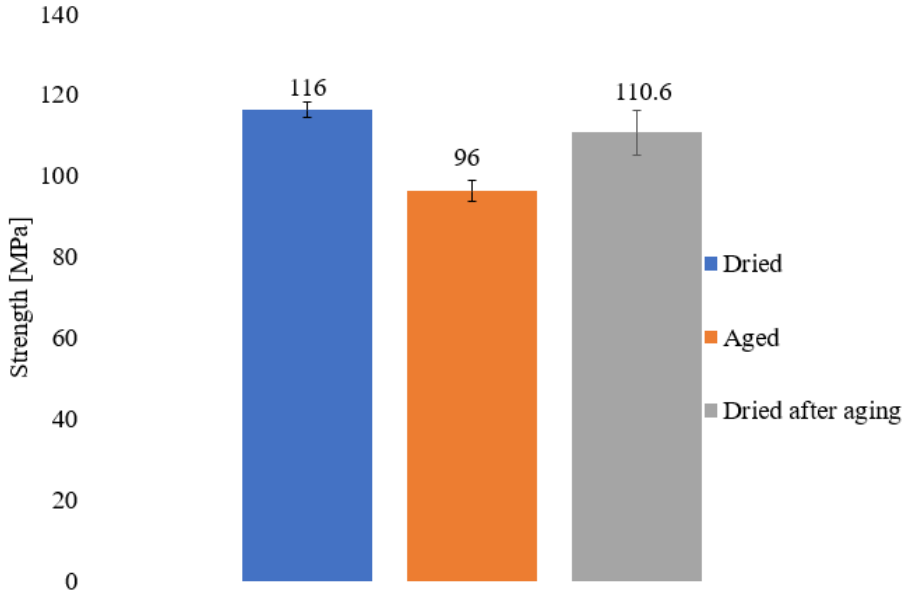

(a) Strength

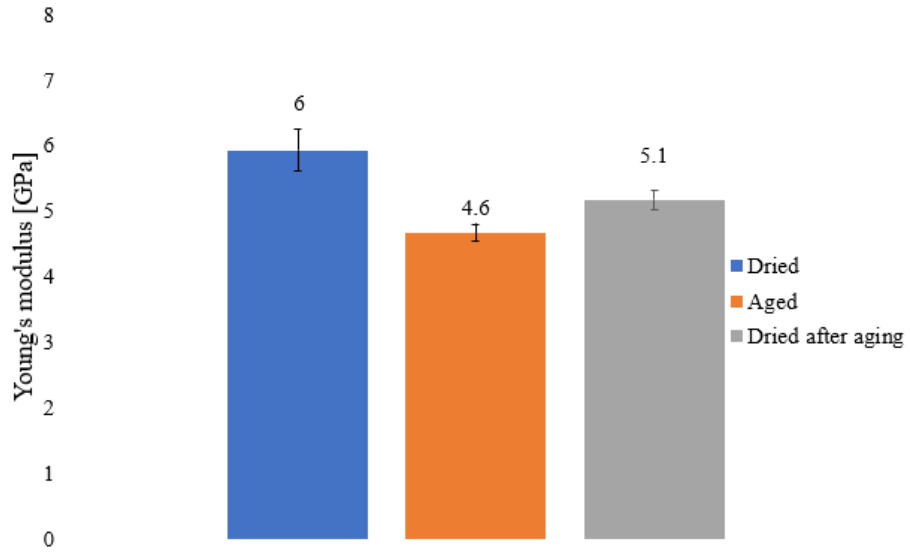

(b) Young's modulus

Figure 18: Mechanical properties of the PBT-GF30 for the different conditions at 130°C

At 130°C, the PBT-GF30 showed the same behavior as for 90°C. Again there was not a significant difference due to the influence of the temperatures and after the water intake the material was not capable of completely restore the previous properties, which leads to concluding more strongly that the PBT-GF30 undergoes degradation of its polymer matrix.

B.4.3 Single lap joint (SLJ)

70°C

Figures 19 and 20 show representative $P - \delta$ curves of the most representative curve for each state and the failure load, respectively.

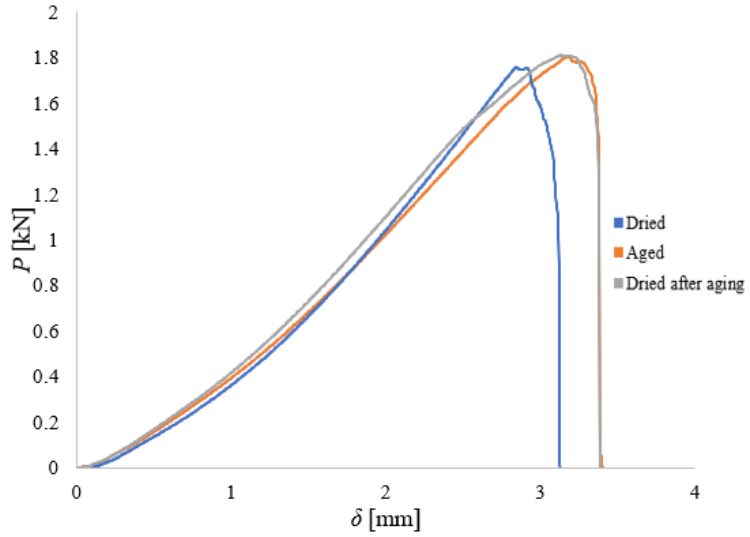

Figure 19: SLJ $P - \delta$ for the different conditions tested at 70°C

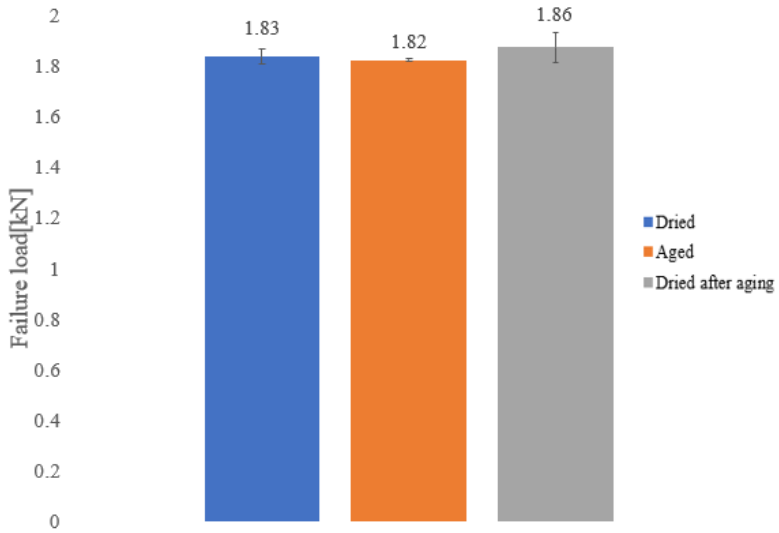

Figure 20: Failure load of the SLJ for the different conditions tested at 70°C

For 70°C, there was not a considerable difference between the three states. While the substrate material, PBT-GF30, decrease its properties, as a studied done by Borges et al. showed that the mechanical properties of the silicone adhesive improved with water intake at 70°C [Borges et al., 2021c]. Therefore, as a result, the SLJ did not show a significant difference between the three conditions. As for the failure type, Figure 21, for

the dried state the failure was cohesive and in aged and dried after aging stage the failure was still cohesive but even closer to the middle of the adhesive. This happens because, with increasing water uptake, the adhesive becomes stronger and stiffness, and since the region of the adhesive closer to the interface absorbs more water, it is stronger, moving failure to the middle of the adhesive.

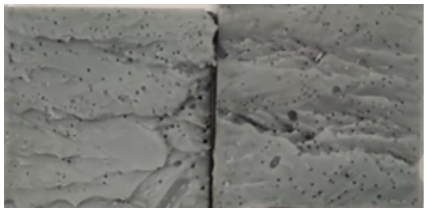

(a) Dried

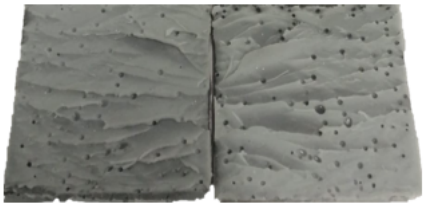

(b) Aged

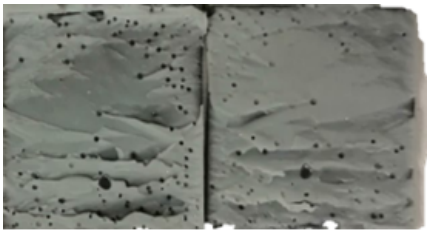

(c) Dried after aging

Figure 21: Failure surface of the SLJ for the different conditions tested at 7°C

90°C

Figures 22 and 23 show representative $P - \delta$ curves of the most representative curve for each state and the failure load, respectively.

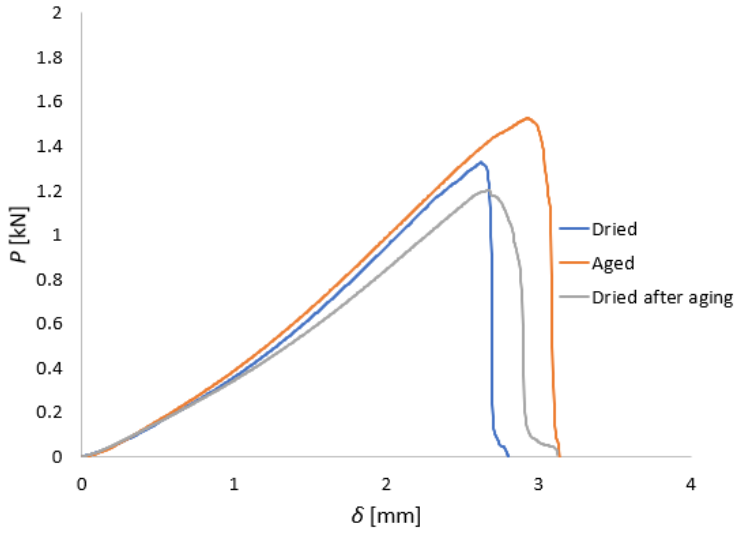

Figure 22: SLJ $P - \delta$ for the different conditions tested at 90°C

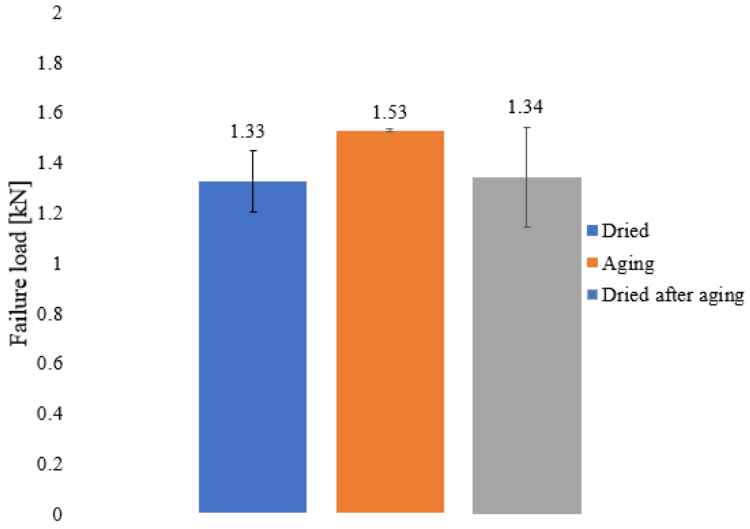

Figure 23: Failure load of the SLJ for the different conditions tested at 90°C

For the dried state at 90°C there was a decrease of 27% on the failure load when compare with the same state at 70°C, since the strength of the adhesive reduces with drying temperature [Borges et al., 2021c]. As for the difference between states at 90°C SLJs, the behavior was similar to the ones obtained at 70°C due to the same explanation. While the mechanical properties of the PBT-GF30 decrease significantly with the water intake, the determining properties to the failure of the joint are those of the adhesive, since in these SLJ testes there was not even plastic deformation of the substrate.

Regarding failure mode, Figure 24, failure moves from cohesive in the dried condition to mixed failure, with adhesive failure regions in the aged condition and a similar failure mode after re-drying.

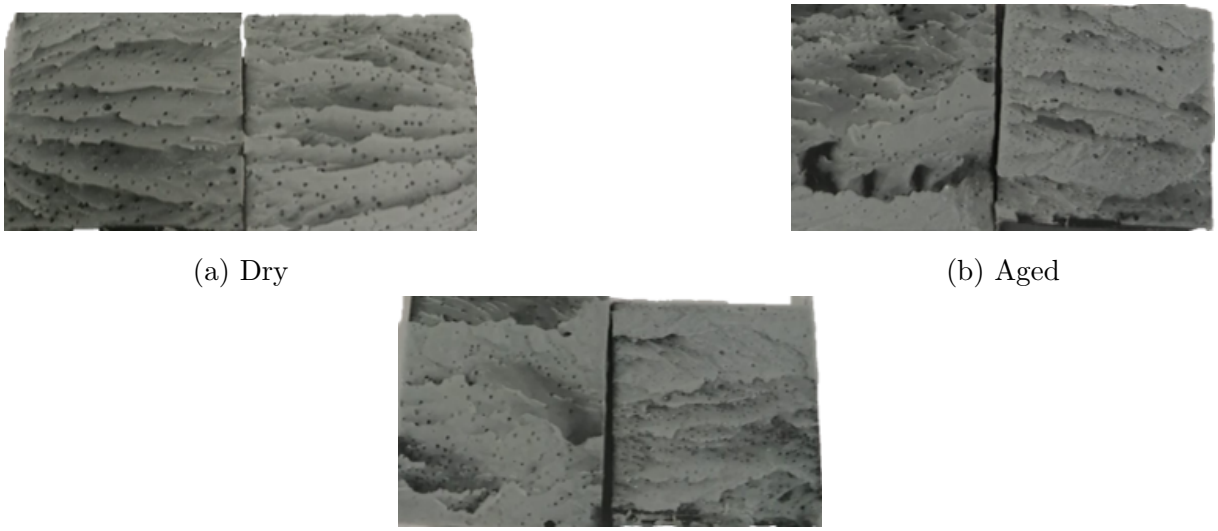

(a) Dry

(b) Aged

(c) Dried after aging

Figure 24: Failure surface of the SLJ for the different conditions tested at 90°C

Although for 70°C failure was closer to the middle of the substrate as the adhesive aged, after water immersion at 90°C [Borges et al., 2021b] there is already chemical degradation of the substrate, which can lead to release of chemical agents to the interface, degrading the bond strength by remaining at the interface of the chemical properties of the adhesive closer to the substrate, if it absorbs these components.

130°C

Figures 25 and 26 show representative $P - \delta$ curves of the most representative curve for each state and the failure load, respectively. The SLJs presented similar behavior as the two previous temperatures, the aged state was the one with higher strength, while the dried and dried after aging were very similar.

In comparison to the dried state at 70°C there was a decrease of 31 % in failure load, as in comparison with 90°C there was 5% decrease. The drop of mechanical behavior of the SLJ was not as pronounced as the temperature increases.

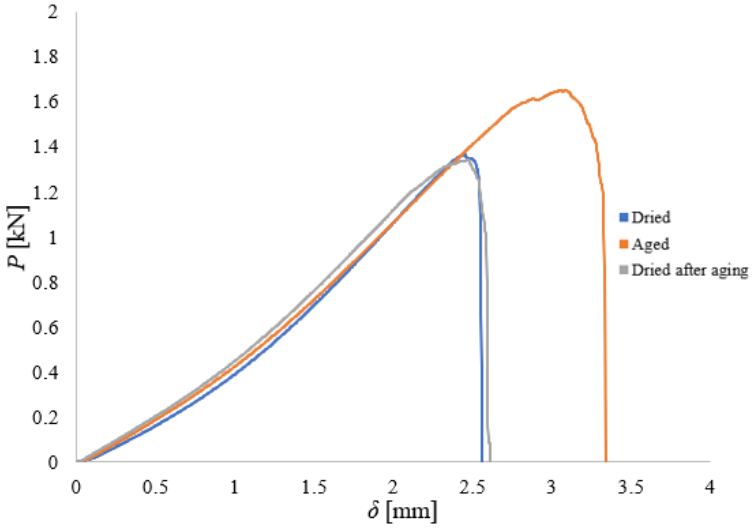

Figure 25: SLJ $P - \delta$ for the different conditions tested at130°C

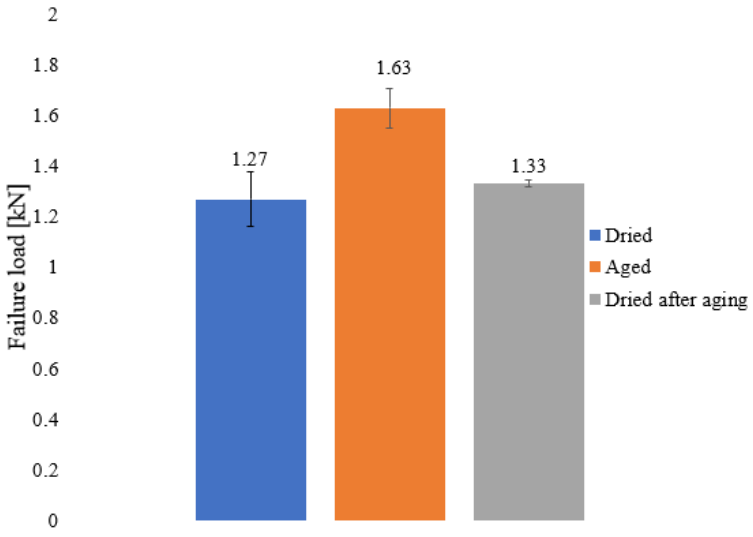

Figure 26: Failure load of the SLJ for the different conditions tested at 130°C

At 130°C the failure type is cohesive near the substrate in all states, however in dried after aging the failure starts to become adhesive. The motive for this is the same presented for 90°C, with temperature degradation playing an even higher role, that is why failure is always closer to the interface, and it increases from dried to aged, to dried after aging and, therefore, with increasing exposure time at 130°C.

(a) Dry

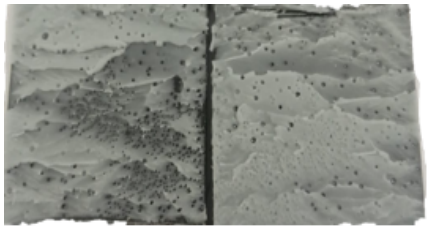

(b) Aged

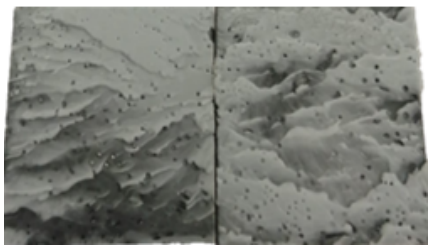

(c) Dried after aging

Figure 27: Failure surface of the SLJfor the different conditions tested at 130°C

B.4.4 Double cantilever beam (DCB)

70°C

In the DCB test, Figure 28, the substrates are under plastic deformation, which means the effect of temperature and himidity condition is going to have a higher weight on the properties of the joint.

Even though the properties of the PBT-GF30 decrease in the aged states, it is clear that the DCB at 70°C, as the SLJs at the three temperatures, increases its peak load and maximum displacement in the aged state, since the adhesive has better properties in this state.

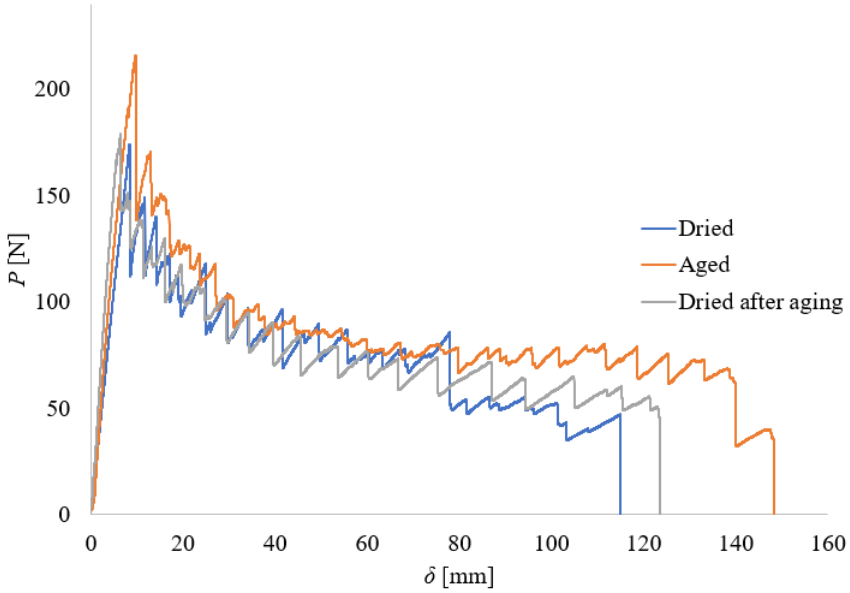

Figure 28: DCB $P - \delta$ for the different conditions tested at 70°C

The failure type, Figure 29, did not change significantly for state to state, being always cohesive near the substrate.

(a) Dry (b) Aged (c) Dried after aging

Figure 29: Failure surface of the DCB for the different conditions tested at 700°C

90°C

At 90°C, Figure 30, the impact of the hydrolysis of the PBT-GF30 with the water intake was noticeable. Comparing with the previous results, there was not an improvement in behavior in the aged state when comparing with the dried state.

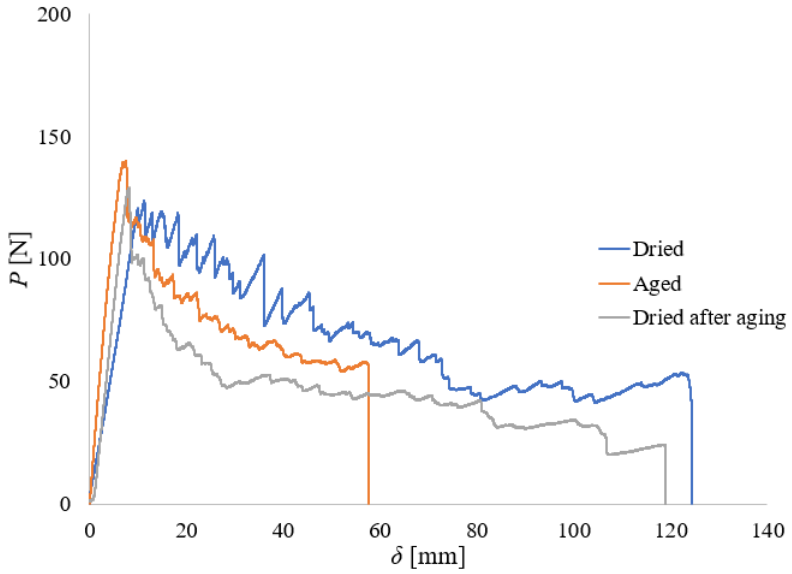

Figure 30: DCB $P - \delta$ for the different conditions tested at 90°C

This was due to the properties of the substrate of the substrate in this test, the substrate was under a significant plastic deformation. In fact, during the aged test, the failure was at the PBT-GF30. As seen previously, the strength of the substrate decreases when aged at 90°C with the aggravating factor of the chemical changes in the material,

which led to failure of the substrate.

When comparing the failure modes, Figure 31, the failure changed from cohesive near the substrate in the dried state to substrate failure in the aged condition. When re-dried, the substrate recovered some of its properties, and failure returned to the adhesive.

(a) Dry (b) Aged (c) Dried after aging

Figure 31: Failure surface of the DCB for the different conditions tested at 90°C

130°C

Regarding the results obtained at 130°C, Figure 32, it can be inferred that, as for 90°C, there was a deteorization of the polymeric matrix of PBT-GF30 in the aged condition due to water ingress that led to a substrate rupture (Figure 33), which explains the severe decrease in maximum displacement for the aged and dried after aging conditions.

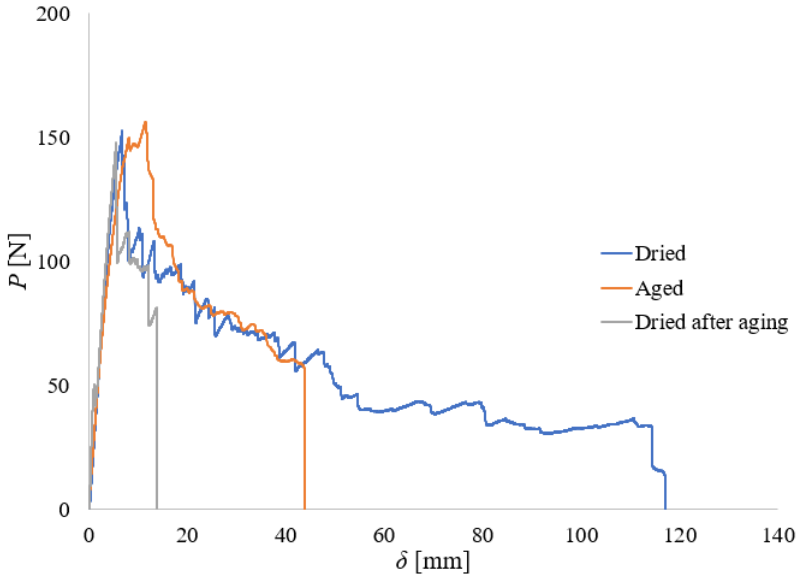

Figure 32: DCB $P - \delta$ for the different conditions tested at 130°C

However, the substrate, did not recover its mechanical properties after re-drying, as

it happened for 90°C, which is agreement to that was found for the bulk tensile tests, the increasing temperature leads to more significant and irreversible damage on the PBT-GF30. However, both the DCB and bulk tensile tests, the specimens were kept in water until saturation is reached and, the joint takes a longer time to saturate, which means the DCB was kept in water for a longer period of time, explaining the more extensive damage.

(a) Dry (b) Aged (c) Dried after aging

Figure 33: Failure surface of the DCB for the different conditions tested at 130°C

B.5 Numerical results

In this section, the water uptake level at the adhesive and substrate for the immersion times analyzed is defined. Additionally, for SLJ and DCB data from the numerical analysis is compared with the experimental data obtain in Section *Experimental results*. As explain in Section *Numerical model*, a SLJ and DCB model was created with the same geometry as the experimental geometry. The mechanical properties used in the simulations were obtained from the bulk tensile test of the adhesive [Borges et al., 2021c] and the PBT-GF30. The results are divided into joint geometry and temperature.

B.5.1 Water uptake of the joints

The water uptake as a function of time, as well as the time at which the joints were removed from water at the three temperatures, are presented in Figure 34. It should be noticed that, for SLJs, the respective immersion times of 30 days for 70 °C, 15 days for 90 °C and 1 day for 130 °C lead to the same water uptake in the adhesive and substrate.

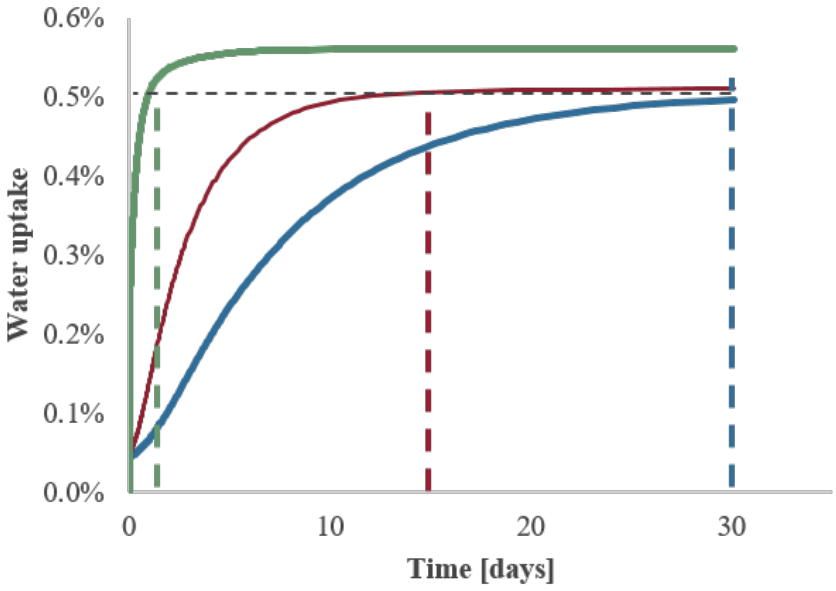

(a) Water uptake of the adhesive

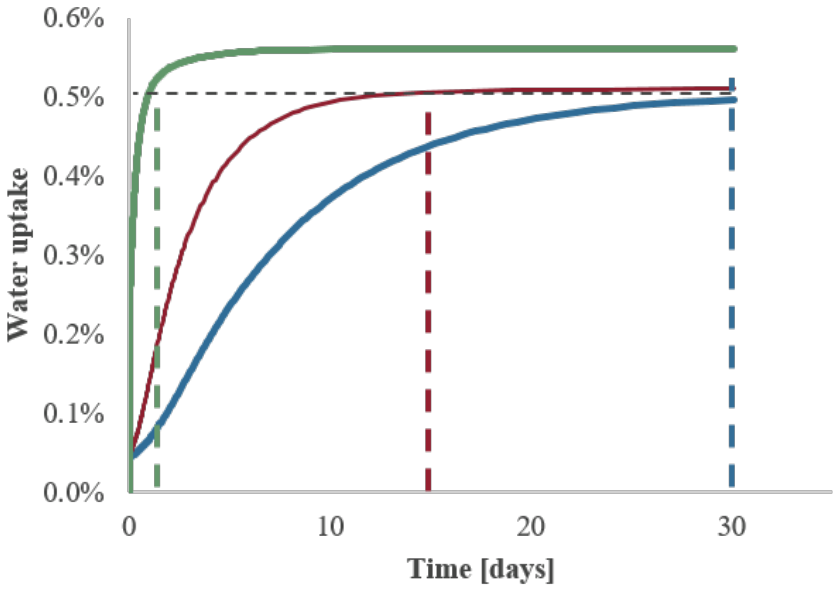

(b) Water uptake of the substrate

Figure 34: Numerical simulation of the water uptake in SLJs at the three temperatures considered

The same immersion times were considered for DCBs, for the time exposed to high temperatures humid environments to be similar. However, in these joints the water uptake, particularly at the substrates at higher temperatures, was smaller, since the substrate area exposed to water also decreased, Figure 35.

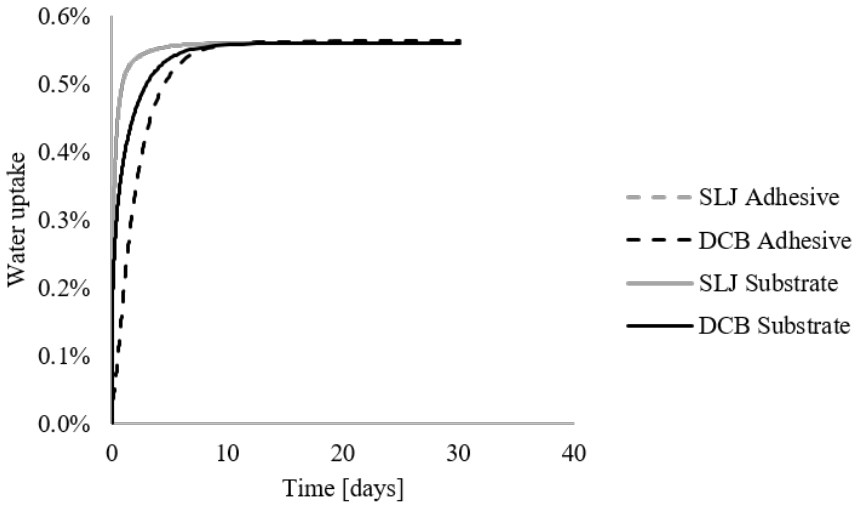

(a) 70 °C

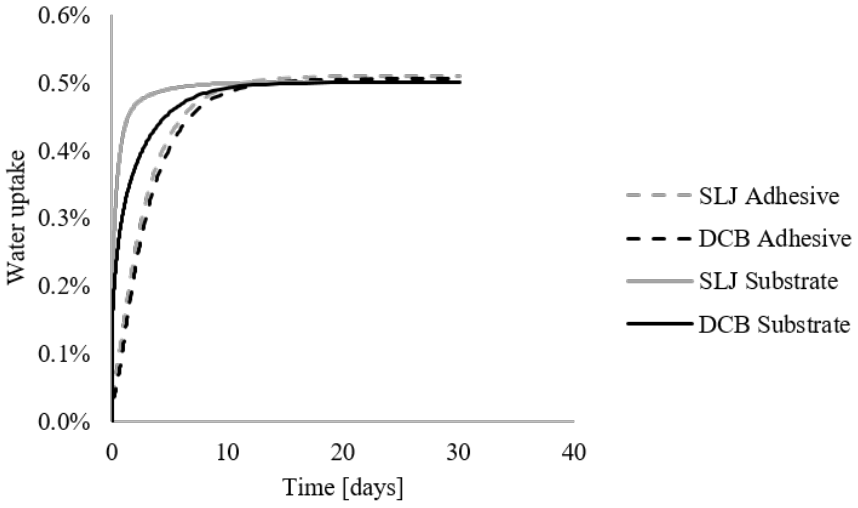

(b) 90 °C

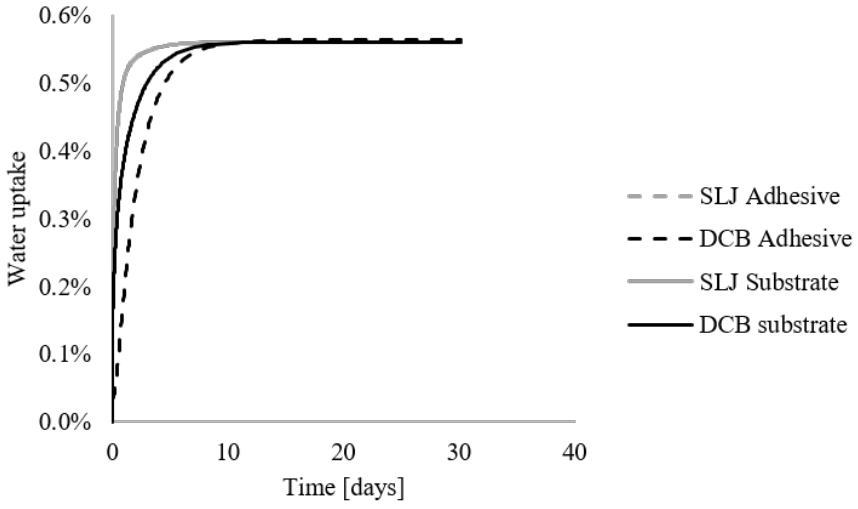

(c) 130 °C

Figure 35: Numerical simulation of the water uptake in the substrates and adhesive of SLJs and DCBs for the three temperatures considered.

B.5.2 Single lap joints(SLJ)

70°C

The Figures 36, 37 and 38 , show a comparison of the numerical results with the experimental results at the dried, aged and dried after aging state at 70°C. In general, the numerical failure load did not exhibit a significant difference. The $P-\delta$ curves were a good agreement with the experimental results. This numerical approach is valid to simulate the experimental result obtain at 70°C. However, the stiffness in the early part of the curve (produced by the SLJ test's non-linearity) is not represented by the numerical model, since the boundary conditions are intrinsically stiffer than those imposed on the experimental specimen [Machado et al., 2018].

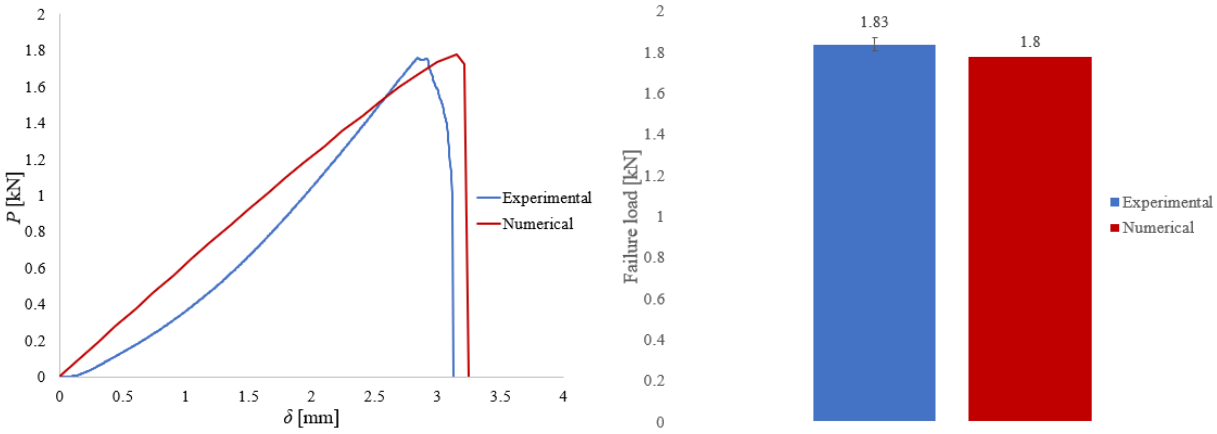

(a) P-δ (b) Failure load

Figure 36: Numerical results of the dried at 70°C SLJ model.

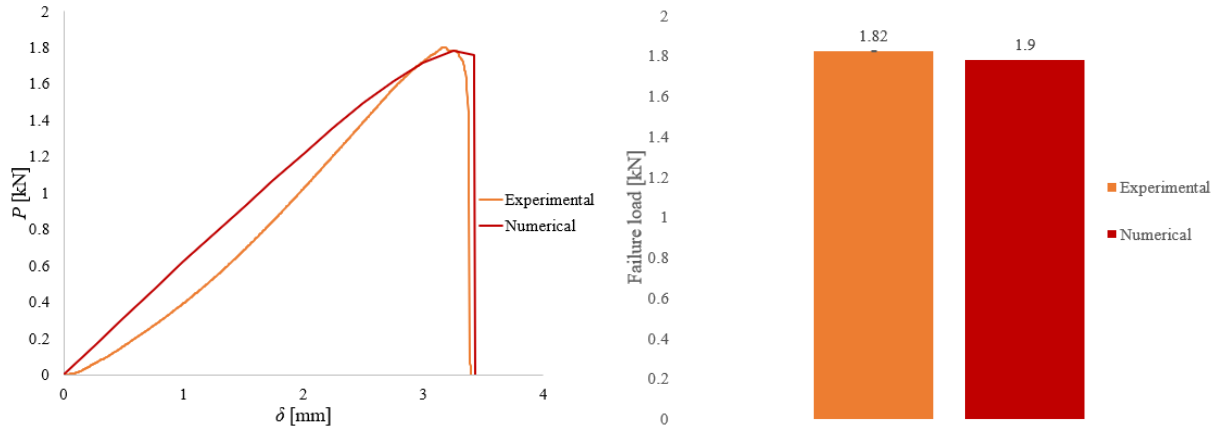

(a) P-δ (b) Failure load

Figure 37: Numerical results of the aged at 70°C SLJ model.

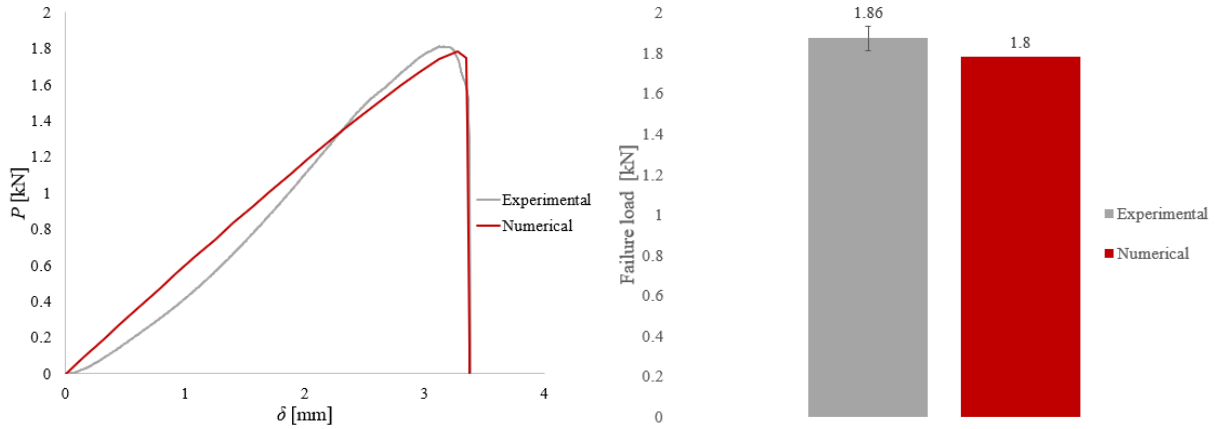

(a) P-δ (b) Failure load

Figure 38: Numerical results of the dried after aging at 70°C SLJ model.

The results being so accurately simulated from the bulk properties of the PBT-GF30 and silicone for each condition under analysis shows that, although there is some water being absorbed by the adhesive/substrate interface, it does not have a preponderant weight on the water uptake or failure of the adhesive joints, since the behavior of the joint can be simulated by the adhesive and substrate property variation.

90°C

The numerical results obtain for the three different states at 90°C are presented in Figures 39, 40, 41. The results showed a good agreement with the experimental results, although the stiffness, in the beginning, was not possible to of reproducing, as explain previously. The failure load obtain numerically were slightly higher for this temperature.

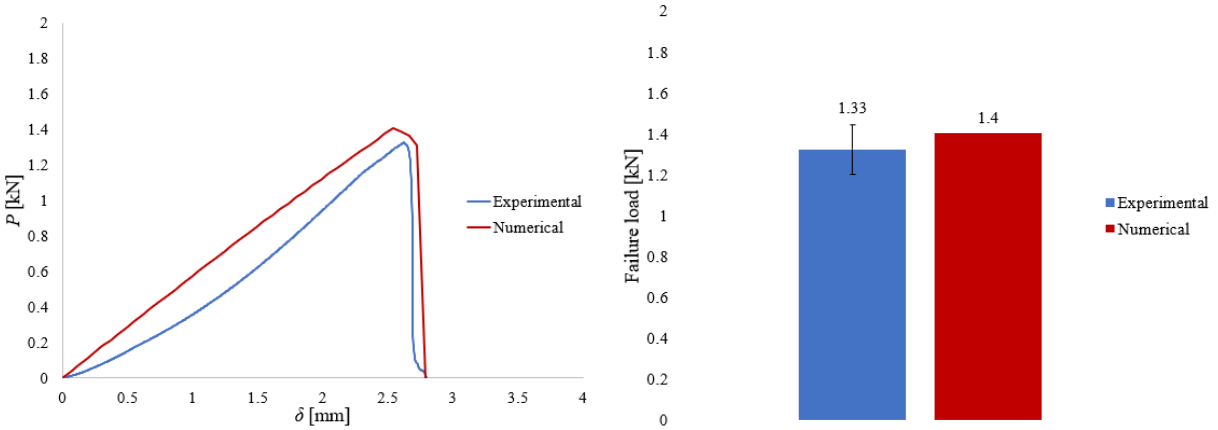

(a) P-δ (b) Failure load

Figure 39: Numerical results of the dried at 90°C SLJ model.

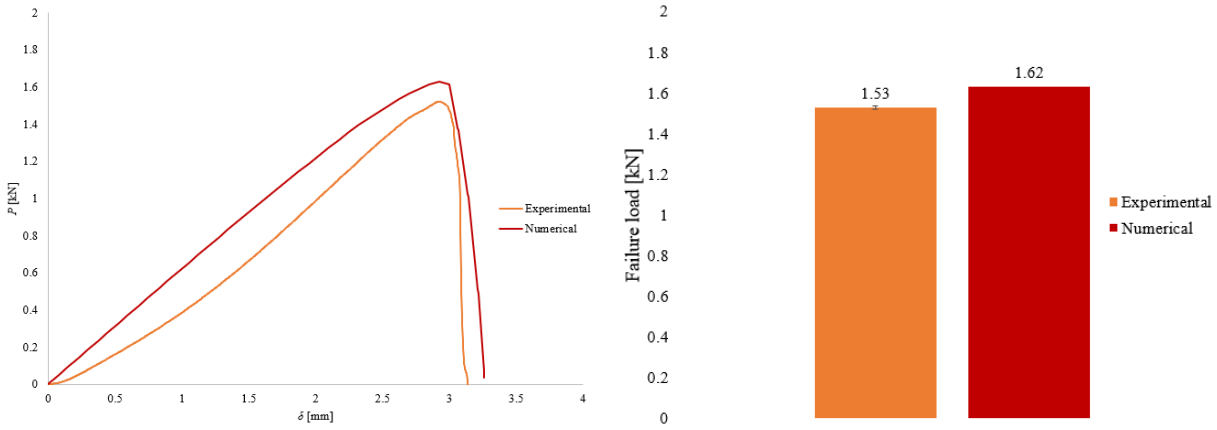

(a) P-δ (b) Failure load

Figure 40: Numerical results of the aged at 90°C SLJ model.

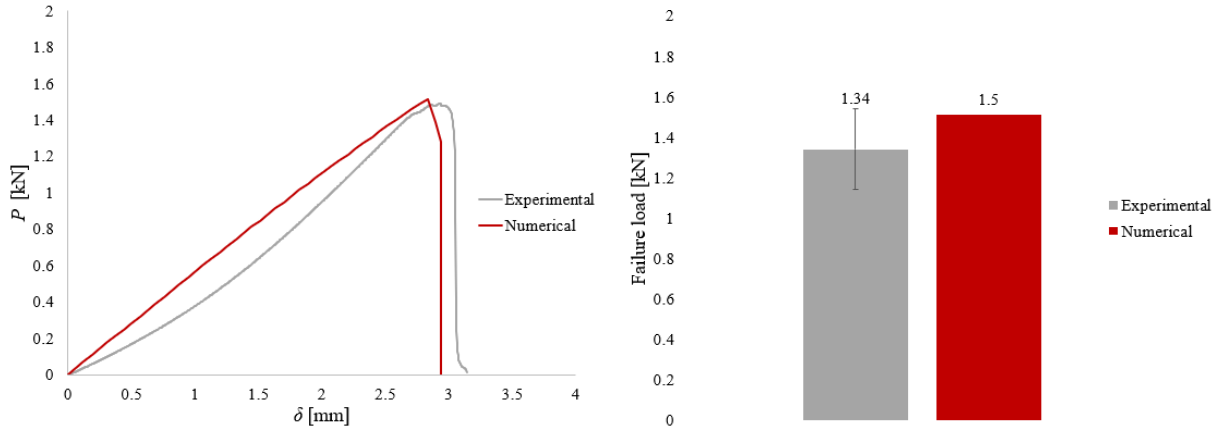

(a) P-δ (b) Failure load

Figure 41: Numerical results of the dried after aging at 90°C SLJ model.

130°C

For 130°C, the numerical model proved to be capable of simulate the experimental results obtained. Again, the failure load in the numerical model was slightly higher, while the $P - \delta$ curves showed a good approximation.

The numerical model for SLJ reproduce results that validated the experimental results of both bulk tensile tests of the PBT-GF30 and silicone as the SLJ of the PBT-GF30/silicone.

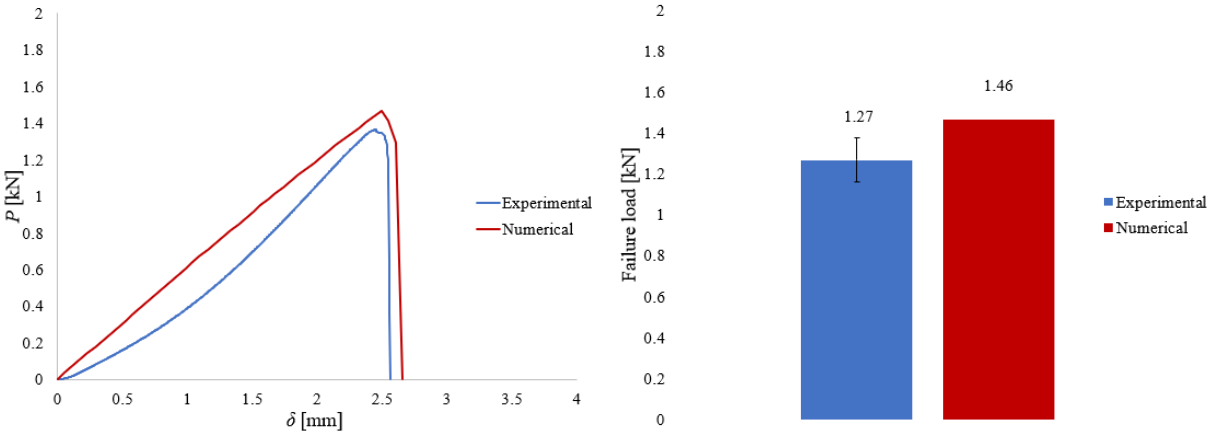

(a) P-δ (b) Failure load

Figure 42: Numerical results of the dried at 130°C SLJ model.

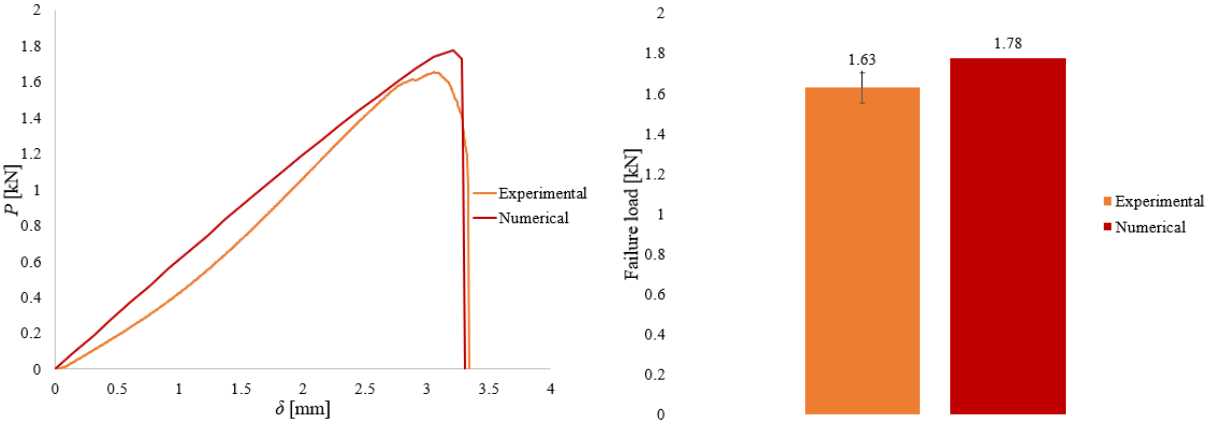

(a) P-δ (b) Failure load

Figure 43: Numerical results of the aged at 130°C SLJ model.

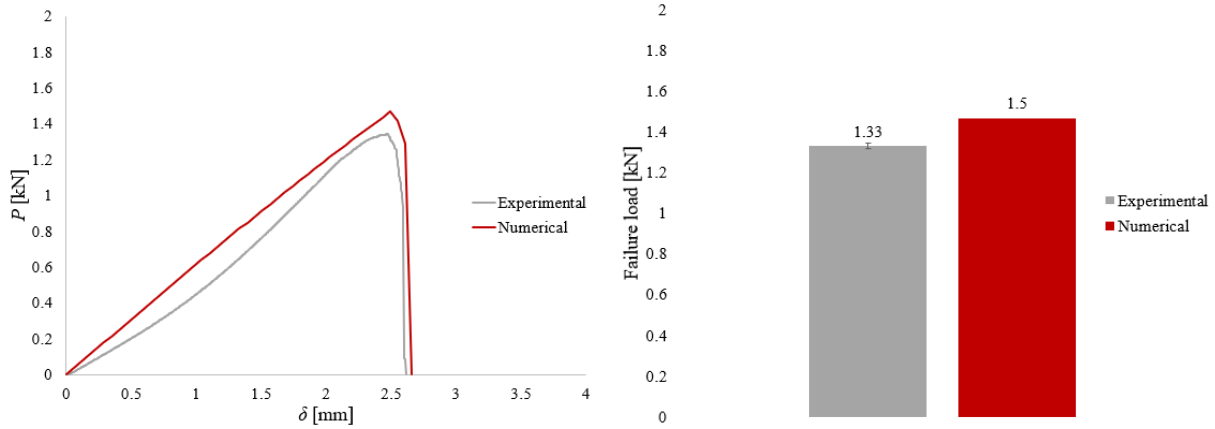

(a) P-δ (b) Failure load

Figure 44: Numerical results of the dried after aging at 130°C SLJ model.

B.5.3 Double cantilever beam (DCB)

70°C

In Figures 45, 46 and 47, a comparison between the numerical model $P-\delta$ curve with the mechanical properties obtain in the bulk tensile test of the substrate and adhesive, and the experimental $P-\delta$ curve are showed. The stiffness of the numerical model was almost equal to the experimental one, the dropping after the failure load was a good approximation. However, it was not possible to reproduce the end of the curve numerically.

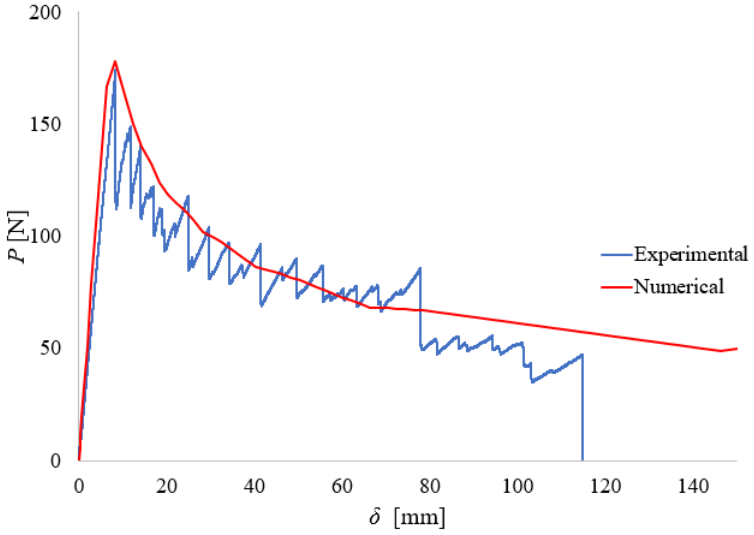

Figure 45: P-δ of the dried at 70°C DCB model

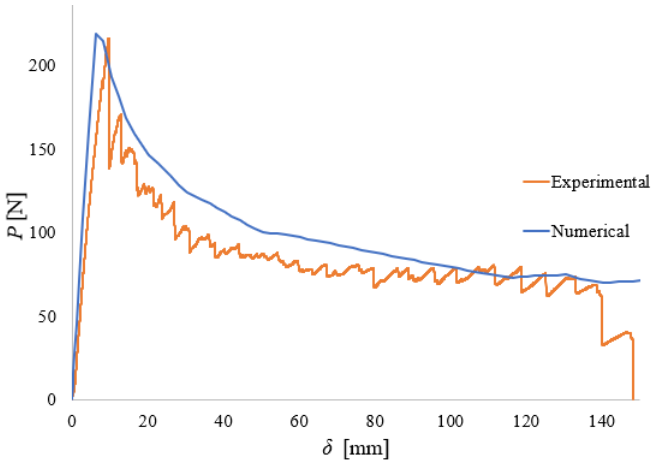

Figure 46: P-δ of the aged at 70°C DCB model

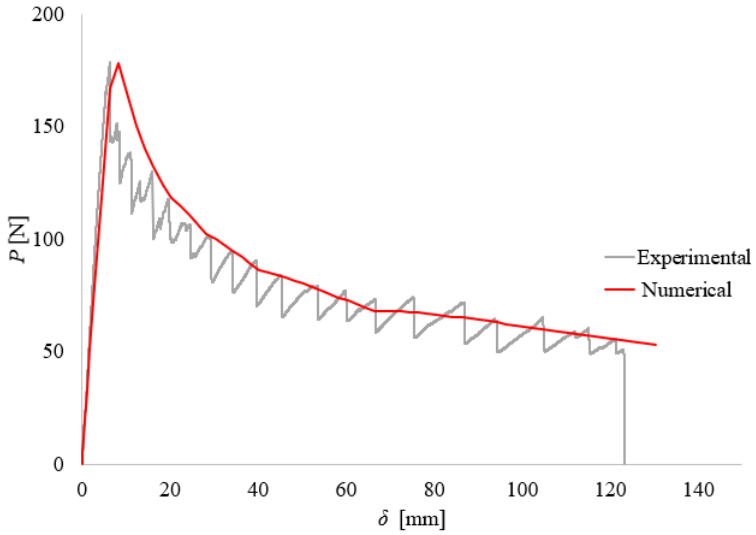

Figure 47: P-δ of the dried after aging at 70°C DCB model

90°C

At 90°C the results were similarly to the ones at 70°C, with basically the same stiffness as the experimental results and a good approximation of the failure load and dropping afterwards. Since the substrate broke in the aged state, the maximum strength value obtained in the bulk tensile test was imposed in the simulation, using the Von Mises stress criterion. When the substrate reached this value, it was assumed that the substrate would fail, and the simulation ended there. This approach showed a good approximation to the experimental $P - \delta$, as shown in Figure 49. The rest of the results are presented in Figures 48 and 50.

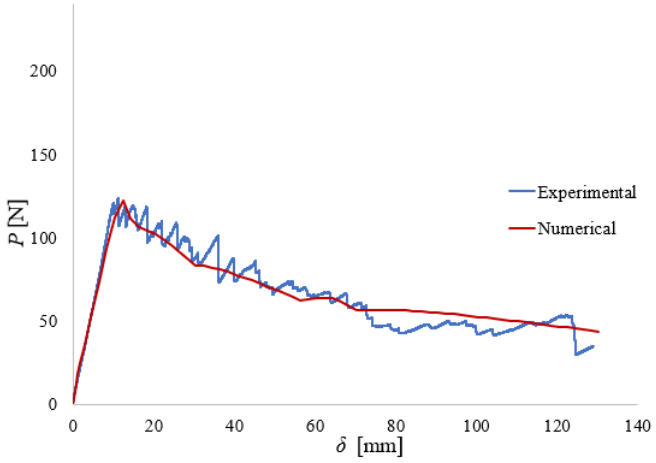

Figure 48: P-δ of the dried at 90°C DCB model

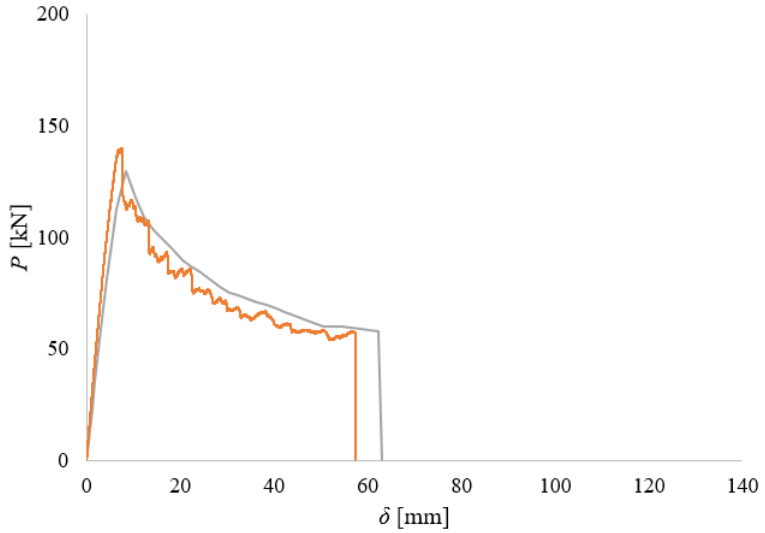

Figure 49: P-δ of the aged at 90°C DCB model

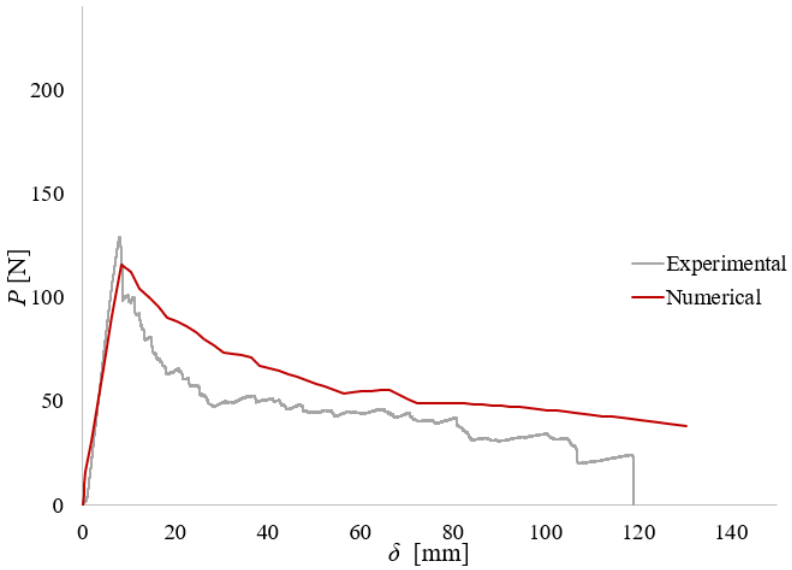

Figure 50: P-δ of the dried after aging at 90°C DCB model

130°C

Regarding the simulation for the 130°C experimental $P - \delta$ the same approach was taken. The experimental bulk tensile test values of the substrate and adhesive for each state were used. Again, the maximum stress obtained from the bulk tensile test of PBT-GF30 was imposed in the simulation of the aged and dried after aging states, since the substrate broke experimentally. When this value was reached, it was admitted that the simulation ended since the substrate broke. The results, again, showed an excellent approximation to the experimental results, which validates these and numerical approach. These simulations are shown in Figures 51, 52 and 53.

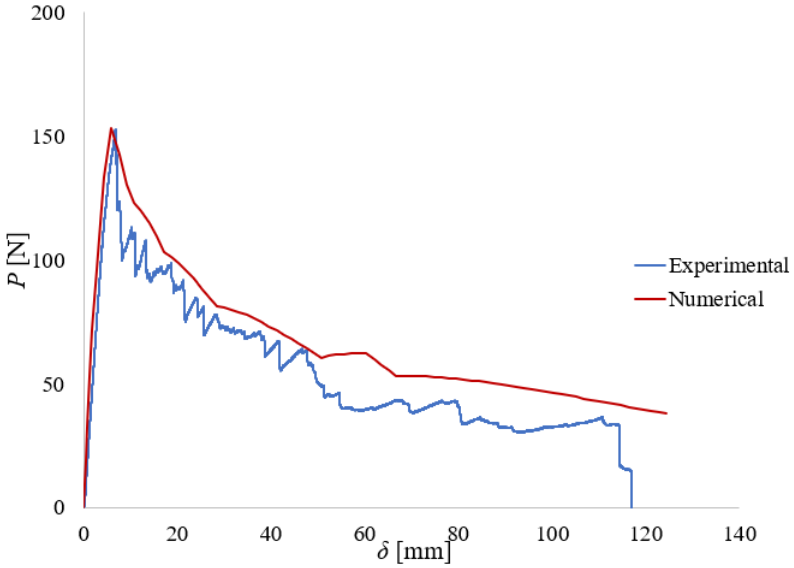

Figure 51: P-δ of the dried at 130°C DCB model

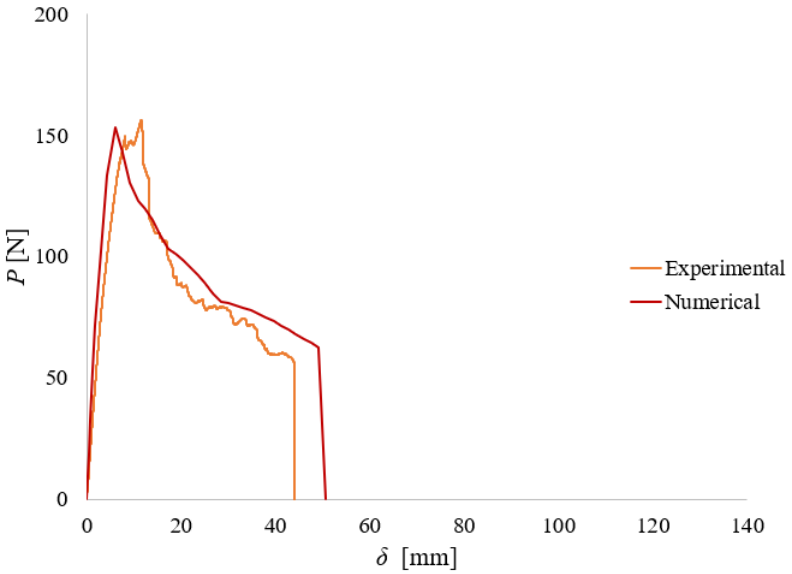

Figure 52: P-δ of the aged at 130°C DCB model

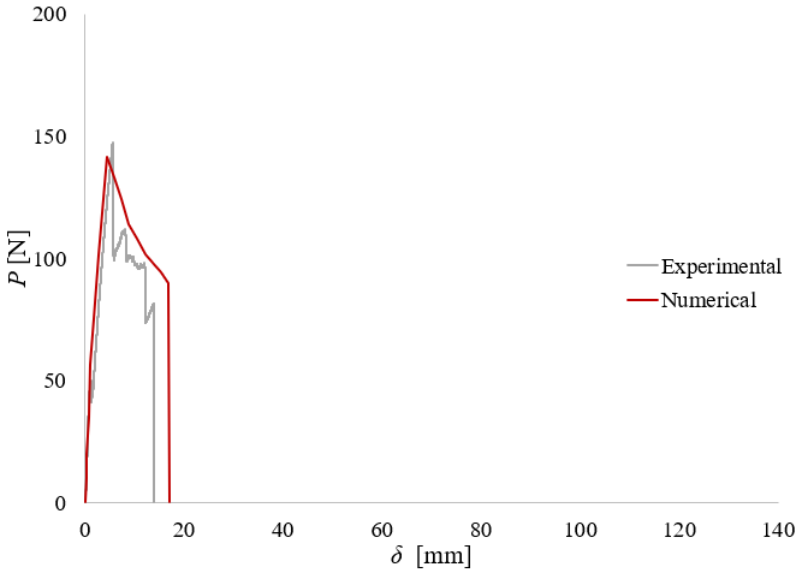

Figure 53: P-δ of the dried after aging at 130°C DCB model

B.6 Conclusions

In this study, the effects of humidity and immersion temperatures of the properties and failure mode of PBT-GF30/silicone bonded joints were analyzed. Three different temperatures and three different states were applied to "dogbones" of PBT-GF30, SLJ and DCB with PBT-GF30/silicone. Afterwards, a numerical model was created with the experimental values of the substrate from this work and the silicone values from [Borges et al., 2021c]. It is possible to conclude the following:

- The PBT-GF30 decreases its strength and Young's modulus with temperature and water intake.

- Almost all of the joints analyzed exhibited a better mechanical behavior when aged, since the strength of the adhesive increases with humidity.

- The exceptions were, for the DCBs, the aged joint at 90°C and the aged and dried after aging joints at 130°C, which failed on the substrate. This happens due to chemical changes in the PBT-GF30 after water immersion at temperatures above 85°C. Additionally, it was seen on the DCB and not on the SLJ because the loading of the substrate was more severe, with the substrate experiencing plastic deformation.

- With increasing temperature, there was a decrease in the mechanical behavior of the joints, regarding all humidity conditions, due to the decrease of strength of the adhesive with immersion temperature and the chemical changes and degradation of the substrate.

- With the experimental results of the tensile bulk tests of the PBT-GF30 and silicone from [Borges et al., 2021c], it was possible to simulate the joint behavior (for SLJ and DCB), achieving good agreement with the experimental results. This shows that the interface does not have a preponderant role in these phenomena.

References

[Borges et al., 2021a] Borges, C., Marques, E., Carbas, R., Ueffing, C., Weißgraeber, P., and da Silva, L. (2021a). Review on the effect of moisture and contamination on the interfacial properties of adhesive joints. *Proceedings of the Institution of Mechanical Engineers, Part C: Journal of Mechanical Engineering Science*, 235(3):527–549.

[Borges et al., 2021b] Borges, C. S., Akhavan-Safar, A., Marques, E. A., Carbas, R. J., Ueffing, C., Weissgraeber, P., and da Silva, L. F. (2021b). Effect of water ingress on the mechanical and chemical properties of polybutylene terephthalate reinforced with glass fibers. *Materials*, 14(5):1261.

[Borges et al., 2021c] Borges, C. S., Brandão, R., Akhavan-Safar, A., Marques, E. A., Carbas, R. J., Ueffing, C., Weissgraeber, P., and da Silva, L. F. (2021c). Influence of water and surfactant contamination on the properties of a silicone adhesive, before and after curing.

[Bowditch, 1996] Bowditch, M. (1996). The durability of adhesive joints in the presence of water. *International Journal of Adhesion and Adhesives*, 16(2):73–79.

[Carlberger et al., 2009] Carlberger, T., Biel, A., and Stigh, U. (2009). Influence of temperature and strain rate on cohesive properties of a structural epoxy adhesive. *International Journal of Fracture*, 155:155–166.

[da Silva et al., 2018] da Silva, L. F., Ochsner, A., and Adams, R. D. (2018). *Handbook of adhesion technology*. Springer Science & Business Media.

[Eftekhari and Fatemi, 2016] Eftekhari, M. and Fatemi, A. (2016). Tensile behavior of thermoplastic composites including temperature, moisture, and hygrothermal effects. *Polymer Testing*, 51:151–164.

[Errajhi et al., 2005] Errajhi, O., Osborne, J., Richardson, M., and Dhakal, H. (2005). Water absorption characteristics of aluminised e-glass fibre reinforced unsaturated polyester composites. *Composite Structures*, 71(3):333–336.

[Fan et al., 2019] Fan, J., Wang, Z., Zhang, X., Deng, Z., Fan, X., and Zhang, G. (2019). High moisture accelerated mechanical behavior degradation of phosphor/silicone composites used in white light-emitting diodes. *Polymers*, 11(8).

[F.Loureiro, 2020] F.Loureiro, R. . R. (2020). J-integral analysis of the mixed-mode fracture behaviour of composite bonded joints. *The Journal of Adhesion*, 96(1-4):321–344.

[Gustafson and Waas, 2009] Gustafson, P. A. and Waas, A. M. (2009). The influence of adhesive constitutive parameters in cohesive zone finite element models of adhesively bonded joints. *International Journal of Solids and Structures*, 46(10):2201–2215.

[Högberg et al., 2007] Högberg, J., Sørensen, B., and Stigh, U. (2007). Constitutive behaviour of mixed mode loaded adhesive layer. *International Journal of Solids and Structures*, 44(25):8335–8354.

[ISO, 2001] ISO, B., . (2001). Fibre-reinforced plastic composites. determination of mode i interlaminar fracture toughness, gic, for unidirectional reinforced materials.

[ISO294-3, 2002] ISO294-3 (2002). Plastics-injection moulding os test specimens of thermoplastic materials, part 3: Small plates.

[Kashi et al., 2018] Kashi, S., Varley, R., Souza, M. D., Al-Assafi, S., Pietro, A. D., de Lavigne, C., and Fox, B. (2018). Mechanical, thermal, and morphological behavior of silicone rubber during accelerated aging. *Polymer-Plastics Technology and Engineering*, 57(16):1687–1696.

[K.H. Jürgen Buschow, 2001] K.H. Jürgen Buschow, Robert W. Cahn, M. C. F. B. I. E. J. K. S. M. P. V. (2001). Fracture toughness testing of metallic materials. pages 3336–3340.

[Kurtz, 2016] Kurtz, S. M. (2016). 29 - characterization of physical, chemical, and mechanical properties of uhmwpe. pages 531–552.

[Loh et al., 2005] Loh, W., Crocombe, A., Abdel Wahab, M., and Ashcroft, I. (2005). Modelling anomalous moisture uptake, swelling and thermal characteristics of a rubber toughened epoxy adhesive. *International Journal of Adhesion and Adhesives*, 25(1):1–12.

[Machado et al., 2018] Machado, J., Marques, E., Silva, M., and da Silva, L. F. (2018). Numerical study of impact behaviour of mixed adhesive single lap joints for the automotive industry. *International Journal of Adhesion and Adhesives*, 84:92–100.

[Mohd Ishak et al., 2000] Mohd Ishak, Z., Ishiaku, U., and Karger-Kocsis, J. (2000). Hygrothermal aging and fracture behavior of short-glass-fiber-reinforced rubber-toughened poly(butylene terephthalate) composites. *Composites Science and Technology*, 60(6):803–815.

[Oldfield and Symes, 1996] Oldfield, D. and Symes, T. (1996). Long term natural ageing of silicone elastomers. *Polymer Testing*, 15(2):115–128.

[Rice, 1968] Rice, J. R. (1968). A path independent integral and the approximate analysis of strain concentration by notches and cracks. *Journal of Applied Mechanics*, 35(2):379–386.

[Viana et al., 2017] Viana, G., Costa, M., Banea, M. D., and da Silva, L. F. M. (2017). Behaviour of environmentally degraded epoxy adhesives as a function of temperature. *The Journal of Adhesion*, 93(1-2):95–112.

[White et al., 2009] White, C., Tan, K., wolf Andreas, and Carbary, L. (2009). *Advances in Silicone Adhesives*. Advances in Structural Adhesive Bonding, Woodhead Publishing Limited, Cambridge, -1.

[Wu et al., 2017] Wu, J., Dong, J., Wang, Y., and Gond, B. K. (2017). Thermal oxidation ageing effects on silicone rubber sealing performance. *Polymer Degradation and Stability*, 135:43–53.

[Zhu et al., 2009] Zhu, Y., Liechti, K. M., and Ravi-Chandar, K. (2009). Direct extraction of rate-dependent traction–separation laws for polyurea/steel interfaces. *International Journal of Solids and Structures*, 46(1):31–51.

C Paper C

Effect of surfactant contamination on the properties of aluminum/silicone adhesive joints.

R.Brandão[1], C.S.P. Borges[2], E.A.S. Marques[2], R.J.C. Carbas[2], A. Akhavan-Safar[2], P. D. P. Nunes[2], C. Ueffing[3], P.Weiβgraeber[3],F. Schmid[3], L.F.M. da Silva[1]

1 Departamento de Engenharia Mecânica, Faculdade de Engenharia (FEUP), Universidade do Porto, Portugal

2 Instituto de Ciência e Inovação em Engenharia Mecânica e Engenharia Industrial (INEGI), Portugal

3 Robert Bosch GmbH, Corporate Research and Advance Engineering, 71272 Renningen, Germany

Abstract: Adhesives are used to joint and seal electronic packaging. In these application, they are often used to bond aluminum components and, during the process of machining aluminum, oils and lubricants are used to facilitate the process. To remove these fluids, detergents such as surfactants are often used. However, if the surfactant itself is not removed completely and remains in the aluminum, it can affect the bond properties of the joint, leading to abrupt joint failure. In this work, adhesive joint properties as a function of the amount of surfactant at the surface were studied. For this, double cantilever beam (DCB) single lap joints (SLJ) were used. An additional scanning electron microscopy (SEM) analysis was conducted to clarify the results. It was found that the adhesive bond strength cohesive stress continuously decreases with increasing amount of contaminant. Similarly, the failure type progressively changed from cohesive to adhesive, which was attributed to the adhesive at the interphase absorbing the contaminant during curing, moving the failure to this region, until the absorption limit of the adhesive is surpassed and the surfactant remains at the interface, leading to interfacial failure. A numerical model was created to simulate the behavior of the experimental joints and obtain the properties of the interphase by applying the indirect method, and a numerical study was done on the sensitivity of the model to variations in cohesive properties in mode I for the DCB and in mode II for the SLJ.

C.1 Introduction

Adhesives are used in several applications due to their high strength to weight ratio, as well as not needing the introduction of holes or local heating of the components to join two materials [da Silva et al., 2018]. As a result, they are a better option in a wide range of scenarios, particularly when bonding notch sensitive composite materials, for instance the polybutylene terephthalate with 30% of glass fiber (PBT-GF30) housings for electronic components to the aluminum heat sinks found in vehicles. The components of this housing are often bonded using silicone, since high strength and stiffness are not a requirement in these applications, and thermal insulation and sealing are crucial. Prior to bonding, the aluminum is processed to obtain the final component desired and oils are used in the procedure. These oils are then cleaned using a detergent, containing surfactactants, which, if it is not carefully rinsed, can remain at the substrate surface and act as a contaminant.

When two substrates are joined using an adhesive, an interphase is formed between the adhesive and the substrate [Borges et al., 2021a]. This interphase layer, created upon adhesive bonding due to the adhesive/substrate interations, has specific chemical, physical and mechanical properties, different from those of the adhesive and of the substrate [Montois et al., 2006]. Possart et al. stated that, in adhesive joints with metallic substrates, this interphase is created due to a segregation of components at the metal interface or at the air, leading to heterogeneities in the liquid stage [Possart et al., 2006]. Thus, a specific layer, containing all those heterogeneities was formed between the adhesive and substrate and, since it has a gradient in chemical composition, chemical reactions during the curing of the adhesive also happen at different rates in this layer, thus leading to the conclusion that the cured interphase properties become field variables [Possart et al., 2006]. The exact size of this layer has not been determined, but it was said that it extended over a long range of some hundred micrometers in a three-dimensional structure. A work carried out by Roche et al. affirmed that in metal/epoxy adhesive joints, the glass transition temperature (T_g), the extent of the curing reaction between amine and epoxy, the interphase thickness, the residual stresses within the interphase and Young's modulus of the interphase all depend heavily on the amine nature [Roche et al., 2002], since it is the one that bonds with the metallic oxides on the surface of the substrate, creating organometallic complexes [Grangeat, 2019]. Voyutskii et al. explains adhesion as the result of interdiffusion of the macromolecules of the two material being bonded at the interphase [Voyutskii, 1963]. This interphase arises from a chemical bond created between the metallic oxide at the substrate surface and the amine monomer from the adhesive. The reaction with the amine groups, that can be from an isophorone diamine (IPDA) monomers, form orgono-metallic complexes. If this concentration is higher than

the solubility product, the complexes can crystallize as sharp needles [Aufray and Roche, 2006]. These crystals perform as short fibers in an organic matrix which leads to improvements of the stiffness, although the practical adhesion decreases since there is a growth of the residual stress when the interphase is formed.

In the case of a contaminated substrate surface, the contaminant can either be absorbed by the adhesive or remain at the adhesive/substrate interface. In both scenarios, the contaminants may affect the mechanical, chemical and thermal properties of the joint. If the contaminant is absorbed by the adhesive, it can affect the mechanical properties, particularly of the interphase layer, since it is the one in close proximity to the contaminated substrate. If the contamainant remain at the adhesive/substrate interface, it forms a thin segregation layer, in a manometric scale, that can severely weaken the adhesive bond due to the physical separation between adhesive and substrate, not allowing mechanical interlocking and also making it difficult to establish chemical bonds. This can promote interfacial defects such as weak bonds or debonding of the adhesive. These interfacial defects are thought to arise either from surface contamination prior to the application of the adhesive, incorrect curing of the adhesive, adhesive chemistry, or due to the environment surrounding the components during its service life or any combination of these causes [Jeenjitkaew et al., 2010]. Weak bonds are very difficult to detect, often being only noticed when they cause premature failure of adhesive joints. Additionally, they are very challenging to reproduce experimentally so that detection mechanisms are developed. Brotherhood et al. and Marty at al. produced weak bonds by contaminating the joint with a very thin layer of several contaminants. In their research, contaminants such as release agents and silicone-based oil, showed promising results as candidates for creating constant zero volume debonds [Brotherhood et al., 2002, Marty et al., 2004]. In addition to manufacturing weak bonds by surface contamination, Drewry et al. created weak joints using a consistent amount of bearing grease (wet lubrication) in single lap joints. These joints showed a reproducible decrease in shear and tensile strength [Drewry et al., 2009]. In general, as seen, contamination studies are challenging since to characterize the effect of the contaminant joints with a constant amount of contaminant, distributed evenly along the overlap must be produced.

To avoid the weak bonds or zero volume debonds and create a strong bond between adhesive and an oil-contaminated metal surface, regardless of surfacial contamination, the adhesive needs to be able to perform two separate jobs. First, the adhesive must be able to move the oil from the metal surface directly. Second, the adhesive must be able to absorb most of the oil [Pramanik et al., 2017]. Greiveldinger et al. studied the diffusion of an industrial mineral oil into an epoxy resin in an adhesive joint. The contaminant was initially placed on the substrate. Once the adhesive begins to cure, the

oil diffuses into the bulk adhesive. This process occurs quickly at the beginning of the curing cycle. Ahead of the adhesive curing, the Fourier-transform infrared spectroscopy (FTIR) profile at the interface is quite similar to that of the oil, showing that the oil is still at the adhesive/substrate interface [Greiveldinger et al., 2000]. However, at the end of the curing process, it resembles the uncontaminated adhesive. After a certain period of time in the curing cycle, it is noticeable that some oil leaves the adhesive, which is related to the crosslinking of the adhesive, since the adhesive shrinks just slightly on crosslinking, and this compression then result in the expelling of some contaminant from the adhesive. Crosslinking of the adhesive is very similar with and without the initial presence of oil at the interface, as far as the contaminant has been mostly absorbed by the adhesive [Borges et al., 2021a, Greiveldinger et al., 2000].

Contamination can have an impact on several stages of adhesion, the wettability of the surface, the curing process and the mechanical properties of the final joint such as strength [Akiyama et al., 2020a] or in the curing process. The process of contamination can happen in different stages of the process, it can occur during manufacturing of the substrate which leads to a change in the surface energy. Hoffmann et al. studied different types of contamination susch as release agents, moisture, fingerprint, thermal degradation and de-icing fluid before being bonded on the metallic stamp. For all types, the different levels of contamination were evaluated and it was noticed a decrease of the adhesion strength for each scenario, especially with the increase of the level of contamination [Hoffmann et al., 2018]. A. N. Rider et al. showed the surface energy changed during pre-treatments of an aluminum substrate and with contaminant post pre-treatments. During the pre-treatments steps, the surfacial levels of hydrocarbon decrease which leads to an increase in surface hydrophicility, which means, an increase of the surface energy what enables the adhesive to wet the substrate and provides a better formation of adhesive bonds [A. N. Rider, 1999].

For a better contact between the substrate and the adhesive, the contaminant should be displaced from the substrate at adhesive application. However, some contaminant can be physically stuck due to the roughness of the substrate, Figure 1. This remaining contaminant must be absorbed by the adhesive to avoid a physical separation between the adhesive and substrate. Nonetheless, as discussed above, when the adhesive absorbs contamination, its properties might be affected. Debski et al. studied this effect, working on the T_g of resins as a function of the oil content. The results stated that T_g during cross-linking was heavily reduced by the oil content, the more contaminant is present the more the effect was noticeable [Debski et al., 1986]. Thus, there is an undeniable change in cross-linking kinetics due to the presence of contaminant.

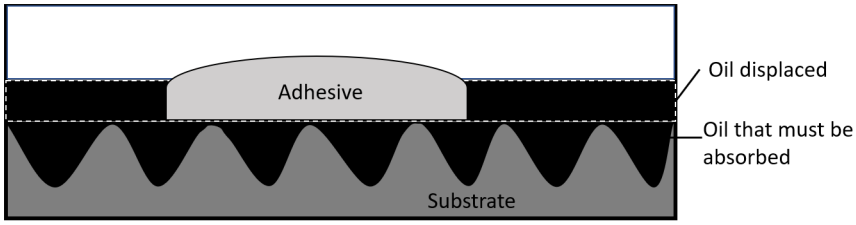

Figure 1: Oil accommodating adhesives

Akiyama et al. examined the effect of various types of contaminants in the properties of two adhesive joints, one using an epoxy adhesive and the other an second generation acrylic (SGA) adhesive. Two of the contaminants were surfactants, stearic acid and dodium dodecyl sulfate (SDS). The authors found that the stearic acid decreased the bond strength of both joints even with a small amount of contaminant, while using SDS only after 5 layers of contaminant there was a breakdown in the properties of the joints [Akiyama et al., 2020b]

As discussed to this point, in the studies found in literature, the adhesives analyzed are usually epoxies. This study strives to enrich the knowledge developed up to this point by analyzing the effect on silicone adhesives.

Due to the low Young's modulus of silicone adhesives, which is generally below 10 MPa, they are usually applied in non-structural and semi-structural applications that require flexible bonding, resistance to severe environmental and high service life. One of the advantages of silicone adhesives is the wettability, silicons wet most substrates, even under bad conditions due to their low surface tension (ca. 21–22 mN m^{-1}). Another advantage is that cured silicone adhesives display good elastomeric properties like movement capability, elastic recovery (85-98 %) and low creep when compared to others organic adhesives, they are much less temperature dependent. Their good fatigue resistance allows them to withstand cyclic loading in the adhesive joint caused by flexible flanges, equipment or component vibration, as well as temperature cycling of joints with high differential thermal expansion of substrates [White et al., 2009].

In this study, the effects of the surfacial application of surfactant on the properties of joints with aluminum substrates and silicone adhesive is going to be studied. For this, different contamination levels, imposed by the amount of contaminant applied, are going to be analyzed. To fully study the effect on the joint, strength tests, such as single lap joints (SLJ) and facture tests, such as double cantilever beam (DCB) are going to be performed. The contaminant used is a surfactant, used in the industry to clean oils or lubricants used during the manufacturing process of aluminum components. To validate

the experimental results, a numerical simulation using *Abaqus* through the inverse method was created. The numerical simulation showed a good approximation to the experimental study. The influence of the cohesive properties of the interface layer on the numerical model was also studied in detail.

C.2 Experimental details

C.2.1 Materials

Adhesive

The adhesive studied in this work is a two-part silicone elastomer adhesive, used both to join and seal the parts of the housing of electronic components used in the automotive industry. The general properties of the adhesive can be seen in Table 1.

Table 1: General properties of the adhesive used.

Type of adhesive	Supplied as	Cure cycle
Silicone elastomer	Two-part	120 °C / 25 min

As for the mechanical properties of the adhesive, Borges et al, performed a work where it was found that Young's modulus and tensile strength of this adhesive [Borges et al., 2021b]. The results are represented in Table 2.

Table 2: Mechanical properties of the adhesive used.

Tensile strength/ MPa	2.72
Young's modulus/ MPa	1.34

Substrate

The substrate used was aluminum 6082-T6. This material has an Young's modulus of 70 GPa and a Poisson's ration of 0.33.

Contaminant

The contaminant considered is a surfactant used to clean oil from aluminum surfaces, Cocosalkylaminethoxylate, supplied by SysKem Chemie GmbH (Wuppertal, Germany).

The general specification are shown in Table 3.

Table 3: Product Specification, given by the supplier [Cocosalkylaminethoxylate, 2020]

Cocosalkylaminethoxylate	
Chemical Name	$Amines, cocoalkyl, ethoxylated$
Appearance	$Brown$
pH	$9 - 11$
Moisture	$max 1.0\%$
Density	0.95

C.2.2 Specimen manufacturing

Surface treatment and contamination

The aluminum substrates were treated using two different methods: sand paper and sulfuric acid anodizing. The sand paper is an intermediate cleaning, removing contaminated layers from the surface. As for the sulfuric acid anodizing, it is employed since it improves porosity, increasing the bond strength and giving the substrates better corrosion resistance. The aluminum substrates are immersed in an aqueous phosphoric acid solution with a concentration of 9% (m/m) during 25 min according to the ASTM D3933 standard [International, 2017]. Afterwards, they are cleaned with distilled water and acetone.

After the pre-treatments, the contaminant was applied through spraying an aqueous solution of contaminant with a concentration of 10 g/L. Four different levels of contamination were considered, governed by the number of sprays applied, ranging from no contamination to 1, 4 and finally 10 sprays. When applying the contaminant, the spray nozzle was kept vertically aligned to the middle of the overlap and at a constant distance of 300 mm to ensure a homogeneous contaminant distribution across the surface area and repeatability of the process.

Finally, the substrates were placed in a climatic chamber at 70°C for 12h to evaporate the water in the solution and ensure that, at the time of adhesive application, only contaminant would be present at the overlap.

Double cantilever beam (DCB)

Aluminum substrates were used for the DCB specimens. The bondline thickness was 1 mm, and it was controlled by the introduction of calibrated tape between the substrates before the application of adhesive, which was removed after curing of the adhesive. The pre-crack was guaranteed through the introduction of a 0.1 mm thick sharp razor blade mid-thickness of the adhesive layer. The geometry of the joint is shown in the Figure 2.

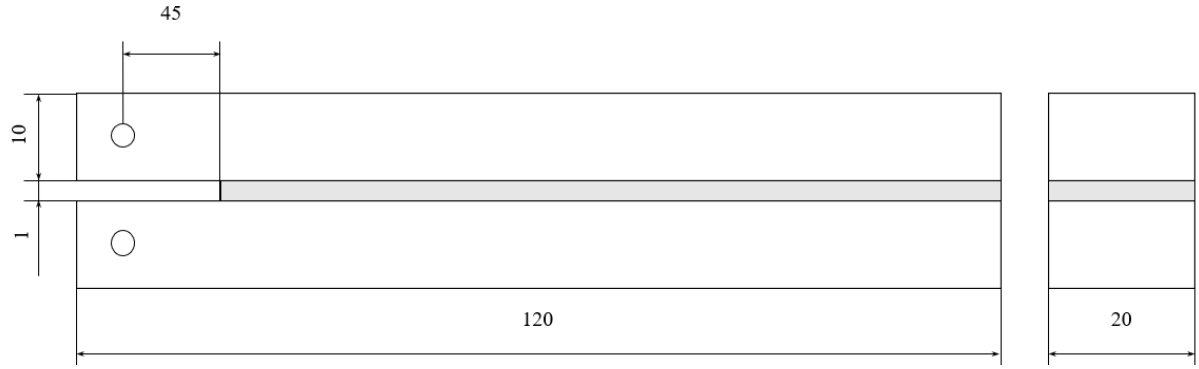

Figure 2: Schematic representation of the DCB, dimensions in mm.

Single lap joint (SLJ)

Aluminum substrates with 2 mm of thickness and 25 mm of width were used for SLJs for all levels of contamination. The overlap length was 25 mm and the bondline thickness of adhesive was 1 mm. In order to achieve that, packing shims were used to provide the necessary spacing between the two substrates. The geometry of the joint is represented in Figure 3.

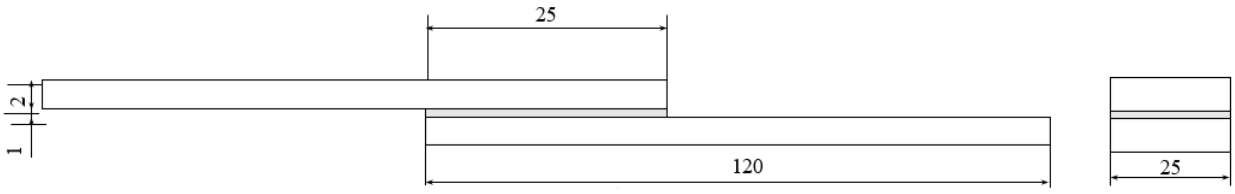

Figure 3: Schematic representation of the SLJ, dimensions in mm.

C.2.3 Scanning electron microscopy (SEM)

Scanning electron microscope (SEM) was employed to analyse the contaminant influence on the substrate, in a joint with contaminant and in bulk adhesive. It was studied if the adhesive had absorbed contaminant particles or if it would only stay in the interface. Clean and contaminated substrates, neat adhesive and joints with contaminant were

compared. To make the effect of contaminant clearly stand out, the higher contamination level (10 sprays) was used.

Borges et al. investigated this effect on the adhesive, analysing both both neat adhesive and with multiple contamination levels, the substrate (without contaminant and contaminated) and a fracture surface of a SLJ were analyzed [Borges et al., 2021c].

C.2.4 Experimental procedures

Double cantilever beam (DCB)

All tests were performed using an INSTRON® 3367 universal test machine (Norwood, MA, USA), with a load cell of 30 kN, at room temperature and constant displacement rate of 2 mm/min. The load–displacement (P–δ) curves for all tests were registered by the universal testing machine and were compared for all contamination levels. At least three specimens were tested for each contamination level.

The fracture toughness of the neat adhesive in mode I, G_{IC}, was determined in a previous work by the same authors using a standard DCB with high strength steel substrates [Brandão et al., 2021].

Single lap joints (SLJ)

The SLJ were vertically placed and fastened using two grips prior to testing (pressure was produced using four bolts and exerting 20 Nm of torque to each bolt). Metal tabs were placed beneath one side of each substrate of the SLJs to keep the specimens horizontal when handled. During testing, two center pins were also used to control appropriate placement of the SLJ.

Load–displacement (P–δ) curves were obtained for all SLJs tested. At least three specimens were tested for each contamination level.

Scanning Electron Microscopy (SEM)

Two distinct SEM microscopes were used for the analysis: JEOL JSM 6301F/Oxford INCA Energy 350/Gatan Alto 2500 (Tokyo, Japan) and FEI Quanta 400FEG ESEM / EDAX Genesis X4M (Tokyo, Japan) (Hillsboro, Oregon, United States). The research was carried out at CEMUP (University of Porto, Portugal). Using the SPI Module Sputter Coater, the samples were sputtered with an Au/Pd thin film for 120 seconds at a current of 15 mA.

C.3 Numerical model

In this study, four numerical models were implemented using the Finite Element Method (FEM) in *Abaqus* (Dassault Systèmes Simulia Corp.Providence, USA). Two different models were created for SLJ and DCB: one for the uncontaminated joints and other for the contaminated joints

The aim of the numerical model is obtaining the properties of the interphase, through reverse engineering, since the properties of the substrate and adhesive are known. For each level of contamination, with the load displacement curve from the DCB test, the tensile strength and mode I fracture toughness of the contaminant is tuned. Afterwards, with the load displacement curve of the SLJ, the shear strength and mode II fracture toughness of the contaminated layer are imposed.

Models for uncontaminated joints

The substrate and the adhesive were modeled as elastic and cohesive elements, respectively. The model has the same geometry as the experimental specimens. The two-dimensional (2D) mesh applied to the models was constructed with plain strain four-node quadrilateral solid finite elements (CPE4) for the aluminum substrates, and four-node cohesive elements (COH2D4) for the silicone adhesive. The mesh was refined to reduce element size in regions with large stress gradients. The mesh size of the cohesive elements was 0.08 mm, with one element across the overlap thickness. The triangular CZM was chosen since the material does not present plastic deformation.

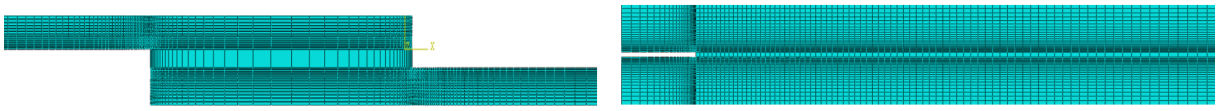

(a) SLJ (b) DCB

Figure 4: Mesh of the numerical model without contaminant

Regarding the SLJ model, the boundary conditions were set as indicated in Figure 5. At one end of the specimen, a clamp condition was added to simulate the static grip of the tensile machine while at the other end a longitudinal displacement was applied, retained in the perpendicular direction of displacement, thus simulating the grip that applies the force during the test.

Figure 5: SLJ without contaminant boundary conditions

As for the DCB model, a node on the edge of the lower substrate was restrained in the plane, and a node on the edge of the upper substrate was held horizontally and pulled vertically. Figure 6 shows the boundary conditions of the DCB numerical model.

Figure 6: DCB without contaminant boundary conditions

Models for contaminated joints

The substrate and adhesive were modelled as elastic elements, while the contaminant layer was modelled as cohesive elements, Figure 7. In the model for uncontaminated adhesive joints the cohesive elements were placed in the adhesive since the failure was cohesive through the adhesive, however, the contaminated joints fail through the interphase. Therefore, the cohesive elements are placed in this section. The sum of the heights of the contaminant layer and adhesive layer must be equal to 1 mm, since it is the distance between the substrates imposed in the experimental work. Although various authors state that the interphase has a size between 1 and 100 μm [Gao and Mäder, 2002]. The size of 0.1 mm was applied in *Abaqus*, however, it is important to emphasize that cohesive zone models are not especially affected by the size of the elements [Avendaño et al., 2016, Araújo et al., 2017].

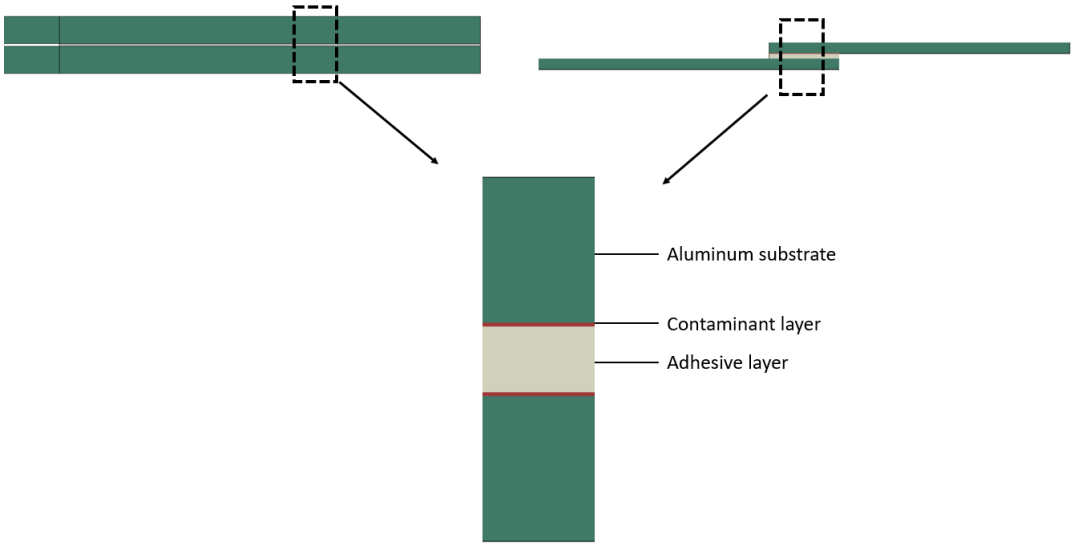

Figure 7: Numerical model of DCB and SLJ with a contaminant layer

A two-dimensional (2D) mesh was used, with plain strain four-node quadrilateral solid finite elements (CPE4) for the substrate and adhesive, and four-node cohesive elements

(COH2D4) for the contaminant layer. As in the uncontaminated model, the mesh was refined to reduce element size in regions with large stress gradients. The mesh size of the cohesive elements was 0.08 mm, with one element across the overlap thickness. The meshes of both SLJ and DCB are shown in Figure8.

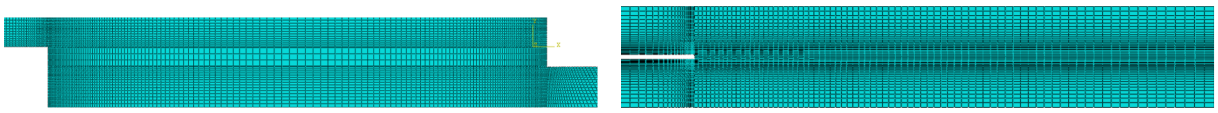

(a) SLJ (b) DCB

Figure 8: Mesh of the numerical model with a contaminant layer

C.4 Experimental results and discussion

C.4.1 Double cantilever beam (DCB)

The load-displacement, P-δ curves of the DCB tests are shown in Figure 9, through a representative curve. The results show that, as the amount of surfactant contamination raises, the failure load decreases. It would appear that the stiffness of the joint would slightly increase from no contaminant to the DCB with 1 spray, however this appears to be an outlier, since the trend is not followed for the other levels of contamination.

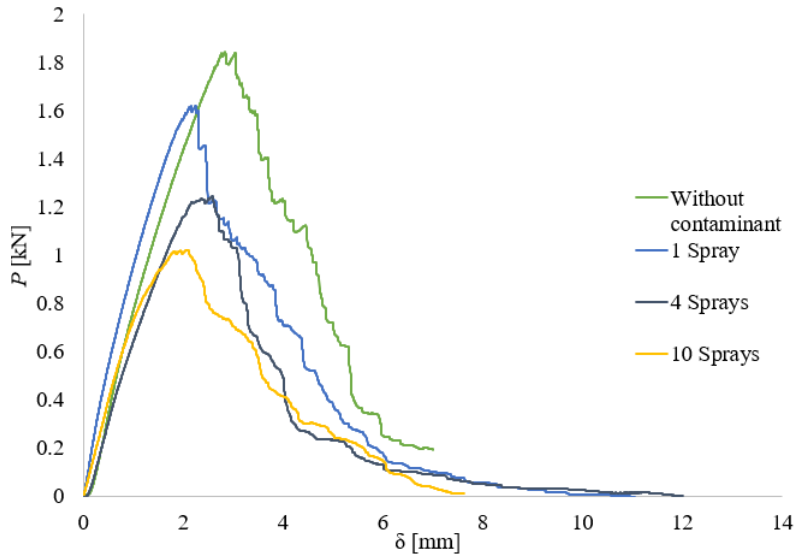

Figure 9: Representative P-δ curves for all the conditions tested

Figure 10, shows representative images of the failure surface of the DCB joints with different levels of contamination. When analyzing the failure surfaces it is noticeable that, as the amount of contaminant increases, the failure moves increasingly towards the interface. The joint without contamination exhibits cohesive failure through the middle of the adhesive. With 1 spray, the failure is still cohesive through the adhesive however, it is

closer to the interface, at the interphase. With 4 sprays failure is adhesive in most of the overlap, with some areas of cohesive failure near the substrate. Finally, with 10 sprays, failure is predominantly adhesive. As observed by Borges et al., the adhesive strength and stiffness decreases with increasing amount of contaminant included in the adhesive prior to curing [Borges et al., 2021c]. In this case, between the uncontaminated joint and the joint with 1 spray, it is thought that the adhesive at the interphase absorbs the contaminant placed in the substrate prior to bonding therefore, its strength decreases, leading failure to move closer to the interface. Increasing the contamination level, and reaching 10 sprays, the adhesive at the interphase absorbs as much contaminant as possible, however, there is still contaminant at the interface. At this point, because there is contaminant that remains at the interface, acting as a physical separation, the failure is adhesive.

(a) Without (b) 1 Spray (c) 4 Sprays (d) 10 Sprays

Figure 10: Failure surface of the different DCB conditions tested.

C.4.2 Single lap joint (SLJ)

Representative load-displacement P-δ curves for the SLJ tested are shown in Figure 11a. The results for the SLJ failure load for all levels of contamination are presented in Figure 11b. The results show that there is a big decrease in the failure load from the uncontaminated SLJ to the SLJ with one spray and then a steady decrease between sprays. Likewise, the displacement did suffer a decrease in relation to the SLJ without contamination, however between the different levels of contamination there was not a significant difference.

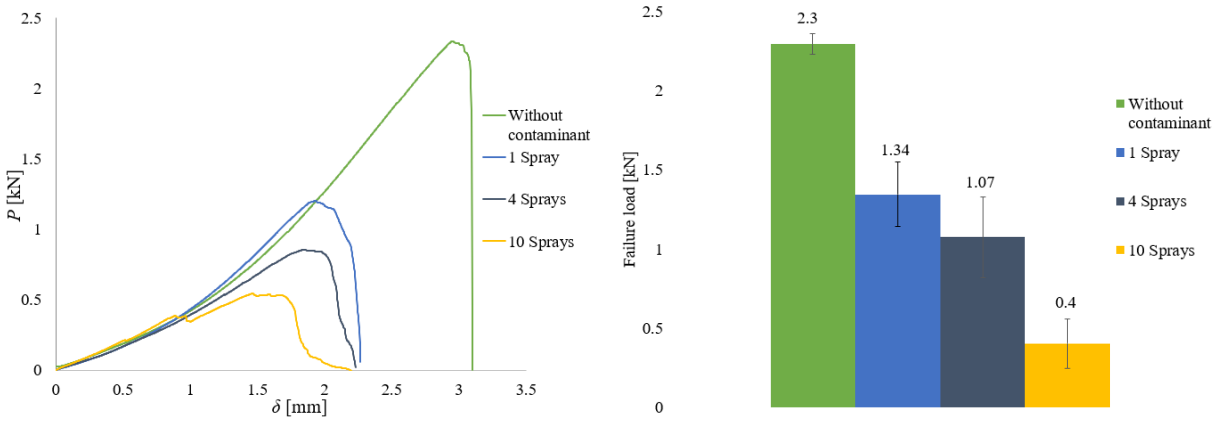

(a) P-δ (b) Failure load

Figure 11: Representative curves obtained using SLJ and failure loads

Representative images of the fracture surface of each condition tested are shown in Figure 12. The failure clearly shifts to the interface as the contamination level increases, changing from cohesive failure through the middle of the adhesive for the uncontaminated joint, to cohesive failure near the interface for 1 spray of contaminant, mixed failure (with areas of adhesive failure and mainly cohesive failure in the adhesive near the interface) for 4 sprays and adhesive failure for 10 sprays. The motives behind these failure modes are the same presented for DCB tests.

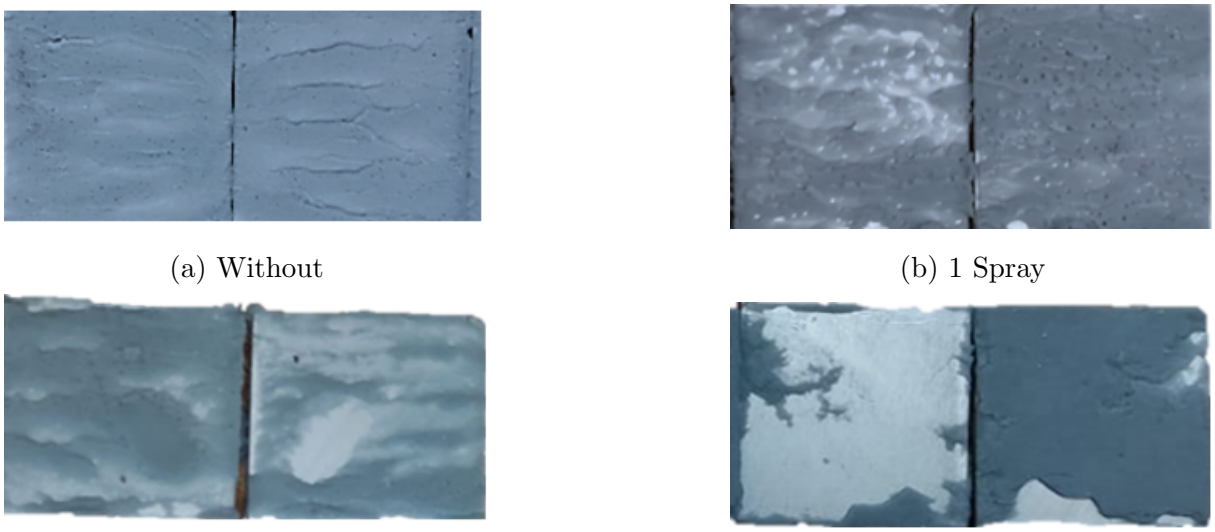

(a) Without (b) 1 Spray

(c) 4 Sprays (d) 10 Sprays

Figure 12: Failure surface of the SLJs for the different conditions tested

From the results presented, it is clear that the existence of a layer of contaminant in the interface prior to adhesion has an impact in the bonding properties in SLJs. With the increase of the amount of contaminant, the average shear strength of the SLJ suffer a steady decrease and the failure path moved from cohesive to adhesive.

C.4.3 SEM analysis

Figure 13, shows a SEM image of the adhesive and the EDS profile obtained. As expected, discussing a silicone adhesive, it is clear that it has carbon, silicon and oxygen(Figure 13b).

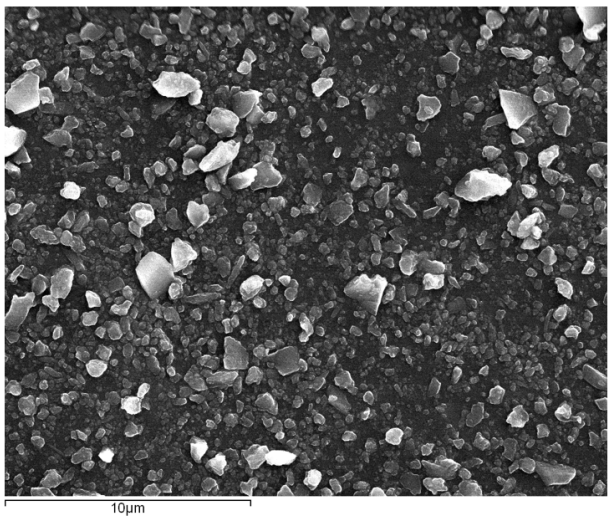

(a) Image of the neat silicone adhesive

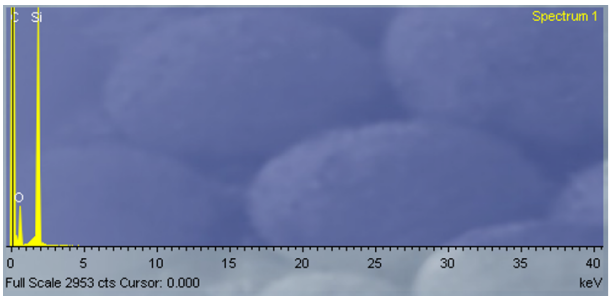

(b) Energy-dispersive X-ray spectroscopy of the neat silicone adhesive

Figure 13: SEM analysis of neat silicone adhesive

Two substrates were also analyzed. One without contaminant (Figure 14) and one with the highest amount of contaminant, 10 sprays (Figure 15). It was clear that there is a considerable difference in the roughness of the substrate, the substrate became smother and the quantity of carbon detected in the substrate with contaminant was higher, showing there was a second carbon rich component, which in this case is the contaminant.

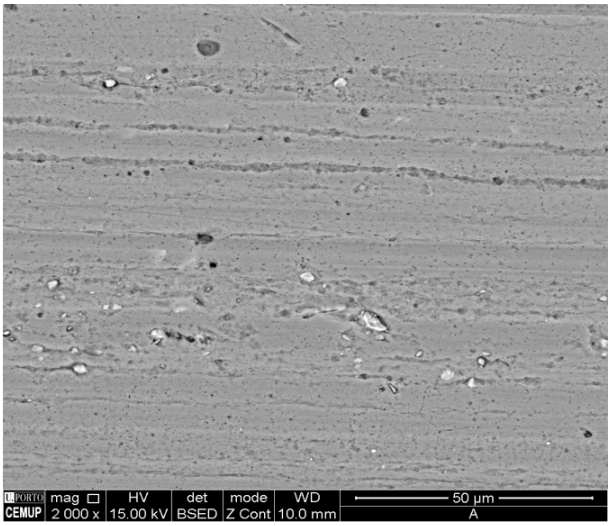

(a) Image of the substrate without contaminant

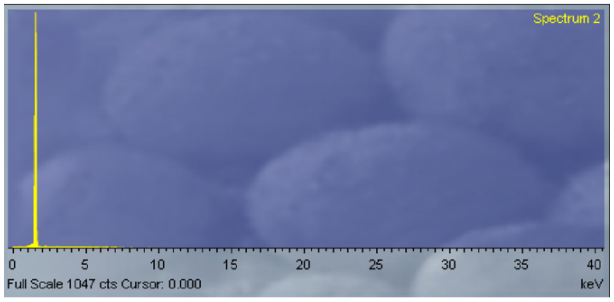

(b) Energy-dispersive X-ray spectroscopy of the substrate without contaminant

Figure 14: SEM analyis of substrate without contaminant

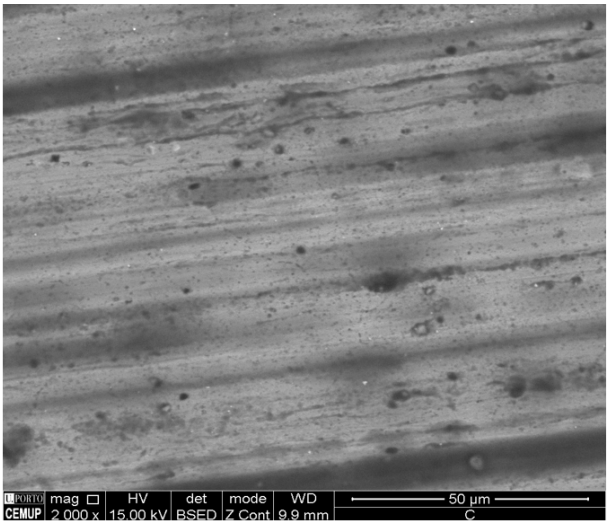

(a) Image of the contaminated substrate

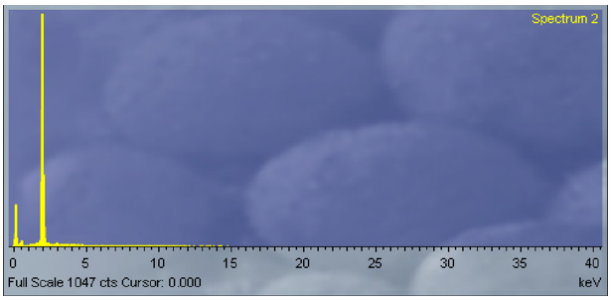

(b) Energy-dispersive X-ray spectroscopy of the contaminated substrate

Figure 15: SEM analysis of substrate with contaminant

This explains the difficulty silicone has in the mechanical interlocking to the aluminum, which causes a decrease in bondability between them. At this point, when the substrates are bonded, the adhesive has two main alternatives: absorbing the contaminant, decreasing the strength of the adhesive close to the substrate and exhibiting cohesive failure in the adhesive but at the interphase (as seen for 1 and 4 sprays of contaminant), or if the adhesive reaches a point where it can not absorb more contaminant, it is going to remain at the adhesive/substrate interphase during curing, creating a physical separation between them (as seen for 10 sprays). Since in the SEM analysis the 10 sprays condition is being analyzed, the second behavior is expected.

Therefore, in order to fully understand if in fact that was the explication, an adhesive joint with 10 sprays of contaminant was also analyzed (Figure 16).

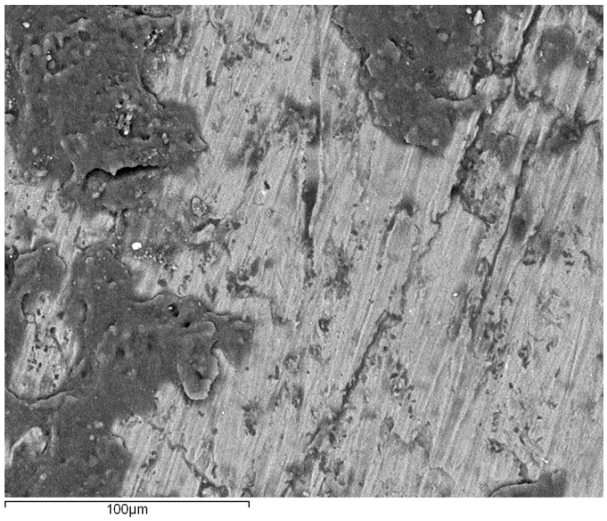

(a) Image of fracture surface

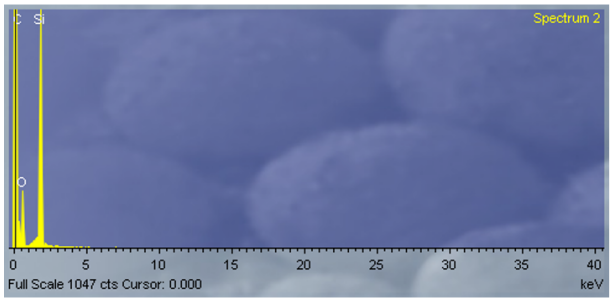

(b) Energy-dispersive X-ray spectroscopy of the adhesive

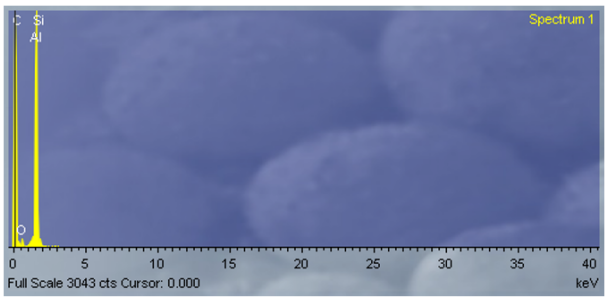

(c) Energy-dispersive X-ray spectroscopy of the substrate

Figure 16: SEM analysis of fracture surface

Although failure in these joints is mainly adhesive, it is clear that there is some adhesive that remains in small areas at the substrate, being detected in the EDS analysis. In this image, the remaining of contaminant at the substrate is not clear since the composition of the surfactant, in terms of chemical elements, is close to that of the adhesive. However, it is clear that the adhesive remains on small areas of substrate, but the failure is mostly interfacial, supporting the idea that the surfactant contamination is higher that what the adhesive can absorb.

C.5 Numerical results

Models for uncontaminated joints

All cohesive parameters were previously determined experimentally in other works. Brandão et al. determined the G_{IC} for an uncontaminated DCB [Brandão et al., 2021], while Borges et al. produced a detailed study on silicone adhesive used in this work, showing the values of the stiffness and strength as a function of the amount of contaminant added to the adhesive prior to curing [Borges et al., 2021b]. These values are presented in Table 4.

Table 4: Cohesive properties of the adhesive applied in the numerical mode.

G_{IC} [N/mm]	3.3
Tensile strength [MPa]	2.72
Young's modulus [MPa]	1.34

Figure 17 presents P-δ curves of the uncontaminated DCB, both representative experimental results and the curves numerically obtained. As on the Figure 18, the experimental and numerical results for the SLJ are compared through the P-δ curves and the failure load. From these results, it is clear that the CZM and numerical model developed is capable of simulating the behavior of the silicone adhesive on the joints under analysis, though the properties previously determined using standard tests.

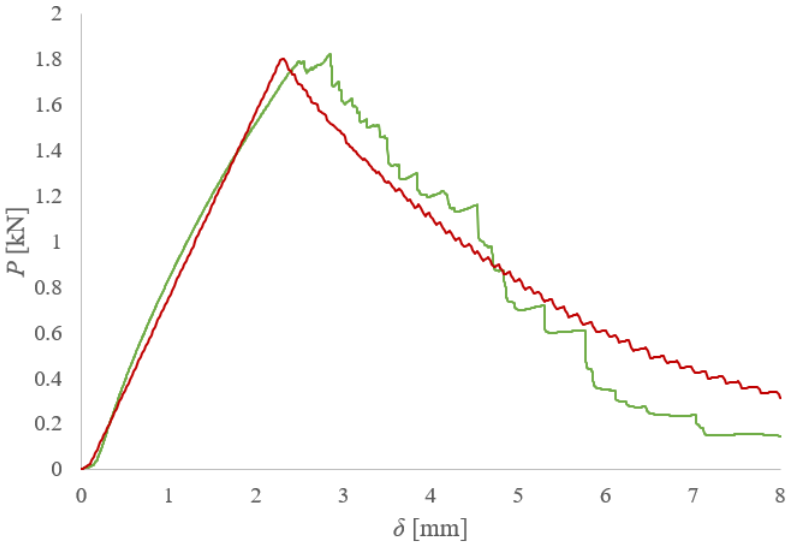

Figure 17: P-δ of the DCB uncontaminated model

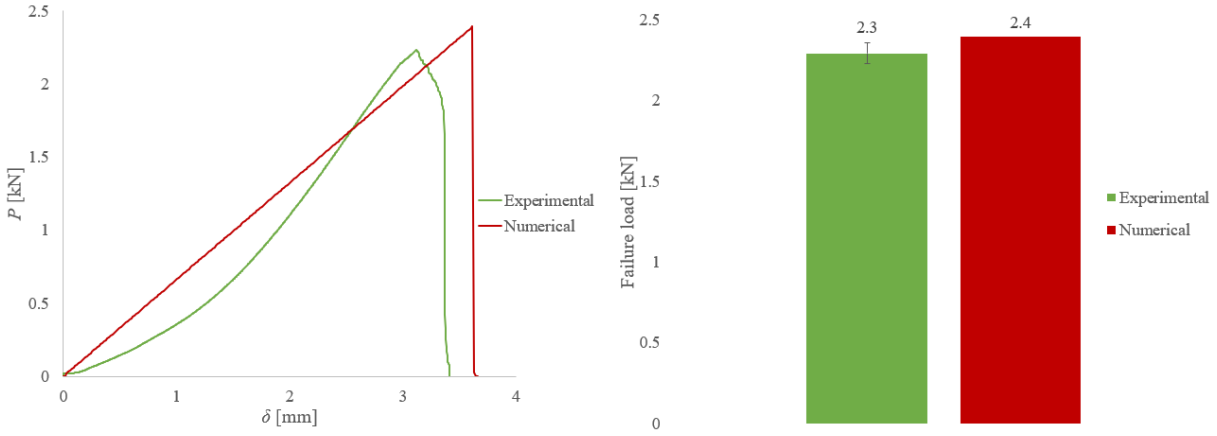

(a) P-δ (b) Failure load

Figure 18: Numerical results of the SLJ uncontaminated model

Models for contaminated joints

In this model, the cohesive parameters of the contaminant layer were obtain with an inverse method, fitting the numerical P-δ curves to the experimental ones and enabling a full characterization of the properties of the contaminant layer as a function of the quantity of contaminant applied in the substrate prior to adhesive bonding. This method consisted in inputting the Young's modulus (E), the tensile stress (σ) and the G_{IC} in the respective DCB model, as a function of the quantity of contaminant. As for the elastic elements of the "neat adhesive" layer, the same Young's modulus as the one in the numerical model without contaminant was considered.

In Figures 19 20 21, experimental and numerical P-δ of the DCB specimens with 1, 4 and 10 sprays, respectively, are shown.

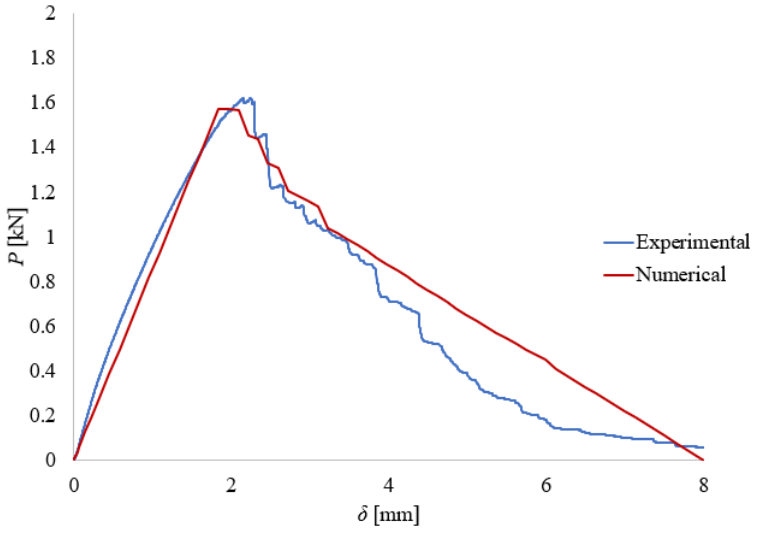

Figure 19: P-δ of 1 spray model

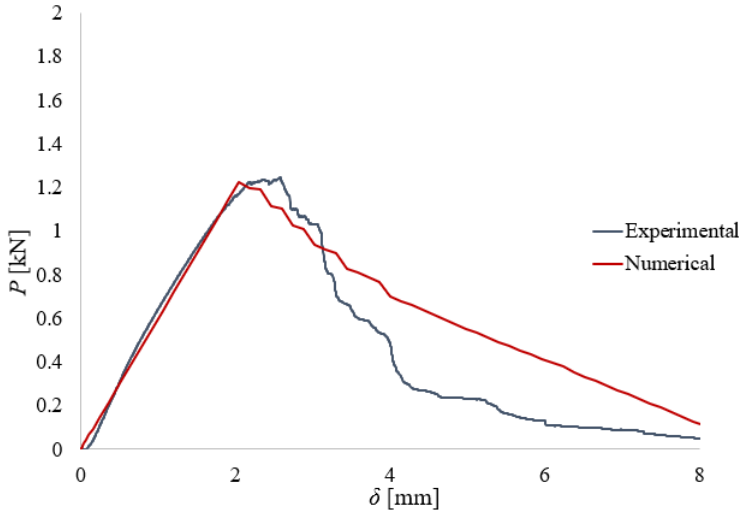

Figure 20: P-δ of 4 spray model

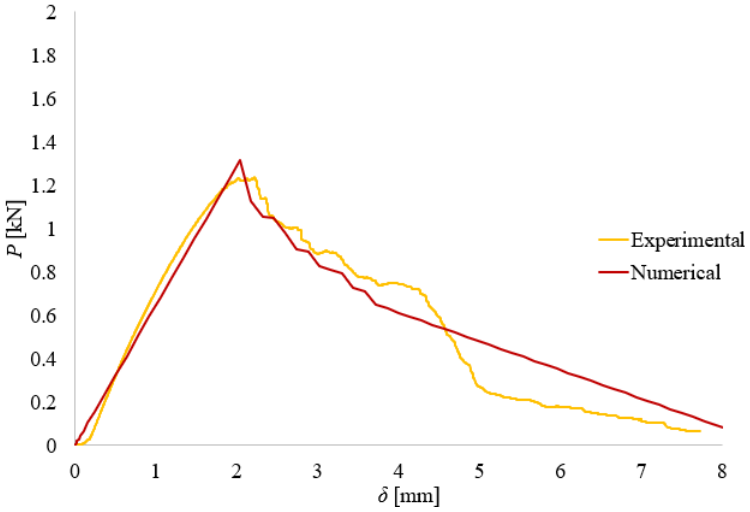

Figure 21: P-δ of 10 spray model

While for DCB models, the G_{IC} is the predominant parameter in obtaining a good model [Gustafson and Waas, 2009], for our range of values, which is reduced [0.1-0.08 N/mm], the model showed to be mostly insensitive to the variation. Regarding strength, it was very sensitive to small variations in the range of values for the σ [4-5.5 MPa]. This result is in line with a study done by Banea et al. who stated that to low values of the cohesive strength (under 7 MPa) this type of numerical model is very sensitive to cohesive strength while, for high values of cohesive strength, G_{IC} is the predominant parameter [Banea et al., 2011].

In order to confirm these results, a sensitivity study to mode I parameters was performed in the model for 1 spray DCB, since it was the model with higher strength (5.5 MPa). First, it was compared how the P-δ curve changed with the G_{IC}, the value applied in our numerical model for 1 spray was 0.08 N/mm, so a comparison was made either

for a value well above and below. We increase until 1 N/mm which (125% higher) and decrease until 0.05 N/mm. The results are shown in 22a. Secondly, the same analysis was done for σ and the results are presented in 22b.

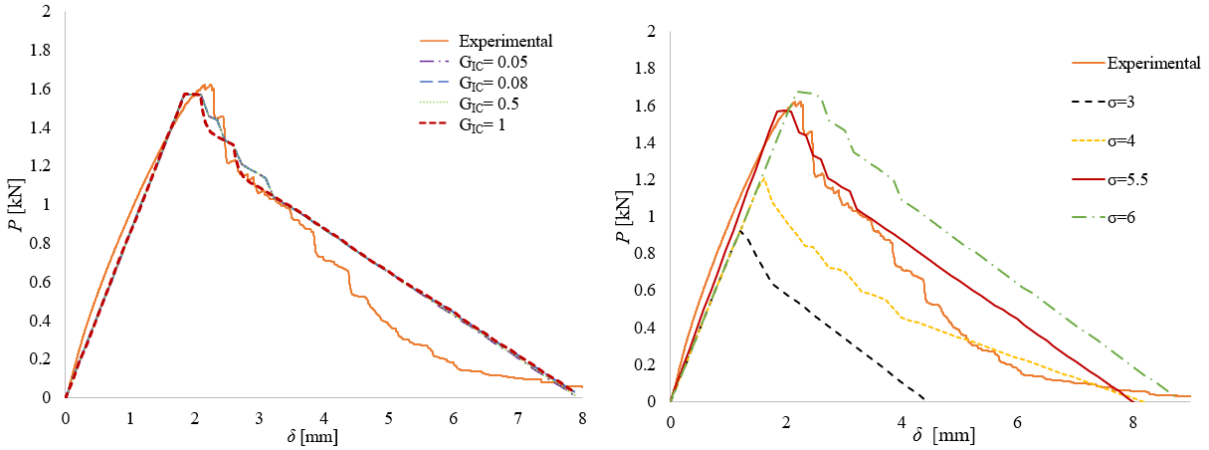

(a) G_{IC} sensitivity (b) σ sensitivity

Figure 22: Numerical model sensitivity to Mode I parameters

In Figure 23 a schematic representation is showed how the cohesive strength in mode I varied for the models used. There is a decrease of the property as the number of sprays increase.

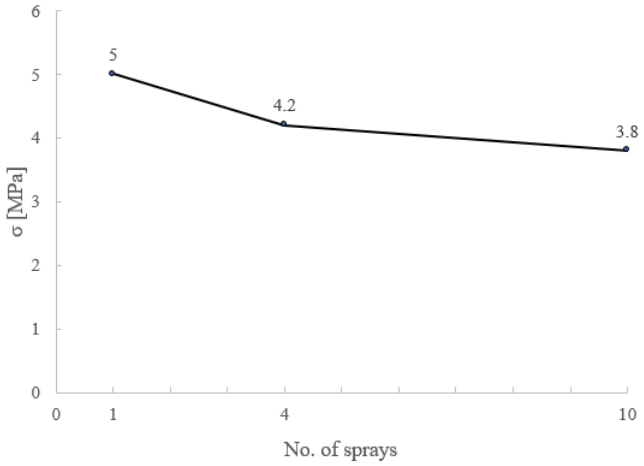

Figure 23: σ used in the three models

It is clear that the model is in reality very insensitive to changes in G_{IC} and really susceptible to changes in σ, what confirms what was previously stated.

Afterwards, to further validate this method and to obtain a more complete characterization of the cohesive values of the contaminated layer, we repeated the process in a SLJ. This time, the values previously obtain in mode I (E, σ, G_{IC}) were used and found the

remaining mode II parameters using the inverse method, fitting the numerical P-δ curves to the experimental ones.

In Figures 24, 25 and 26, experimental and numerical P-δ as well the failure load graphic to represent the difference of the failure load of the SLJ with 1, 4 and 10 sprays, respectively, are shown.

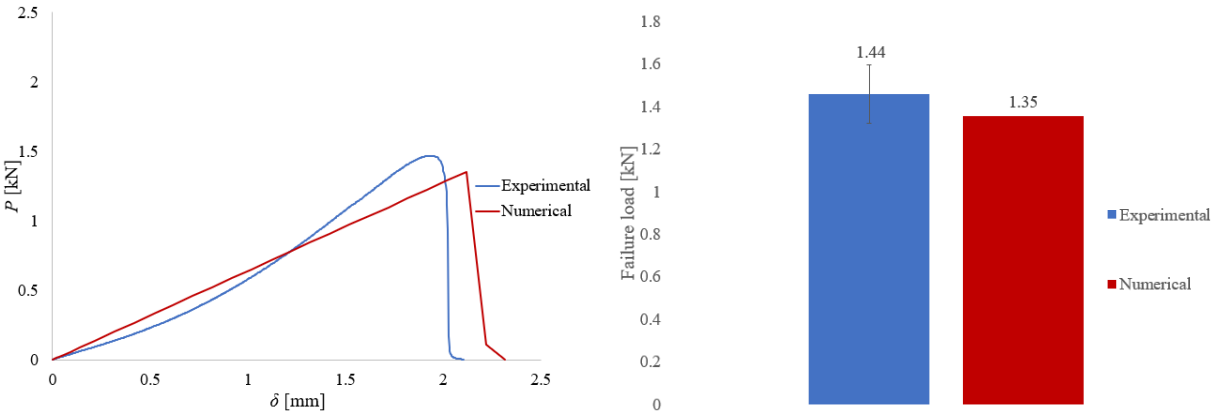

(a) P-δ (b) Failure load

Figure 24: Numerical model of SLJ with 1 spray

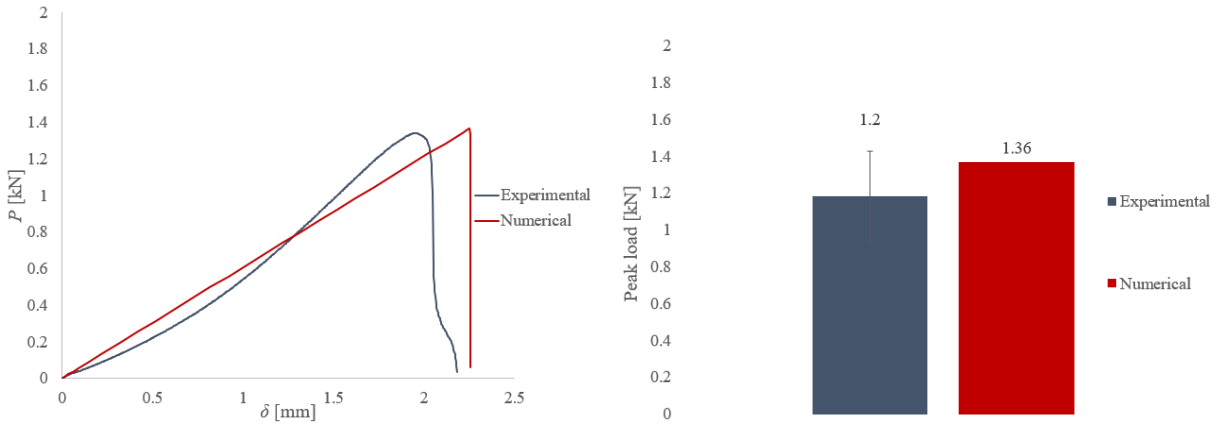

(a) P-δ (b) Failure load

Figure 25: Numerical model of SLJ with 4 spray

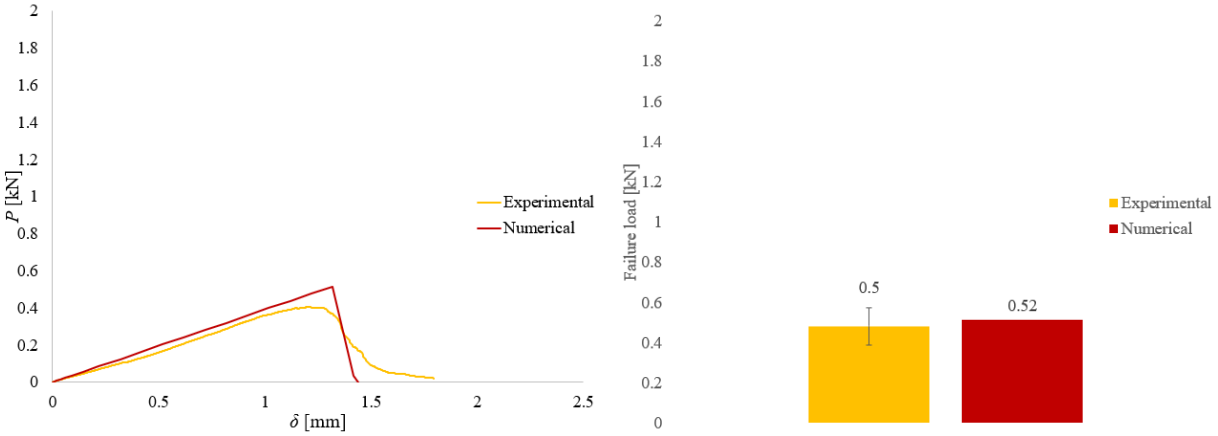

(a) P-δ (b) Failure load

Figure 26: Numerical model of SLJ with 10 spray

For all levels of contamination, by applying this method it was possible to reach a good prevision of the real properties of the contaminated layer, since the numerical curves of the SLJ model is very similar to the experimental one, reaching a good result.

Regarding the model sensibility to the cohesive parameters in mode II, the SLJ model was not very affected by the G_{IIC} values, and the parameter that had the most influence was the critical shear stress (τ_{IIc}). These results are in agreement with Gustafson et al. who stated that for low G_{IIC}, the maximum load is primarily dependent. on τ_{IIc} [Gustafson and Waas, 2009].

To prove these results, a sensitivity study to mode II parameters was performed in the model for the SLJ with 1 spray of contaminant, as it was done for the DCB test. To analyze the sensitivity of G_{IIC}, a range of [0.05-1] N/mm was utilized and, for all the values input, there was not a considerable difference, which leads to the conclusion that, in this range of critical shear stress, the G_{IIC} does not significantly influence the model, Figure 27a. To study the influence of the τ_{IIc} in the SLJ model, a range of values was applied and, for all the values inputted, the results significantly changed, Figure 27b.

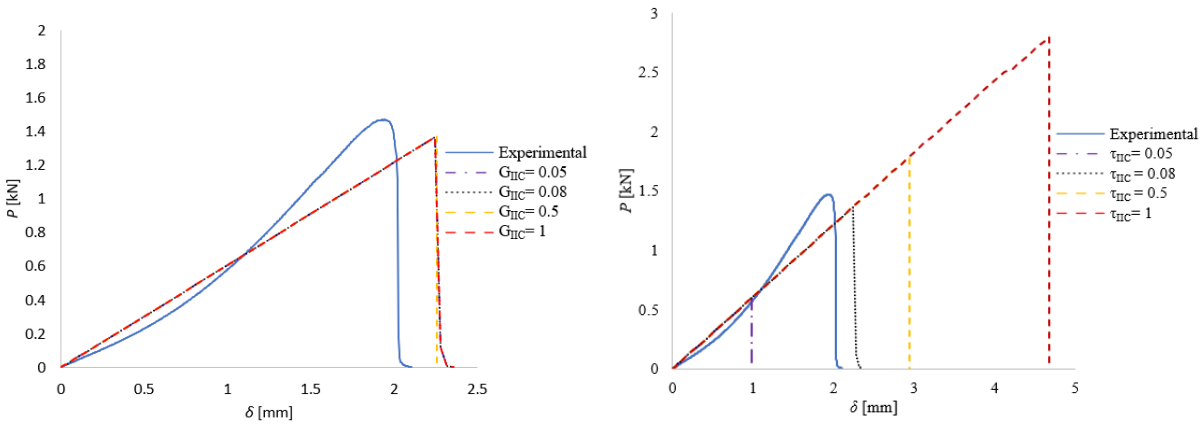

(a) G_{IIC} sensitivity (b) τ_{IIc} sensitivity

Figure 27: Numerical model sensitivity to Mode II parameters

In Figure 28 shows how the critical shear stress varied for the models used. As the number of sprays increases, the property value decreases.

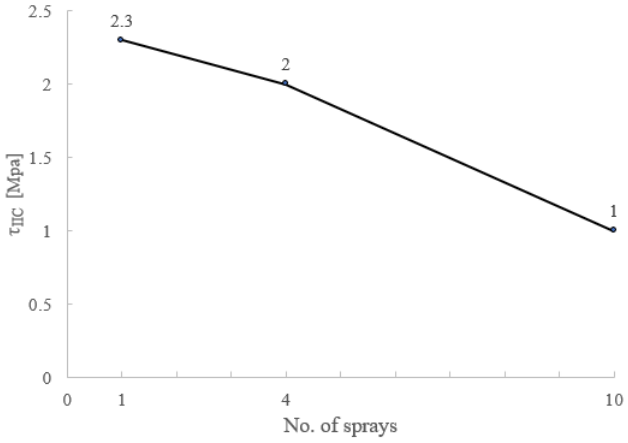

Figure 28: τ_{IIC} used in the three models

C.6 Conclusions

In this study, the effects of the surfacial application of surfactant on the properties of joints with aluminum substrates and silicone adhesive were studied. Different levels of contamination were applied in aluminum substrates before adhesive bonding. SLJ and DCB were used. Afterwards, a numerical model was created to verify the experimental results. The main conclusion are as follows:

- The application of a surfactant before bonding decreases the joint strength of DCB and SLJ. The deterioration of the properties varied directly with the amount of surfactant applied.

- In both SLJs and DCBs, the failure surface became increasingly interfacial as the amount of contaminant increased, changing from cohesive failure for the joints without surfactant application to adhesive failure for the maximum level of contamination. For the medium levels of contamination, the failure was cohesive near the substrate.

- The adhesive at the interphase absorbs the contaminant (decreasing its strength and stiffness), changing the failure from cohesive through the middle of the adhesive to cohesive at the interphase. As the contamination level is increases, the adhesive reaches a limit of contaminant it can absorb, and the remaining contaminant is left at the interface, acting as a physical separation turning the failure adhesive.

- It was possible to simulate this behavior with *Abaqus*, using a model with a contaminated layer as cohesive elements. With the indirect method, good approximations of the $P - \delta$ curves of both SLJ and DCB were obtained.

- In addition, a cohesive properties' sensibility study was made. The results stated that, for this type of simulation with low tensile stress (under 5.5 MPa), the G_{IC} does not have an impact on the behavior of the model, for mode I the model was most sensitive to tensile stress variations. As for the mode II properties, the one that have the bigger impact was the shear stress.

References

[A. N. Rider, 1999] A. N. Rider, C. L. Olsson-Jacques, D. R. A. (1999). Influence of adherend surface preparation on bond durability. *Surface and interfacial analysis*, 27:1027–1118.

[Akiyama et al., 2020a] Akiyama, H., Fukata, T., Sato, T., Horiuchi, S., and Sato, C. (2020a). Influence of surface contaminants on the adhesion strength of structural adhesives with aluminium. *The Journal of Adhesion*, 96(15):1311–1325.

[Akiyama et al., 2020b] Akiyama, H., Fukata, T., Sato, T., Horiuchi, S., and Sato, C. (2020b). Influence of surface contaminants on the adhesion strength of structural adhesives with aluminium. *The Journal of Adhesion*, 96(15):1311–1325.

[Araújo et al., 2017] Araújo, M., Machado, J., Marques, E., and da Silva, L. (2017). Dynamic behaviour of composite adhesive joints for the automotive industry. *Composite Structures*, 171:549–561.

[Aufray and Roche, 2006] Aufray, M. and Roche, A. A. (2006). Residual stresses and practical adhesion: effect of organo-metallic complex formation and crystallization. *Journal of Adhesion Science and Technology*, 20(16):1889–1903.

[Avendaño et al., 2016] Avendaño, R., Carbas, R., Marques, E., da Silva, L., and Fernandes, A. (2016). Effect of temperature and strain rate on single lap joints with dissimilar lightweight adherends bonded with an acrylic adhesive. *Composite Structures*, 152:34–44.

[Banea et al., 2011] Banea, M., da Silva, L., and Campilho, R. (2011). Mode i fracture toughness of adhesively bonded joints as a function of temperature: Experimental and numerical study. *International Journal of Adhesion and Adhesives*, 31(5):273–279.

[Borges et al., 2021a] Borges, C., Marques, E., Carbas, R., Ueffing, C., Weißgraeber, P., and da Silva, L. (2021a). Review on the effect of moisture and contamination on the interfacial properties of adhesive joints. *Proceedings of the Institution of Mechanical Engineers, Part C: Journal of Mechanical Engineering Science*, 235(3):527–549.

[Borges et al., 2021b] Borges, C. S., Brandão, R., Akhavan-Safar, A., Marques, E. A., Carbas, R. J., Ueffing, C., Weissgraeber, P., and da Silva, L. F. (2021b). Influence of water and surfactant contamination on the properties of a silicone adhesive, before and after curing.

[Brandão et al., 2021] Brandão, R., Borges, C. S., Akhavan-Safar, A., Marques, E. A., Carbas, R. J., Ueffing, C., Weissgraeber, P., and da Silva, L. F. (2021). The influence of humidity and immersion temperature on the properties and failure mode of pbt-gf30/silicone bonded joints.

[Brotherhood et al., 2002] Brotherhood, C., Drinkwater, B., and Guild, F. (2002). The effect of compressive loading on the ultrasonic detectability of kissing bonds in adhesive joints. *Journal of Nondestructive evaluation*, 21(3):95–104.

[Cocosalkylaminethoxylate, 2020] Cocosalkylaminethoxylate (2020). Syskem chemie gmbh. *Accessed June 3, 2021*, https://www.syskem.de/index$_e$.*html*.

[da Silva et al., 2018] da Silva, L. F., Ochsner, A., and Adams, R. D. (2018). *Handbook of adhesion technology*. Springer Science & Business Media.

[Debski et al., 1986] Debski, M., Shanahan, M., and Schultz, J. (1986). Mechanisms of contaminant elimination by oil-accommodating adhesives part 1: Displacement and absorption. *International Journal of Adhesion and Adhesives*, 6(3):145–149.

[Drewry et al., 2009] Drewry, M. A., Smith, R. A., Phang, A. P., Yan, D., Wilcox, P., and Roach, D. P. (2009). Ultrasonic techniques for detection of weak adhesion. *Materials evaluation*, 67(9):1048–1058.

[Gao and Mäder, 2002] Gao, S.-L. and Mäder, E. (2002). Characterisation of interphase nanoscale property variations in glass fibre reinforced polypropylene and epoxy resin composites. *Composites Part A: Applied Science and Manufacturing*, 33(4):559–576.

[Grangeat, 2019] Grangeat, R. (2019). *Durabilité des assemblages collés en environnement humide: instrumentation par capteurs à fibre optique*. PhD thesis, Nantes.

[Greiveldinger et al., 2000] Greiveldinger, M., Shanahan, M. E. R., Jacquet, D., and Verchère, D. (2000). Oil-covered substrates: A model study of the evolution in the interphase during cure of an epoxy adhesive. *The Journal of Adhesion*, 73(2-3):179–195.

[Gustafson and Waas, 2009] Gustafson, P. A. and Waas, A. M. (2009). The influence of adhesive constitutive parameters in cohesive zone finite element models of adhesively bonded joints. *International Journal of Solids and Structures*, 46(10):2201–2215.

[Hoffmann et al., 2018] Hoffmann, M., Tserpes, K., Moutsompegka, E., Schlag, M., and Brune, K. (2018). Determination of adhesion strength of pre-bond contaminated composite-to-metal bonded joints by centrifuge tests. *Composites Part B: Engineering*, 147:114–121.

[International, 2017] International, A. (2017). Astm d3933-98,standard guide for preparation of aluminum surfaces for structural adhesives bonding (phosphoric acid anodizing).

[Jeenjitkaew et al., 2010] Jeenjitkaew, C., Luklinska, Z., and Guild, F. (2010). Morphology and surface chemistry of kissing bonds in adhesive joints produced by surface contamination. *International Journal of Adhesion and Adhesives*, 30(7):643–653.

[Marty et al., 2004] Marty, P. N., Desai, N., and Andersson, J. (2004). Ndt of kissing bond in aeronautical structures.

[Montois et al., 2006] Montois, P., Nassiet, V., Petit, J. A., and Baziard, Y. (2006). Viscosity effect on epoxy–diamine/metal interphases: Part i: Thermal and thermomechanical behaviour. *International Journal of Adhesion and Adhesives*, 26(6):391–399.

[Possart et al., 2006] Possart, W., Krüger, J. K., Wehlack, C., Müller, U., Petersen, C., Bactavatchalou, R., and Meiser, A. (2006). Formation and structure of epoxy network interphases at the contact to native metal surfaces. *Comptes Rendus Chimie*, 9(1):60–79.

[Pramanik et al., 2017] Pramanik, A., Basak, A., Dong, Y., Sarker, P., Uddin, M., Littlefair, G., Dixit, A., and Chattopadhyaya, S. (2017). Joining of carbon fibre reinforced polymer (cfrp) composites and aluminium alloys – a review. *Composites Part A: Applied Science and Manufacturing*, 101:1–29.

[Roche et al., 2002] Roche, A., Bouchet, J., and Bentadjine, S. (2002). Formation of epoxy-diamine/metal interphases. *International Journal of Adhesion and Adhesives*, 22(6):431–441.

[Voyutskii, 1963] Voyutskii, S. S. (1963). *Autohesion and adhesion of high polymers.*

[White et al., 2009] White, C., Tan, K., wolf Andreas, and Carbary, L. (2009). *Advances in Silicone Adhesives*. Advances in Structural Adhesive Bonding, Woodhead Publishing Limited, Cambridge, -1.